Application of Advanced Thermodynamic Models in the Representation of the Global Phase Behavior of Fluids of Interest in the Oil & Gas Industry

Vinhal, Andre Pinto Coelho Muniz

Publication date:
2018

Document Version
Publisher's PDF, also known as Version of record

Application of Advanced Thermodynamic Models in the Representation of the Global Phase Behavior of Fluids of Interest in the Oil & Gas Industry

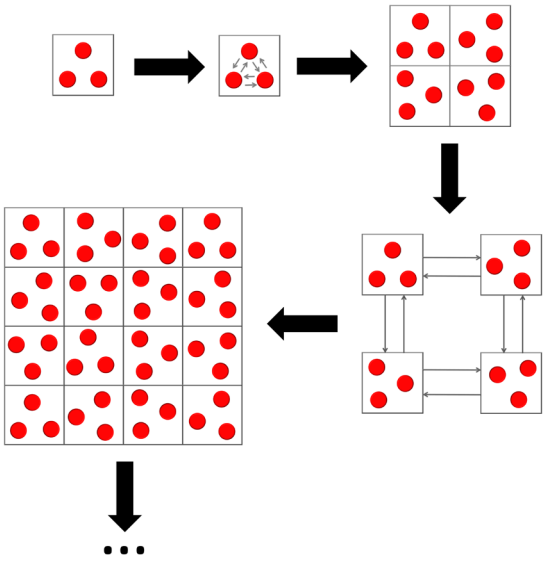

Andre Pinto Coelho Muniz Vinhal
June, 2018

DTU Chemical Engineering
Department of Chemical and Biochemical Engineering

PhD Thesis
Doctor of Philosophy

Application of Advanced Thermodynamic Models in the Representation of the Global Phase Behavior of Fluids of Interest in the Oil & Gas Industry

Andre Pinto Coelho Muniz Vinhal
June 30, 2018

Supervisors:
Professor Georgios M. Kontogeorgis
Associate Professor Wei Yan

Center for Energy Resources Engineering
Department of Chemical and Biochemical Engineering
Technical University of Denmark (DTU)
DK-2800 Kgs. Lyngby, Denmark

DTU Chemical Engineering
Department of Chemical and Biochemical Engineering
Technical University of Denmark

Søltofts Plads
Building 229
2800 Kongens Lyngby, Denmark
Phone +45 4525 2800
kt@kt.dtu.dk
www.kt.dtu.dk

"...though the world does not change with a change of paradigm, the scientist afterward works in a different world."

Thomas Kuhn

Summary

The complexity of industrial processes is increasing rapidly in the last decades, allowing the production of important materials in more efficient ways. Some examples are the use of near-critical and super-critical fluids to substitute traditional separation methods, and the exploitation of unconventional reservoirs. In such cases, the feasible implementation of the processes requires a broad and accurate knowledge of the thermophysical properties of the systems.

The experimental measurement of the thermodynamic properties is extremely important in the understanding of the behavior of fluids, yet, this activity is time-consuming and expensive. An alternative is to use theoretical thermodynamic models to represent the systems, which can also be applied in process simulators for the design of the equipment and optimal control of the operations.

In this work, one of the limitations of the classical thermodynamic models was investigated, that is the incorrect description of the behavior of fluids close to the critical point. In this region, the properties of the system are modified due to the strong fluctuations related to the long-range correlations between the molecules. Classical equations of state (EoS), like Soave-Redlich-Kwong (SRK) and Cubic-Plus-Association (CPA), are based on a mean-field theory, in which an average interaction potential is assumed for the particles, therefore they do not account for these long-range fluctuations. The improvement of such models is fundamental for the correct simulation of processes in the near-critical regions, and for the modeling of operations encompassing a wide range of conditions, which is relevant to the oil & gas industry and other sectors.

The incorporation of the long-range fluctuations into the classical EoS, i.e. SRK and CPA, was achieved using a recursive procedure developed by White and co-workers, following the renormalization group (RG) treatment proposed by Wilson. It is a simple method that consists of a set of recur-

sive relations where the fluctuations with respect to the density are considered in several iterations. The procedure yields a model that possesses a non-analytical/asymptotic behavior close to the critical point, but reduces to the traditional equation far from the critical region. The extended models are called the crossover SRK and crossover $CPA\ EoS$, and they are capable of accurately representing the phase behavior of fluids far away and close to the critical point. However, while the first one is only used to describe the properties of systems with non-associating species, the latter can be used to model the phase behavior of highly non-ideal systems composed of molecules that form hydrogen bonds, due to an additional term that explicitly accounts for the association between molecules.

The non-mean-field equations were compared with different classical thermodynamic models in the representation of the experimental saturated and critical properties of pure fluids. In addition to the SRK and $CPA\ EoS$, the Patel-Teja (PT) EoS was also used for the comparisons. The results of the computations indicated that only the crossover equations were able to describe both the saturated and critical properties with high accuracy for non-associating and associating species. Moreover, a new method for rescaling the pure component parameters of CPA was tested, but it showed some of the intrinsic limitations of mean-field equations, that is, different parameters might enhance the models' performance for certain regions. Nonetheless, large deviations regarding some properties, either critical or sub-critical, will be observed, as long as an average potential is used for describing the interactions between the particles.

Afterward, the calculations were extended to binary and ternary mixtures. Several groups of systems containing n-alkanes, n-alkanols, and carbon dioxide were studied. This is an important test to evaluate the capacity of the models to represent the different phase type behaviors that are observed in some homolog series, e.g. methane/n-alkane. Additionally, the comparison with experimental data showed the importance of the renormalization group corrections for the precise description of the volumetric properties of mixtures of non-associating components in near-critical regions. Furthermore, the calculations indicated that the performance of the models deteriorated due to asymmetry, i.e. the difference in size between the components.

In the case of systems with hydrogen bonding components, the incorporation of density fluctuations in the classical models proved to be even more crucial. This is due to the fact that the overestimation of the critical properties

with CPA is higher for associating components, which affects the representation of the phase behavior of mixtures, and cannot be completely corrected with the used of binary interaction parameters. On the other hand, the classical cubic models cannot represent the correct behavior of such systems, because they do not account for the formation of hydrogen bonds in the fluid.

Further evaluation of the crossover models to describe other systems, e.g. different associating species like glycols and very asymmetric mixtures, are needed to expand the applicability of the non-mean-field equations in the oil & gas sector. However, the current work has already shown that the utilization of the recursive procedure based on RG theory corrects the behavior of the classical models near the critical point, thus becoming a relevant and useful tool for engineering applications, which include the design of equipment and control of the operation of complex processes.

Resumé (Summary in Danish)

Kompleksiteten af industrielle processer er steget hurtigt i de sidste årtier. Det gør det muligt at producere vigtige materialer på mere effektive måder. Nogle eksempler er brugen af nærkritiske eller superkritiske væsker til at erstatte traditionelle separationsmetoder eller udnyttelsen af ukonventionelle kulbrinters reservoirer. I disse tilfælde kræver den profitable gennemførelse af processer et bredt og præcist kendskab til de termofysiske egenskaber af systemet.

Den eksperimentelle måling af de termofysiske egenskaber er meget vigtigt for forståelsen af væskers adfærd. Imidlertid er aktiviteten tidskrævende og dyr. Et alternativ er at bruge teoretiske termodynamiske modeller til at repræsentere systemer. Derudover kan de anvendes i processimulatorer til udformningen af udstyret og optimal styring af processen.

I denne Ph.d.-afhandling undersøges en af begrænsningerne af de klassiske termodynamiske modeller, dvs. modellerne der ikke er i stand til at repræsentere adfærden af væsker tæt på det kritiske punkt. Systemets egenskaber er modificeret i denne region på grund af de stærke fluktuationer som er tilknyttet til langtrækkende korrelationer mellem molekylerne. Klassiske tilstandsligninger, fx. Soave-Redlich-Kwong (SRK) og Cubic-Plus-Association (CPA), er baseret på en middelfeltteori, som antager et gennemsnitligt interaktionspotentiale for partiklerne. Derfor tager tilstandsligningerne ikke højde for disse langtrækkende fluktuationer. Forbedringen af de klassiske ligninger er vigtig for den korrekte modellering af processer i de nærkritiske regioner, men også for den nøjagtige repræsentation af operationer, der omfatter brede temperaturområder og trykbetingelser, der er relevante for olie og gas industrien.

Indførelsen af de langtrækkende fluktuationer i de klassiske tilstandsligninger, dvs. SRK og CPA, blev udført med anvendelse af en rekursiv procedure udviklet af White m.fl. efter en renormaliseringsgruppebehandling (RG) skabt af Wilson. Det er en enkel metode, som består af et sæt rekursive ligninger hvor fluktuationerne, med hensyn til densiteten, er inkluderet i flere iterationer. Proceduren giver en model som har en ikke-analytisk / asymptotisk adfærd nær det kritiske punkt, imens den reduceres til de traditionelle tilstandsligninger langt fra det kritiske område. De udvidede modeller bliver refereret til som crossover SRK og crossover CPA, og de er i stand til at repræsentere faseopførsel af væsker langt fra og tæt på det kritiske punkt. Crossover CPA kan derimod bruges til at modellere faseadfærd af væsker sammensat af molekyler, der danner hydrogenbindinger, på grund af et yderligere udtryk, der eksplicit tager højde for hydrogenbindinger via et associationsled.

Ikke-middelfeltligningerne blev sammenlignet med forskellige klassiske termodynamiske modeller i repræsentationen af de eksperimentelle faseligevægte og kritiske egenskaber af rene væsker. Desuden blev Patel-Tejas (PT) modellen også anvendt til sammenligningerne. Resultaterne af beregningerne viste, at kun crossover ligningerne var i stand til at beskrive begge typer af egenskaber med høj nøjagtighed for ikke-associerende og associerende komponenter. Derudover blev en ny metode til evaluering af CPA's komponentparametre testet, og det viste nogle af de egentlige begrænsninger af middelfeltligningerne, dvs. parametrene er optimale for nogle bestemte betingelser. Faktisk overholdes store afvigelser vedrørende nogle egenskaber, så længe der anvendes et gennemsnitligt potentiale til at beskrive samvirkninger mellem partiklerne.

Derefter blev ligningerne udvidet til binære og ternære blandinger. Flere grupper af systemer der indeholder n-alkaner, n-alkanoler og carbondioxid blev undersøgt. Det er en vigtig test for at evaluere modellernes evne til at repræsentere de forskellige fasetypeadfærd, der ses i nogle homologserier, fx. methan/n-alkan. Derudover viste sammenligningen med eksperimentelle data, at renormaliseringsgruppens korrektioner er væsentlige for den præcise beskrivelse af de volumetriske egenskaber for blandinger af ikke-associerende komponenter i nærkritiske regioner. Yderligere viste beregningerne, at præcisionen af modellerne blev reduceret på grund af asymmetrien, dvs. forskellen i størrelse mellem komponenterne.

I tilfælde af systemer med hydrogenbindende komponenter, var indførelsen af langtrækkende fluktuationer i de klassiske modeller endnu mere afgørende.

Overvurderingen af de kritiske egenskaber med CPA er højere for associerende komponenter, som påvirker repræsentationen af faseopførsel for blandinger hvilket ikke kan korrigeres ved anvendelse af binære interaktionsparametre. På den anden side kan de kubiske tilstandsligninger ikke repræsentere den rigtige opførsel af sådanne systemer, fordi de ikke tager højde for dannelsen af hydrogenbindinger i væsker.

Yderligere evaluering af crossover modellerne til beskrivelse af andre systemer, fx. forskellige associerende komponenter som glykoler og meget asymmetriske blandinger, er nødvendige for at udvide relevansen af ikke- middelfeltligningerne i olie og gas industrien. Det nuværende arbejde har imidlertid allerede vist, at anvendelsen af en rekursiv procedure baseret på RG teori korrigerer adfærden af de klassiske ligninger nær det kritiske punkt, og dermed bliver et relevant og nyttigt værktøj til tekniske applikationer, bl.a. udformning af udstyr og kontrol af driften af komplekse processer.

Preface

This thesis is submitted in partial fulfillment of the requirements to obtain the Doctor of Philosophy degree at the Technical University of Denmark (DTU). The work has been carried out at the Center for Energy Resources Engineering ($CERE$), at the Department of Chemical and Biochemical Engineering, under the supervision of Professor Georgios M. Kontogeorgis and Associate Professor Wei Yan.

The scholarship of the author was financially supported by the program Science Without Borders (Ciência sem Fronteiras), a program of the Brazilian National Council for Scientific and Technological Development ($CNPq$), under the Ministry of Science and Technology. The author gratefully acknowledges this support.

I would also like to acknowledge my supervisor Professor Georgios M. Kontogeorgis for his assistance over this entire project, and for always being available to answer the many questions I had. Additionally, I admire his enthusiasm, which is a great inspiration for pursuing the development of the field of thermodynamics.

I want to express my gratitude to my co-supervisor Associate Professor Wei Yan, for his insightful suggestions and comments over the several reports and discussions since I started the PhD program. His ideas were highly appreciated and important for the outcome of the project.

In addition to my supervisors, I want to say thanks to my colleagues at KT and Kemi departments. I have enjoyed working with them all. This project would not be the same if not for the countless coffee breaks and seemingly meaningless debates, which, contrarily, inspired me profoundly.

I am deeply thankful to all my friends and family in Brazil that, although being roughly 10000km away, have always been by my side. A special thanks to my dearest friends Zim and Mendin, my brother Ricardo, my father Ricardo

and my mother June. They have definitely made this work possible by shaping my personality.

Finally, to my wife and most important person to me: Claudia. The meaning of my life. Without her understanding and comprehension in needed times, but also firm opinions in others, but above all... her love; this would not have been possible.

Andre Vinhal

June 30, 2018

Contents

Nomenclature

Below are the list of symbols used in this work.

Abbreviations:

AAD	Average Absolute Deviations
$CCPA$	Crossover Cubic-Plus-Association
CPA	Cubic-Plus-Association
$CR1$	Combining Rule 1
$CSRK$	Crossover Soave-Redlich-Kwong
$DIPPR$	The Design Institue for Physical Properties
ECR	Elliot Combining of Rule
EoS	Equation of State
EOR	Enhanced Oil Recovery
LLE	Liquid-liquid Equilibrium
$LCEP$	Lower Critical End Point
LPG	Liquefied Petroleum Gas
$NIST$	National Institute of Standards and Technology
OF	Objective Function
PR	Peng-Robinson
PSO	Particle Swarm Optimization
PT	Patel-Teja
RG	Renormalization Group
$RKPR$	Redlich-Kwong-Peng-Robinson
$SAFT$	Statistical Associating Fluid Theory
SRK	Soave-Redlich-Kwong
SW	Schmidt-Wenzel
$UCEP$	Upper Critical End Point
VLE	Vapor-liquid Equilibrium

$VLLE$	Vapor-liquid-liquid Equilibrium

Roman characters:

a	Constant of the attractive term in a EoS
a_0	Parameter of the constant of the attractive term of the physical part of CPA
A	Helmholtz energy
b	Constant of the repulsive term in a EoS
b_{LM}	Universal linear-model parameter
c	Constant of the attractive term in a EoS
c_1	Parameter of the temperature-dependent part of the constant in the attractive term of the physical part of CPA
C_v	Isochoric heat capacity
d	Dimensionality, or rectilinear diameter of the coexistence curve
f	Free energy density
f_0	Initial free energy density in White's recursive procedure
F	Free energy
g	Radial distribution function
G	Function to calculate the density fluctuations in White's recursive procedure
Gi	Ginzburg number
K	Kernel term, or constant in White's recursive procedure
k_b	The Boltzmann's constant
k_{ij}	Binary interaction parameter of the attractive term constant in a EoS
$k_{\alpha,\beta,\gamma,\delta}$	Critical amplitudes
L	Cut-off length parameter, or correlation length
l_{ij}	Binary interaction parameter of the repulsive term constant in a EoS
m	Mass of a particle
N	Number of particles, or experimental points
p	Momentum of a particle
P	Pressure
q	Renormalized distance from the critical point
r	Random vectors for the PSO algorithm

R	Universal gas constant, or function of the renormalized distance to the critical point
T	Temperature
T_r	Reduced temperature
u	Interaction potential of the long-rang attractive forces, or constant of the attractive term in the $SW\ EoS$
v	Molar volume, or velocity of a particle
V	Volume
V_{ex}	Excluded volume
w	Constant of the attractive term in the $SW\ EoS$
x	Position of a particle, or mole fraction
X_{A_i}	Monomer fraction
Y	Crossover function
Z	Partition function, or compressibility factor

Greek characters:

α	Temperature-dependent function of the constant of the attractive term in a EoS, or critical exponent
β	Dimensionless inverse temperature, or critical exponent
$\beta^{A_iB_j}$	Association volume parameter
β_c	Function of the acentric factor used to determine the critical compressibility factor of the $SW\ EoS$
γ	Critical exponent
δ	Critical exponent, or parameter in the $RKPR\ EoS$
δf	Corrections to the free energy density due to fluctuations of the order parameter
Δ_1	Critical exponent
$\Delta^{A_iB_j}$	Association strength
$\Delta\eta$	Dimensionless reduced volume
$\varepsilon^{A_iB_j}$	Association energy parameter
ζ_c	Critical compressibility factor of the SW and $PT\ EoS$
η	Critical exponent
κ	Function of the acentric factor, or critical amplitude
κ_T	Isothermal compressibility
λ	Parameter of the PSO algorithm
μ_0	Analytic function of temperature
ν	Critical exponent

ρ	Density
σ	Parameter of the PSO algorithm
τ	Dimensionless reduced temperature
ϕ	Average interaction potential, or parameter related to the initial shortest wavelength of density fluctuations
Φ	Interaction potential between particles
ω	Acentric factor, or correction-to-scaling exponent
$\Omega_{a,b,c}$	Terms for calculating the constants of the attractive and repulsive term in the EoS, or term that accounts the density contributions in White's recursive procedure

Subscripts and superscripts:

c	Critical property
d	Dimensionality
$calc$	Calculated value
exp	Experimental value
i, j	Index to label a molecule in a system
l	Long-range interactions
liq	Liquid phase property
n	Iteration index of White's recursive procedure, or PSO algorithm
s	Short-range interactions
sat	Saturated property
rep	Repulsive part of the free energy
vap	Vapor phase property
$^-$	Renormalized variable, or correction to the free energy density in White's recursive procedure

List of Figures

List of Tables

Chapter 1

Introduction

Industrial processes in the field of chemical and petroleum engineering usually require a detailed knowledge of the phase behavior and the thermophysical properties of fluids for an efficient design of equipment and control of the operations [35]. One of the approaches for obtaining the information regarding the properties of the systems involved in industrial processes is via experimental measurements. The acquisition of reliable data, i.e. data that are consistent, and can be utilized as a benchmark for a certain system in the validation or development of predictive models, is an expensive and time-consuming process [36]. Due to these reasons, high-quality experimental data sets for different pure fluids and mixtures over a wide range of temperature and pressure conditions are scarce. Therefore, the use of predictive models, capable of accurately representing the phase behavior of the systems, is of great importance to the oil & gas and other industrial sectors.

The most common thermodynamic models used to represent the properties of fluids in the oil & gas industry are the cubic equations of state (EoS). Cubic EoS are simple models that can be rewritten as a cubic function in terms of the molar volume, and are adequate for simulating industrial processes in the petroleum sector because of their capability to correctly describe the phase behavior of hydrocarbon-gas mixtures up to high pressures. As an example, such models are extensively utilized in compositional reservoir simulators, which are tools to represent the phase and flow behavior involved in the displacement of fluids in hydrocarbon reservoirs. Compositional models simulate the complex multiphase flow in a reservoir, where the composition of a phase at equilibrium changes with space and time, and the EoS is em-

ployed to determine the number of equilibrium phases and the mole fractions of the components at each phase [37]. The advantage of cubic models in comparison to more advanced ones, like the Statistical Association Fluid Theory ($SAFT$) and Cubic-Plus-Association (CPA) EoS, is related to the reduced computational effort in the phase equilibrium calculations.

Nevertheless, challenging situations are often observed in the modeling of processes with highly non-ideal systems, e.g. molecules that form hydrogen bonds [38], or processes in conditions close to the critical point of the fluid, where the thermodynamic behavior of the system becomes non-analytical [39]. In both cases, simple theoretical formulations fail to represent the phase behavior of the fluids.

Regarding the first issue, it is known in the literature that cubic EoS often cannot satisfactorily represent complex multicomponent systems containing hydrogen bonding compounds [40]. In fact, the description of the binary systems is also problematic when the vapor-liquid equilibria (VLE) and liquid-liquid equilibria (LLE) are of interest over a range of extended temperatures and pressures. This is seen in the simulation of enhanced oil recovery (EOR) methods, which are techniques applied to improve the recovery of hydrocarbons by the injection of materials that are not normally present in the reservoir. The most commonly applied EOR methods are steam flooding and miscible gas injection, e.g. CO_2, which considerably increases the complexity of the system's phase behavior. At high temperatures - over 150^oC - the solubility of water in the hydrocarbons phases is substantial, generating deviations in the equilibrium calculations. These deviations happen because associative components forms clusters through hydrogen bonds. Besides, water molecules forms three-dimensional structures that changes rapidly with the variation of temperature [41].

In order for a model to take into account the polar/association effects, an additional term should be added to the EoS. There are several ways of developing expression for the association contribution, using either perturbation, chemical or lattice theories [42], but in many cases they yield essentially identical expressions for the association contribution [43]. Hence, the choice of the model to describe the hydrogen bonds is usually related to the ability of the theory to cover different types of association schemes. In this sense, Wertheim's association term from perturbation theory is more successful than the others, and it is used in $SAFT$ [44] and CPA [45]. The latter model is widely applied to describe a variety of systems and compounds of interest

to the oil & gas industry (hydrocarbons, gases, water, alcohols, glycols), because it reduces to the $SRK\ EoS$ when no hydrogen bonding compounds are involved [40, 46]. Nevertheless, this approach is only useful for representing the behavior of associating systems far from the critical point, where the fluctuations of the order parameter are negligible [47].

In the vicinity of a critical point, the thermodynamic properties of fluids cannot be accurately described by classical EoS [39]. The classical formulations, also referred to as the mean-field approach, neglect the fluctuations in the order parameter associated with the critical phase transition, hence they predict an analytical behavior of the systems close to the critical point, resulting in an incorrect estimation of the critical exponents and other thermodynamic properties in the near-critical region [48]. This inaccurate representation of the phase behavior of fluids in the critical region might hamper the successful implementation of EOR projects in high-temperature/high-pressure reservoirs with high CO_2 content [49]. Additionally, near-critical and supercritical fluids are becoming more common in different industrial sectors, thus models that are capable of taking into account the long-range interactions that are present in fluids close to the critical point are also useful for the simulation of process like the production of gasoline [50], liquefied petroleum gas (LPG) [51] and methanol [27] from syngas and the production of biofuel using alcohol [52, 53].

Due to the singular behavior of a fluid near the critical point, classical equations of state (EoS) fail to correctly describe the thermodynamic properties of fluids [54]. On the other hand, far away from the critical point, where the inhomogeneities are negligible, classical EoS yields a quantitative representation of the phase behavior of fluids and are important tools for engineering calculations. Therefore, a model that is capable of describing the global phase behavior of thermodynamic systems, i.e. far away and close to the critical point, is of great scientific and technical relevance [55].

Several efforts have been made in the last decade towards the development of a global EoS with a crossover treatment that corrects the mean-field behavior in the critical region. This correction is done by introducing the fluctuations in the order parameter, which for the vapor-liquid critical phase transition is the density, into the mean-field EoS. There are two main approaches to develop a crossover EoS based on the renormalization group (RG) theory. The first is done using a renormalized Landau expansion [48, 56], and the second one is based on Wilson's phase-space cell approximation [57] developed

by White and coworkers [58–61]. The last procedure has the advantages of having fewer additional parameters, in comparison to the first approach, and due to the independence of the numerical procedure in relation to the underlying model, allowing the implementation of different mean-field models with less effort. Moreover, the isomorphism assumption can be used in order to extend the procedure to mixtures [62]. This means that the thermodynamic potential of a mixture is considered to have the same universal form of the one-component fluid, additionally, the mole fraction is used as an independent variable instead of the chemical potential [56].

In summary, global thermodynamic models are equations in which RG methods are used to correct the classical EoS close to the critical point, while far away from the critical regions, they behave like the mean-field thermodynamic equations, yielding accurate descriptions of the thermodynamic properties of real fluids in a wide range of conditions. Such models are useful for representing several different industrial processes, as mentioned previously. Therefore, this work is intended to improve the EoS that are largely applied in the oil & gas industry by introducing long-range fluctuations in density, improving the performance the theoretical models and increasing the reliability of the simulations of complex industrial processes.

1.1 Objectives

The goal of this work is to evaluate and improve the thermodynamic models usually applied in the description the phase equilibrium and critical properties of fluids relevant to the oil & gas industry and other sectors. This task requires the comparison of the experimental thermodynamic properties with the calculations using different mean-field models, thus revealing the shortcomings and advantages of the different implementations. An additional goal is to compare the traditional models with the crossover EoS, i.e. equations that take into account the density fluctuations in the near-critical region, in an attempt to demonstrate the improvements that are obtained when the non-mean-field are used in the representation of the phase behavior of fluids. These comparisons of the phase equilibria and critical properties are done over a wide range of conditions for pure fluids and mixtures containing non-associating and associating, with the aim to obtain a broad knowledge of the developed models.

1.2 Organization of the thesis

Following this general introduction, the next chapter presents an overview of the classical models, which consider an average potential for describing the interaction between the particles in a system. The chapter illustrates the limitations pertaining all traditional EoS; however, it shows some of the approaches to improve the description of complex systems and the usual extension for mixtures.

Chapter 3 is dedicated to show some of the non-mean-field approaches and explain how they take into account the fluctuations of the order parameter, which are related to the singular and asymptotic behavior of systems close to the critical point. In addition, it describes the main features of the critical point both for pure fluids and binary mixtures.

Chapters 4 and 5 contain the results of the phase equilibria and critical point calculations using different thermodynamic models for pure fluids and mixtures, respectively. In the first section of chapter 4, the calculations with the classical EoS are compared with experimental data. The following ones are related to the representation of the phase equilibrium and critical properties using non-mean-field EoS. Chapter 5 begins with a section regarding the results for the VLE region for non-associating and associating species. In the following sections, the performance of the models to represent the LLE region and critical lines are evaluated.

Finally, chapter 6 summarizes the conclusions obtained in this work and outlines the suggestions for future research.

Chapter 2

Mean-field Models

In this chapter, a description of the thermodynamic models widely applied in the oil & gas industry for the representation of the properties of fluids is given. The chapter also explains some of the combining and mixing rules used to extend the Equations of State (EoS) to mixtures. However, before the elucidation of the more useful models, a derivation of the van der Waals model is done, in order to demonstrate certain specific features and limitations pertaining to all classical models.

2.1 The Mean-field Equation of State

From a microscopic viewpoint, the classical theory of the critical point corresponds to a mean-field approximation that neglects the fluctuations of the order parameter, e.g. density. A mean-field model considers that a system composed of a large number of interacting particles can be simplified by approximating the effect of all other particles on a given one by a single averaged effect. In other words, this approach reduces a complex multi-body problem to a one-body problem by the utilization of an average effective field, having an equal effect on each molecule. A typical mean-field model is the van der Waals EoS [63].

In real fluids, all atoms or molecules interact with each other through some potential, $\Phi\left(\{\mathbf{x}_i\}\right)$. The partition function of a system of N classical particles is given by [64]:

$$Z = \frac{1}{N!h^{3N}} \int \int \exp\left\{-\beta \left[\sum_i \frac{p_i^2}{2m} + \Phi\left(\{\mathbf{x}_i\}\right)\right]\right\} d^d\mathbf{p} d^d\mathbf{x} \tag{2.1}$$

where Z is the partition function, N is the number of particles, β is the dimensionless inverse temperature, m is the mass of the particle, p is the momentum, Φ is the potential energy at the position x in space and i labels the molecule in the system. In order to make Z a dimensionless quantity, it is divided by h^{3N}, where h is the Planck constant, and $N!$ is used to not overcount the number of micro-states in the system. The mean-field theory of a non-ideal gas supposes that the action on each particle by the other particles in a system can be represented as an effective single-particle potential $\phi(\mathbf{x})$, in which all the molecules may be assumed to move. The total potential energy then decomposes into a sum of terms, one for each particle:

$$\Phi\left(\{x_i\}\right) \approx \sum_i \phi\left(x_i\right)$$

The integral in Equation (2.1) can be factorized, thus yielding the expression:

$$Z = \frac{1}{N!h^{3N}} \left[\int \int \exp\left\{-\beta \left[\frac{p^2}{2m} + \phi\left(x\right)\right]\right\} d^d\mathbf{p} d^d\mathbf{x}\right]^N \tag{2.2}$$

The momentum and position integrals can be separated, and the first is neglected since it will generate a volume-independent term to the free energy, which is not useful for the calculation of the pressure exerted by the gas [64].

The optimum form of the function $\phi(x)$ will depend on the original potential Φ. Assuming that it has a particularly simple form, i.e. supposing that it excludes each molecule from some volume of space (V_{ex}) by means of an infinite potential barrier, and taking some finite value u elsewhere, which will be negative because of the long-range attractive forces acting between the molecules. Then, the position integration in Equation (2.2), neglecting the volume-independent factor, yields the following expression for the partition function:

$$Z = \left[\left(V - V_{ex}\right) \exp(-\beta u)\right]^N \tag{2.3}$$

where V is the total volume of the system. Furthermore, the equation to calculate the free energy of the system is related to the partition function, Equation

(2.3), through the formula:

$$F = -Nk_BT\left[\ln\left(V - V_{ex}\right) - \beta u\right] \tag{2.4}$$

where k_B is the Boltzmann's constant and T is temperature.

The expression for calculating the pressure of the system (P) is obtained by differentiating Equation (2.4) with respect to volume at constant temperature:

$$P = -\left(\frac{\partial F}{\partial V}\right)_T = \frac{Nk_BT}{V - V_{ex}} - N\left(\frac{\partial u}{\partial V}\right)_T \tag{2.5}$$

The constants of proportionality for each of the right-hand side terms of Equation (2.5) are determined by considering that the excluded volume is proportional to N:

$$V_{ex} = Nb \tag{2.6}$$

where b is a constant of the repulsive term, i.e. the second term on the right-hand side of Equation (2.7), while u is proportional to the density of molecules in the gas ($u \propto \frac{N}{V}$) as given by:

$$u = -a\frac{N}{V} \tag{2.7}$$

where a is a constant of the attractive term, i.e. the first term on the right-hand side of Equation (2.7).

Substituting equations (2.6) and (2.7) into (2.5) one obtains:

$$P = \frac{Nk_BT}{V - nb} - \frac{n^2a}{V^2} \tag{2.8}$$

which is the classical representation of the van der Waals equation of state [65].

Equation (2.8) is not only useful because of its simple form, but also becuase it is able to qualitatively represent the phase transitions in fluids. For example, it can simultaneously estimate the properties of the liquid and vapor phase in equilibrium [66]. Nevertheless, one of the problems of this equation and any other model that uses an effective average potential for representing the interactions between the particles of the system is seen in the calculation of the critical exponents, i.e. values that describe the phase behavior of physical quantities near continues phase transitions or critical points. Table

2.1 shows the critical exponents calculated with a mean-field model like the van der Waals EoS, Equation (2.8). On the other hand, the comparison with the universal values of the critical exponents obtained experimentally, e.g. the value of β is approximately 0.326 [67], indicates that classical EoS are not capable of describing the behavior of fluids close to the critical point. In fact, this discrepancy cannot be eliminated by any traditional improvement of the classical EoS, correcting or adding the mean-field terms, since it is caused by a fundamental deficiency: mean-field models do not incorporate the fluctuations of the order parameter associated with the critical-point phase transition [39], which for the liquid-vapor transitions is the difference between the density of the phases in equilibrium (see chapter 3).

Table 2.1: Classical critical exponents.

α	β	γ	δ	ν	η
0	$\frac{1}{2}$	1	3	$\frac{1}{2}$	0

The approaches for introducing the density fluctuations into classical EoS will be presented in the next chapter. Nevertheless, it is important to note that far from the critical region, where density inhomogeneities are negligible, the mean-field approximation is useful for describing the thermodynamic properties of fluids [47].

Finally, due to the simplified form of potential utilized in the van der Waals EoS, this model can only qualitatively represent the thermodynamic properties of the phases in equilibrium, e.g. vapor-liquid phase transitions [68]. Thus, for quantitative representations of the phase behavior of fluids, it is necessary to modify Equation (2.8) [69], which is discussed in the next section.

2.2 Classical Equations of State

The accuracy of the representation of the thermodynamic properties of fluids is directly related to the EoS applied in the calculations [63]. Equations of State provide a relation between pressure, temperature, volume and composition of a fluid.

Cubic EoS are widely applied in process design [35] and are built on the model proposed by van der Waals [65], which was derived in the previous section and can be written as:

$$P = \frac{RT}{v-b} - \frac{a}{v^2} \tag{2.9}$$

where R is the universal gas constant, or Nk_B, and v is the molar volume, i.e. $\frac{V}{N}$. The constants a and b are usually calculated using the inflection condition of the critical isotherm [66], which is given by the expressions:

$$\begin{aligned} \left(\frac{\partial P}{\partial v}\right)_{T=T_c} &= 0 \\ \left(\frac{\partial^2 P}{\partial v^2}\right)_{T=T_c} &= 0 \end{aligned} \tag{2.10}$$

The values of the constants of the van der Waals EoS are obtained by solving equations (2.9) and (2.10). The solution for a and b is:

$$a = \frac{27R^2T_c^2}{64P_c} \tag{2.11}$$

$$b = \frac{RT_c}{8P_c} \tag{2.12}$$

where T_c and P_c are the critical temperature and pressure, respectively.

As stated before, the model developed by van der Waals is important for historical reasons since it was the first thermodynamic model to qualitatively represent the coexistence of the vapor and liquid phases. Nevertheless, Equation (2.9) is even incapable of correctly describing the saturation pressures and densities of simple molecules. Thus many other authors attempted to improve the representation of the thermodynamic properties of fluids by modifying the van der Waals EoS [69].

One of the first successful alterations were proposed by Redlich and Kwong [70], where the authors changed the attractive term of Equation (2.9) by making it dependent on temperature. This modification allowed good results for the description of non-polar pure gases and its mixtures. The Redlich-Kwong (RK) EoS is given by:

$$P = \frac{RT}{v-b} - \frac{a}{T^{1/2}v(v+b)} \tag{2.13}$$

where the parameters a and b are calculated by:

$$a = 0.4278\frac{R^2T_c^{2.5}}{P_c} \tag{2.14}$$

$$b = 0.0867\frac{RT_c}{P_c} \tag{2.15}$$

Soave [71] improved Redlich-Kwong's model by introducing, into the attractive term, a temperature-dependent function (α) related to the acentric factor (ω). This allowed the precise description of the vapor pressure of hydrocarbons and other fluids from the triple to the critical point. Consequently, the modeling of high-pressure vapor-liquid equilibrium was possible with the Soave-Redlich-Kwong (SRK) EoS, which is given by:

$$P = \frac{RT}{v-b} - \frac{a\alpha\left(T\right)}{v(v+b)} \tag{2.16}$$

where a, b and $\alpha\left(T\right)$ are calculated by the equations:

$$a = 0.42747\frac{R^2T_c^2}{P_c} \tag{2.17}$$

$$b = 0.08664\frac{RT_c}{P_c} \tag{2.18}$$

$$\alpha = \left\{1 + \left(0.480 + 1.57\omega - 0.176\omega^2\right) \times \left[1 - \left(\frac{T}{T_c}\right)^{0.5}\right]\right\}^2 \tag{2.19}$$

With the aim to improve the saturated liquid phase description of the SRK model, Peng and Robinson [72, 73] modified the attractive term of Equation (2.16), obtaining:

$$P = \frac{RT}{v-b} - \frac{a\alpha}{v(v+b)+b(v-b)} \tag{2.20}$$

where a, b and $\alpha\left(T\right)$ are:

$$a = 0.45724\frac{R^2T_c^2}{P_c} \tag{2.21}$$

$$b = 0.07780\frac{RT_c}{P_c} \tag{2.22}$$

$$\alpha = \left\{1 + \left(0.37464 + 1.5422\omega - 0.26922\omega^2\right) \times \left[1 - \left(\frac{T}{T_c}\right)^{0.5}\right]\right\}^2 \tag{2.23}$$

Two-constant thermodynamic models (a and b), like the ones presented previously, give a fixed critical compressibility factor ($Z_c = \frac{P_c v_c}{RT_c}$) independently of the substance. This behavior does not correspond to real fluids since Z_c

varies according to the species, e.g. the range of the critical compressibility factors of hydrocarbons lies between 0.24 and 0.29 [68]. The critical compressibility factors for the SRK and $PR\ EoS$ are component-independent and are equal to 0.301 and 0.333, respectively.

In order to improve this feature, Schmidt and Wenzel [74] developed a model, where the critical compressibility factor is dependent on the substance. The Schmidt-Wenzel (SW) EoS is given by:

$$P = \frac{RT}{v-b} - \frac{a\alpha\left(T\right)}{v^2 + ubv + wb^2} \tag{2.24}$$

where u and w are determined by:

$$u + w = 1 \tag{2.25}$$

$$w = -3\omega \tag{2.26}$$

while a, b and $\alpha\left(T\right)$ are given by:

$$a = \Omega_a \frac{R^2 T_c^2}{P_c} \tag{2.27}$$

$$b = \Omega_b \frac{RT_c}{P_c} \tag{2.28}$$

$$\alpha = \left\{1 + \left[\kappa + \frac{\left(5\frac{T}{T_c} - 3\kappa - 1\right)^2}{70}\right]\left[1 - \left(\frac{T}{T_c}\right)\right]\right\}^2 \tag{2.29}$$

In equations (2.27) to (2.29), the terms κ, Ω_a and Ω_b are described by the expressions:

$$\kappa = 0.465 + 1.347\omega - 0.528\omega^2 \tag{2.30}$$

$$\Omega_b = \beta_c \zeta_c \tag{2.31}$$

$$\Omega_a = \left\{1 - \zeta_c\left(1 - \beta_c\right)\right\}^3 \tag{2.32}$$

where Ω_a is the smallest positive root, and ζ_c and β_c are defined by:

$$\zeta_c = \frac{1}{3\left(1 + \beta_c\omega\right)} \tag{2.33}$$

$$(6\omega + 1)\,\beta_c^3 + 3\beta_c^2 + 3\beta_c - 1 = 0 \tag{2.34}$$

The solution for the term β_c is easily found if a second order method is applied using the following initial estimate:

$$\beta_c = 0.25989 - 0.0217\omega + 0.00375\omega^2 \tag{2.35}$$

Schmidt and Wenzel [74] compared the performance of their model with the SRK and $PR\ EoS$ for describing the vapor pressures of pure fluids, and concluded that the $SW\ EoS$ is not superior to the traditional thermodynamic models. On the other hand, the inclusion of the two constants (u and w) makes the model more flexible, which enhances the predictions of the density of the saturated liquid phase. Additionally, it yields compound-dependent critical compressibility factors.

With the aim to improve the $SW\ EoS$, Patel and Teja [75] developed a thermodynamic model ($PT\ EoS$) containing three constants given by:

$$P = \frac{RT}{v - b} - \frac{a\alpha\,(T)}{v\,(v + b) + c\,(v - b)} \tag{2.36}$$

In the case of non-polar substances, the authors defined a correlation for the critical compressibility factor (ζ_c) according to the expression:

$$\zeta_c = 0.329032 - 0.076799\omega + 0.0211947\omega^2 \tag{2.37}$$

and the constants a and b are given by equations (2.27) and (2.28), respectively, while c is:

$$c = \Omega_c \frac{RT_c}{P_c} \tag{2.38}$$

The terms Ω_a, Ω_b and Ω_c of the $PT\ EoS$ are calculated according to the expressions:

$$\Omega_a = 3\zeta_c^2 + 3\,(1 - 2\zeta_c)\,\Omega_b + \Omega_b^2 + 1 - 3\zeta_c \tag{2.39}$$

$$\Omega_b^3 + (2 - 3\zeta_c)\,\Omega_b^2 + 3\zeta_c^2\Omega_b - 3\zeta_c^3 = 0 \tag{2.40}$$

$$\Omega_c = 1 - 3\zeta_c \tag{2.41}$$

where Ω_b is the smallest positive root of Equation (2.40) and the α-function has the following form:

$$\alpha\left(T\right)=\left\{1+\left(0.452413-1.30982\omega-0.295937\omega^{2}\right)\left[1-\left(\frac{T}{T_{c}}\right)^{0,5}\right]\right\} \quad (2.42)$$

Due to its importance in engineering applications, cubic EoS are still being developed. Cismondi and Mollerup [76] created a 3-parameter cubic model ($RKPR\ EoS$), with the intention to improve the representation of the volumetric properties in comparison to traditional EoS, and changed the attractive term of van der Waals' model, obtaining the pressure explicit expression given by:

$$P=\frac{RT}{v-b}-\frac{a\left(T\right)}{\left(v+\delta_{1}b\right)\left[v+\left(1-\frac{\delta_{1}}{1+\delta_{1}}\right)b\right]} \quad (2.43)$$

where δ_1 is a constant dependent on the critical compressibility factor of a fluid. The authors also changed the temperature-dependent function of the attractive term constant a, because of its imprecision for high temperatures, using the following equation:

$$a\left(T\right)=a\left(\frac{3}{2+{}^{T}/_{T_{c}}}\right)^{k}$$

and k is a parameter regressed for each component. The $RKPR\ EoS$ was compared to traditional and three constant cubic EoS and it was found superior to these models, due to its improved descriptions of the liquid phase densities in sub-critical conditions and the representation of isotherms in supercritical conditions for pure non-associating molecules.

The cubic models with three constants mentioned in this work describe with greater accuracy the phase behavior of non-polar fluids when compared to the traditional cubic EoS, i.e. SRK and PR model, eespecially for the representation of the saturated liquid phase volume. Nevertheless, for highly non-ideal systems, e.g. fluids containing associating species, cubic equations of state are not reliable [74], because they do not take into account effects like the formation of aggregates due to the hydrogen bonding interactions [77, 78].

Thermodynamic models especially developed for describing associating fluids can be classified among chemical, lattice and perturbation theories [43]. The most successful approach for modeling hydrogen bonding fluids relevant to the oil & gas industry comes from perturbation theory and it was elaborated

by Chapman et al. [44]. These authors developed an association equation of state called $SAFT$, in which properties like shape, size and association were included in the calculation of the residual Helmholtz energy using Wertheim's expansion theory [79].

Kontogeorgis et al. [45] developed an equation of state denominated Cubic-Plus-Association (CPA), in which the physical interactions are given by SRK and the association term comes from Wertheim's expansion theory. The CPA equation is given by:

$$P = \frac{RT}{v-b} - \frac{a\left(T\right)}{v\left(v+b\right)} - \frac{1}{2}\frac{RT}{v}\left(1+\rho\frac{\partial \ln g}{\partial \rho}\right)\sum_{i} x_i \sum_{A_i}\left(1-X_{A_i}\right) \tag{2.44}$$

where ρ is the molar density and x_i is the mole fraction of the associating components.

The key element of the associative term is X_{A_i}, which represents the molar fraction of sites A of the molecule i that do not bond to other active sites, i.e. the monomer fraction. The term X_{A_i} is related to the association strength, $\Delta^{A_iB_j}$, between two sites belonging to two different molecules and is calculated by:

$$X_{A_i} = \frac{1}{1+\rho\sum_i x_i \sum_{B_j} X_{B_j}\Delta^{A_iB_j}} \tag{2.45}$$

The association strength is given by:

$$\Delta^{A_iB_j} = g\left(\rho\right)\left[\exp\left(\frac{\varepsilon^{A_iB_j}}{RT}\right)-1\right] b_{ij}\beta^{A_iB_j} \tag{2.46}$$

The simplified radial distribution function, $g\left(\rho\right)$, can be determined by the equation:

$$g\left(\rho\right) = \frac{1}{1-1.9\left(\frac{b}{4v}\right)} \tag{2.47}$$

The constants b_i and b_j of the repulsive term of Soave-Redlich-Kwong equation for components i and j, respectively, and are used in the calculation of b_{ij}:

$$b_{ij} = \frac{b_i + b_j}{2} \tag{2.48}$$

The constant a from the attraction term of SRK equation is dependent on

temperature in the form:

$$a = a_0 \left(1 + c_1 \left(1 - \sqrt{\frac{T}{T_c}}\right)\right)^2 \tag{2.49}$$

From equations (2.44) to (2.49) it is seen that CPA has five parameters for associating components: a_0, b, c_1, $\varepsilon^{A_iB_j}$ and $\beta^{A_iB_j}$. These parameters are usually determined through the fitting of the vapor and liquid phase volume, from reduced temperatures in the range of 0.5 to 0.95, since it overpredicts the critical temperature and pressure of the pure components [38]. For non-associating compounds, the equation reduces to SRK. In addition, the association model is also dependent on the type of association, i.e. the number of hydrogen bonding sites per compound. In this work, n-alkanols were considered to have two association sites, as in the $2B$ scheme, while the scheme for water and hydrogen sulfide were defined as $4C$ and $3B$, following the notation of Huang and Radosz [80].

Many other cubic and non-cubic thermodynamic models, as well as EoS that account for association, are found in the literature. However, for applications in the oil & gas industry, CPA has proven to be a useful and reliable equation [40, 46], capable of representing the properties of complex fluids in different conditions, e.g. modeling the phase behavior of hydrocarbons and hydrate inhibitors like methanol or glycols [81], and simulating processes containing asphaltenes [82, 83]. Therefore, in this work, we use it as the main mean-field approach and compare it to cubic and to crossover EoS, which will be explained in the next chapter. Moreover, the use of the aforementioned models in thermodynamic calculations containing more than one component requires the use of mixing and combining rules, which are described in the next section.

2.3 Mixing Rules

The application of an EoS to represent the phase equilibria and critical properties of multicomponent fluids require the use of a mixing rule to define the constants of the model for the system. The constants of the traditional cubic EoS are related to the attractive and repulsive forces between the molecules of a pure substance. In the case of mixtures, these constants are linked to the attractive and repulsive interactions between the different species

in the system [68].

The van der Waals one-fluid mixing rule is the most widely model applied to extend a thermodynamic model to mixtures [38]. In this case, the constants are calculated using a quadratic composition dependency for both constants, as showed in the expressions:

$$a = \sum_{i=1}^{n}\sum_{j=1}^{n} x_i x_j a_{ij} \tag{2.50}$$

$$b = \sum_{i=1}^{n}\sum_{j=1}^{n} x_i x_j b_{ij} \tag{2.51}$$

where x_i and x_j are the mole fractions of the components i and j. In addition to the mixing rules, there are also combining rules for the a_{ij} and b_{ij} terms. In the case of the cross-energy parameter (a_{ij}), a geometric mean is used, while for the co-volume parameter (b_{ij}), an arithmetic mean is utilized [69]. These expressions are given by:

$$a_{ij} = \sqrt{a_i a_j}\,(1 - k_{ij}) \tag{2.52}$$

$$b_{ij} = \frac{(b_i + b_j)}{2}\,(1 - l_{ij}) \tag{2.53}$$

In the equations (2.52) and (2.53), the constants a_i, a_j, b_i and b_j are the pure a and b constants of components i and j, respectively. The terms k_{ij} and l_{ij} are the binary interaction coefficients, which are estimated by fitting the calculated phase equilibrium properties to experimental data. In fact, only the k_{ij} parameter is normally applied to the improvement of the quantitative description of the thermodynamic model, which is the procedure used in this thesis. Nevertheless, for complex polar systems and special cases, e.g. solid-gas phase equilibria (SGE), the second binary interaction coefficient is also used as an adjustable parameter [38]. If the $l_{ij} = 0$, then the co-volume parameter is simplified to:

$$b = \sum_{i=1}^{n} x_i b_i \tag{2.54}$$

Additionally, for the equations of state with three pure component constants, like the $PT\ EoS$, an additional expression is used for calculating the mixture's c parameter, as given by:

$$c = \sum_{i=1}^{n} x_i c_i \tag{2.55}$$

On the other hand, for the $SW\ EoS$, a mixing rule for the acentric factor is necessary, and it is determined by the expression [74]:

$$\omega = \frac{\sum_{i=1}^{n} x_i \omega_i b_i^{0.7}}{\sum_{i=1}^{n} x_i b_i^{0.7}} \tag{2.56}$$

Quadratic mixing and classical combining rules are frequently used for engineering calculations, especially in the oil industry, because accurate representations of vapor-liquid phase equilibria (VLE) are obtained when they are applied with classical EoS. However, these mixing rules are based on random mixing, i.e. it is assumed that the species are irregularly distributed in the system. Nonetheless, due to intermolecular forces, the mixing of molecules is not completely random, hence mixing rules that yield a non-random distribution of the components in the system can lead to better descriptions of the phase behavior [38]. The introduction of local composition models in a EoS is useful for obtaining a quantitative description of complex phase diagrams, i.e. $VLLE$, LLE and SGE, far away from the critical region, of highly polar and hydrogen bonding mixtures. In this work, the traditional approach used in the oil & gas industry is followed, i.e. classical mixing and combining rules are applied in all calculations. Moreover, the hydrogen bonding term from Wertheim's theory is utilized for fluids with associating components, and in the case of two or more hydrogen bonding species, a combining rule is required for the parameters in the association term.

2.4 Combining Rules for the Association Term

Systems containing more than one substance capable of hydrogen bonding need combining rules for the association parameters, i.e. the association energy ($\varepsilon^{A_i B_j}$) and volume ($\beta^{A_i B_j}$). The same is also valid for mixtures with induced association, or solvation, where there is a cross-association between one non-associating compound and one self-associating molecule.

Although many different combining rules have been suggested in the literature, the most successful and usually applied ones are the $CR1$ and Elliot

(ECR) rules [38]. The expression for the cross-association of the energy parameter of the association term using the $CR1$ rule is given by:

$$\varepsilon^{A_iB_j} = \frac{\varepsilon^{A_iB_i} + \varepsilon^{A_jB_j}}{2} \tag{2.57}$$

where $\varepsilon^{A_iB_i}$ and $\varepsilon^{A_jB_j}$ are the pure component association energy parameter and $\varepsilon^{A_iB_j}$ is the cross-association one. It can be seen that the $CR1$ rule uses an arithmetic mean for the association energy parameter, since it is proportional to the enthalpy of association. However, $\beta^{A_iB_j}$ is related to the cross-entropy of the hydrogen bonding, hence a geometric mean should be used. The expression of the $CR1$ rule for the association volume parameter is:

$$\beta^{A_iB_j} = \sqrt{\beta^{A_iB_i}\beta^{A_jB_j}} \tag{2.58}$$

where $\beta^{A_iB_i}$ and $\beta^{A_iB_i}$ are the association volume parameter of the pure compounds and the cross-association volume is $\beta^{A_iB_j}$.

In the case of the ECR combining rule, the cross-association strength is calculated with the expression:

$$\Delta^{A_iB_j} = \sqrt{\Delta^{A_iB_i}\Delta^{A_jB_j}} \tag{2.59}$$

where the association strength of the pure components are $\Delta^{A_iB_i}$ and $\Delta^{A_jB_j}$. From this expression, it is possible to calculate the combining rules for the association energy and volume, which are expressed by:

$$\varepsilon^{A_iB_j} = \frac{\varepsilon^{A_iB_i} + \varepsilon^{A_jB_j}}{2} \tag{2.60}$$

$$\beta^{A_iB_j} = \sqrt{\beta^{A_iB_i}\beta^{A_jB_j}}\frac{\sqrt{b_ib_j}}{b_{ij}} \tag{2.61}$$

where b_i and b_j are the co-volume parameters of the pure species and b_{ij} is calculated with Equation (2.48) association strength of the pure components are $\Delta^{A_iB_i}$ and $\Delta^{A_jB_j}$.

The comparison of equations (2.57), (2.58), (2.60) and (2.61) shows that the difference between the two approaches is related to the evaluation of the cross-association volume; nevertheless, both are based on plausible assumptions regarding the energy and enthalpy of association, plus they yield similar

results for the phase behavior calculations. In this work, we have chosen the $CR1$ rule for the computation of the thermodynamic properties of cross-associating systems.

Finally, another possibility of cross-association occurs for certain systems, like an aromatic compound and a hydrogen bonding one, due to the induced association between the inert and the associating species. These systems are called solvating mixtures, and a modified $CR1$ can be used to improve the representation of the thermodynamic properties [38].

In the modified $CR1$ rule the cross-association energy parameter is given by Equation (2.57), while the cross-association volume is obtained from fitting experimental data. This rule is useful for systems where one of the components is not self-associating, for example CO_2 and aromatics, while the other forms hydrogen bonds; nevertheless, it fails to describe the solvation in some systems, e.g. chloroform and diethyl ether [38].

Chapter 3

Non-mean-field Models

This chapter is intended to give an overview of different non-mean-field models, i.e. equations that take into account the fluctuations of the order parameter, found in the literature. However, for the sake of clarity, this chapter begins with a detailed explanation of the liquid-vapor critical point of a pure substance, as well as the anomalies that are observed in this region, followed by the different phase behavior types of binary mixtures, using the classification of van Konynenburg and Scott [2]. These descriptions are important for introducing some concepts that are the basis of theoretical formulations and will be later addressed in the chapter containing the results of thesis.

3.1 Critical Region

Under ordinary conditions (1.01325bar and 373.15K) the phase transition of water to steam is characterized by a discontinuity in terms of some variables: molar volume, enthalpy, and entropy. These quantities are first derivatives of the free energy and are often discontinuous at the phase transition of the two phases, hence they are called first-order transitions (if the first derivatives are continuous, but the second are discontinuous, then the phase transition is of second order). The first point ($P1$) in Figure 3.1 represents this type of phase transition, where the system is in equilibrium, thus both phases have the same pressure and temperature (Figure 3.1a); nevertheless, they have distinct molar densities, i.e. the inverse of the molar volume (Figure 3.1b).

Although the liquid/vapor phase changes of H_2O and other fluids are usu-

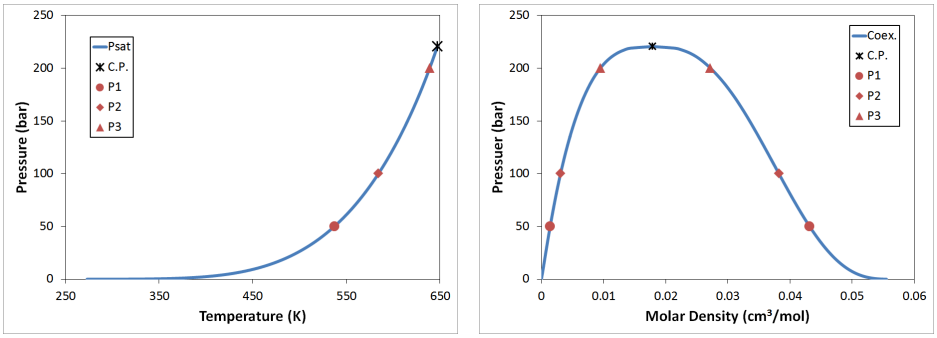

(a) (b)

Figure 3.1: Representation of the liquid-vapor phase transitions of water.

ally classified as first order, there is a condition under which the transition is continuous. This continuous transition can be tracked through a sequence of steadily increasing temperature and pressure steps along the saturated pressure curve (Points $P2$ and $P3$ in Figure 3.1). As the temperature and pressure increase, the differences between the densities of the phases in equilibrium diminish, until they eventually vanish at a point, which is called the critical point. In the case of water, this point is defined by the temperature of 647.10K, the pressure of 220.64bar and the density of 0.0559 $^{mol}/_{cm^3}$ ($C.P.$ in Figure 3.1). At temperatures higher than the critical one, the liquid and vapor phases cease to be distinct entities and the fluid is called supercritical fluids. Phenomena observed near a critical point are referred to as critical phenomena, and are characterized by an order parameter, which represents a measure of the degree of order across the boundaries in a system that undergoes a phase transition. It normally ranges between zero in one phase, normally above the critical point, and nonzero in the other, and in the liquid-vapor transition, this parameter is defined as the difference between the molar density (ρ) of the liquid and vapor phases in equilibrium.

According to Linder [84], the field of thermodynamics appeared logically complete until about 1960, except for the difficulties associated with critical behavior, theoretical models predicted the divergence of the heat capacities, compressibilities, susceptibilities, i.e. a quantification for the change of an extensive property under variation of an intensive property, and other second-order derivatives of the free energy; nonetheless, it failed to correctly describe the non-analytic form of the divergence.

The behavior of some thermodynamic properties in the critical region can be described in terms of scaling laws with critical exponents and scaling functions. In the case of the isochoric heat capacity, the dependence of this property with regard to the temperature is given by the expression:

$$C_v \propto k_\alpha \tau^{-\alpha} \tag{3.1}$$

where $\tau = {}^{T}/_{T_c} - 1$ is the dimensionless reduced temperature, k_α is the critical amplitude and α is the critical exponent related to the isochoric heat capacity close to the critical point. The critical exponents describing the temperature dependence of the coexistence densities (β), isothermal compressibility (γ) and the density dependence of pressure at T_c (δ) are obtained by the equations [63]:

$$\rho_l - \rho_v \propto k_\beta \tau^{\beta} \tag{3.2}$$

$$\kappa_T \propto k_\gamma \tau^{-\gamma} \tag{3.3}$$

$$P - P_c \propto k_\delta \rho^{\delta} \tag{3.4}$$

where k_β, k_γ and k_δ are system dependent coefficients. There are in total 6 of these coefficients, which are called critical amplitudes and, due to the four universal relationship between the critical exponents, only two of the amplitudes are independent. It has been established theoretically and verified experimentally that all the fluids and fluid mixtures belonging to the same universality class have the same critical exponents and amplitude ratio values [39].

In the case of pure fluids, the values of the critical exponents are given in Table 3.1. The analysis of the classical EoS leads to the values of 0 for α, 0.5 for β and 1 and 3 for γ and δ [85], as shown in Table 2.1, while the universal critical values for the exponents are α, β, γ and δ are 0.110, 0.326, 1.237 and 4.879, respectively ([39]). These discrepancies in the critical exponents calculated by the classical models show that they cannot represent the non-analytic behavior of fluids in the vicinity of the critical point.

The reason that classical EoS cannot correctly describe the asymptotic behavior of thermodynamic properties of fluids is related to the presence of fluctuations in the order parameter. To understand the nature of fluctuations

Table 3.1: Universal critical exponents.

α	β	γ	δ	ν	η
0.110	0.326	1.239	4.80	0.630	0.033

in the order parameter one can use the isothermal compressibility (κ_T) as an example. It is seen from Equation (3.3) that just above T_c, κ_T is very large, therefore small changes in the temperature of the system will give rise to large fluctuations in density. The physical origin of these fluctuations is related to the fact that the pressure, which a fluid exerts on any small surface, fluctuates constantly because of the atomic nature of matter. Thus, by dividing the volume of a system into smaller subsets, then each part is subjected to a constantly fluctuating confining pressure from the fluid enveloping it, and, if the compressibility is unusually large, as it is close to the critical point, then the volume of the parcel changes by a correspondingly large amount in response to the fluctuating bounding pressure [64]. In fact, the density fluctuations near the critical point are so large that they are able to interfere with light causing the light scattering phenomena called critical opalescence (Figure 3.2).

The extent of the fluctuations is referred to as correlation length (L), and, due to the special nature of the critical region, this distance becomes much larger than the inter-particle distance. Therefore, the correlation length becomes the scale of theoretical formulations used to define the critical phenomena, especially at the critical point, where L diverges. In this case, the average microscopic interactions, that are usually the basis for the development of classical thermodynamic models, are no longer relevant to represent the critical behavior [86].

In summary, the correct representation of the singular behavior of the critical region requires thermodynamic models to take into account the fluctuations in the order parameter. On the other hand, far from the critical region, theoretical formulations should contemplate the traditional behavior of fluids, where the effects of critical fluctuations become negligibly small [47]. The types of models that are able to change from classical to non-analytical behavior are called crossover EoS and are the main topic of this chapter.

There are two main approaches to build a crossover EoS, one based on the renormalized Landau expansion [47, 48, 56, 87], and the second based on Wilson's phase-space cell approximation [57, 88, 89] developed by White and co-workers [58–61, 90]. With the aim to evaluate the advantages and

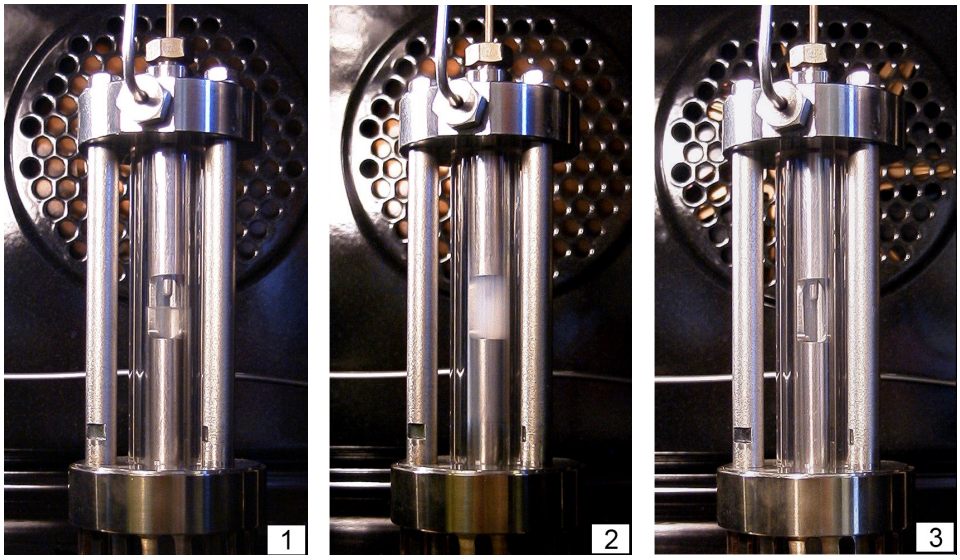

(a) (b) (c)

Figure 3.2: Critical opalescence phenomena in ethane close to the critical point. In Figure (a), the system is in sub-critical conditions, indicated by the phases in equlibrium, while in Figure (b), the system is close to the critical point, indicated by the blurring due to the interaction of the fluctuations with light. The system is in supercritical conditions, indicated by the lack of interface in Figure (c). Figures taken from [1].

disadvantages of each formulation, and to help in the decision of choosing one of the methods for the calculations applied in this work, the last sections of this chapter are devoted to explaining in detail the two approaches. However, before describing the particularities of these models, it is important to explain the different types of critical phase behaviors in mixtures.

The classification of van Konynenburg and Scott [2] is an important tool for defining the different types of critical phase behavior in binary mixtures, as it allows the understanding of the critical phenomena in mixtures. Since most of the applications in industry involve multicomponent mixtures and many of the results obtained in this work are presented in terms of phase diagrams for binary mixtures, these concepts will help in the comparison of the results with experimental data and the correct evaluation of the models in the future chapters.

3.2 Types of Critical Behavior in Binary Systems

The correct representation of the phase behavior of binary mixtures in the critical region is important both due to theoretical and practical reasons, since measurements in this region are difficult and restricted to single concentration points. Besides, there are significant discrepancies between the data reported in the literature for some systems at similar conditions [91], hence the results obtained with an EoS could be used as an indication of the validity of a certain experimental data set, as well as to predict the properties of the system in regions where no data is available.

One of the first classifications of the critical phase behavior of binary fluids was proposed by van Konynenburg and Scott [2]. The authors showed that most of the types of binary fluid-phase equilibria can be qualitatively predicted using the van der Waals EoS and quadratic mixing rules. In fact, they suggested the existence of fluid-phase behavior types, based on the shape of the mixture critical line and on the absence or presence of three-phase lines obtained by their calculations. Nevertheless, due to the limitations of the model, only five of the six types were generated [92]. The schematic representation of the different phase-diagrams is shown in Figure 3.3.

The first type defined by van Konynenburg and Scott is characterized by a continuous gas-liquid curve connecting the pure component critical points. In this type of systems, there is an absence of liquid-liquid miscibility, and the

only phases in equilibrium are a liquid and a gas phase. This behavior is often observed for mixtures where the two components are chemically similar and/or with similar critical points, and some examples are methane/ethane, CO_2/propane or CO_2/n-butane and benzene/toluene.

Type II phase behavior is similar to type I, with the exception there is a three-phase line where the vapor phase is in equilibrium with two liquid phases ($VLLE$), which ends at an upper critical endpoint ($UCEP$), besides the vapor-liquid critical curve connecting both pure component critical points. At the $UCEP$, the gas phase becomes identical with one of the two liquid phases and a critical liquid-liquid line (LLE) goes steeply to high pressures. This behavior is seen in systems like CO_2/n-octane and with hydrocarbons with the correspondent fully or near fully-fluorinated fluorocarbons, e.g. methane/trifluoromethane.

There are two main differences between type II phase behavior and type III. The first one is that at the $UCEP$, the two liquid phases in the three-phase become identical and the vapor-liquid critical line joins the $UCEP$ with the pure component critical point of the lighter species. The second one is that the critical vapor-liquid line starting at the critical point of the less volatile component is not finishing at a critical endpoint, but usually by solidification sometimes at extremely high pressures. If this critical line has a positive slope, then it indicates the existence of gas-gas equilibria, which is when two phases are at equilibrium at a temperature higher than the critical temperature of either pure components. The gas-gas immiscibility is observed for systems like helium/H_2O and helium/xenon, while the other type III diagrams are usually found for mixtures with large immiscibility, such as H_2O/n-alkanes, and CO_2/n-hexadecane.

Type IV phase behavior can be seen as a transition state between types II and III since it has a $VLLE$ line ending in a $UCEP$ and a liquid-liquid critical line that goes steeply to high pressure, as well as a second $UCEP$ that is connected to the critical point of the lightest compound with a vapor-liquid critical line. On the other hand, this type has a third critical line, which is of vapor-liquid nature and starts at the critical point of the heavier component and ends at a Lower Critical End Point ($LCEP$). The $LCEP$ and higher $UCEP$ are linked by a three-phase line. Such phase behavior is shown by ethane/1-propanol, CO_2/n-tridecane and other systems.

In type V systems there are two critical phase lines, and unlike type IV the liquids are completely miscible below $LCEP$, so there are no $VLLE$ lines for

pressures smaller than at this point. The first critical vapor-liquid line begins in the heavier compound and ends at the $LCEP$, while the second one runs from the $UCEP$ to the lighter pure compound. In between the two critical endpoints, there is a three-phase line that connects them. This behavior is observed for systems which contain two asymmetric compounds of the same family, e.g. methane/n-hexane and ethane/n-octadecane.

The last phase behavior type is characterized by a continuous vapor-liquid critical curve linking the pure components' critical points, and a second one that connects the $UCEP$ with the $LCEP$. Examples of this behavior are found for mixtures with strong intermolecular bonding, like water/2-butanol and water/butoxyethanol.

Although most of the phase behavior types can be qualitatively represented even by an oversimplified model, like the van der Waals EoS, in practice the accurate description of experimental measurements is complex, since many mixtures exhibit a transitional behavior between the aforementioned six types, which is usually difficult to accurately model with classical models and traditional mixing and combining rules. For example, systems containing methane with n-alkanes or CO_2 with n-alkanes begin with a type I behavior and end in type III; however, during this transition type II, IV and V behaviors are also observed [91, 93, 94].

The continuous change found for some families and systems, as well as the correct description of complex critical phase behavior, are important tests for evaluating the ability of thermodynamic models to precisely describe the properties of fluids in different conditions. Therefore, a great part of this work is devoted to the calculation of the vapor-liquid critical lines of binary mixtures and the comparison with the experimental data; nonetheless, prior to this comparison, a discussion of the models that take into account the fluctuations of the order parameter is given in the next section.

3.3 Global Equations of State

The previous sections have shown the particularities of the critical region for real fluids and fluid mixtures. In the case of pure components, the physical behavior of these systems in the critical region is defined by the fluctuations in the order parameter. In the case of binary and multicomponent mixtures, it was seen that simple EoS are capable of describing most of the different phase

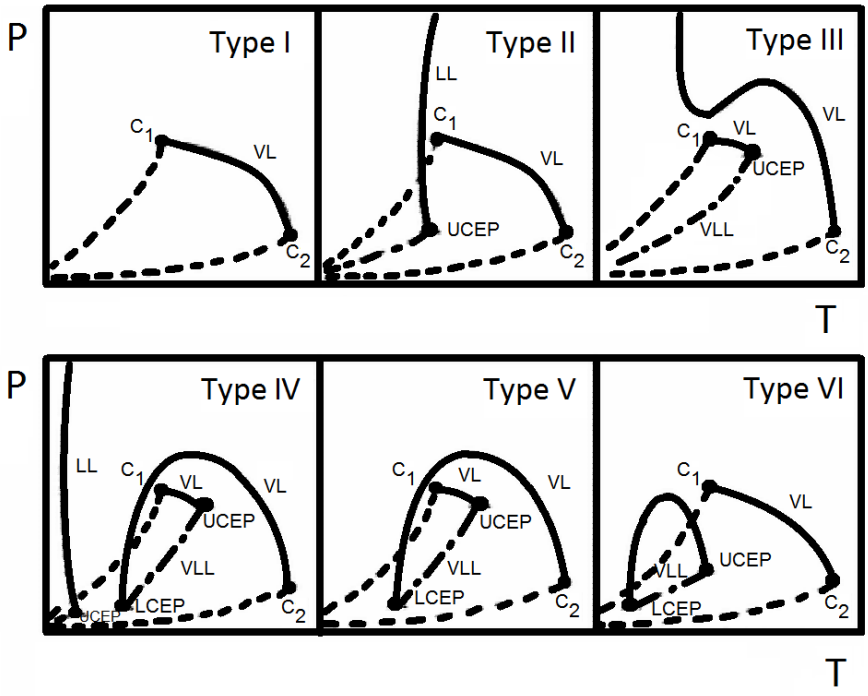

Figure 3.3: Schematic representation of the phase behavior types according to the classification of van Konynenburg and Scott [2].

behavior types; nevertheless, accurate representation of the critical lines in a wide range of conditions requires the precise description of the critical point of the pure components, as it will be shown in future chapters. In both of the cases, the correct modeling of thermodynamic properties is only obtained with a model that incorporate the fluctuations of the order parameter, which becomes especially significant as the critical point is approached [95]. On the other hand, in conditions far away from critical, where the fluctuations are negligible, fluids possess a classical behavior, which is precisely modeled by classical EoS [47].

Models capable of describing both classical and asymptotic behavior of fluids are defined as crossover or global EoS. The procedure to develop these equations consists of combining an approach that incorporates the fluctuation-induced thermodynamic behavior of fluids asymptotically close to the critical point, with a mean-field model that accounts for the classical behavior of thermodynamic properties in conditions far away from the critical point.

Several efforts for the development of global EoS have been attempted in the last decades and the two main approaches found in the literature are the renormalized Landau expansion [47, 48, 87, 96] and the numerical procedure base on Wilson's phase-space cell approximation [55, 59, 97, 98]. The main features of the first procedure will be addressed in the following subsection, using the approach developed by Kiselev and coworkers as an example. Then, we will describe the numerical method created by White and coworkers and the different versions that were developed by other researchers.

3.3.1 Renormalized expansion of the free energy density

The modern representation of the critical phenomena is based on renormalization group (RG) techniques [99]. In this theory, the critical point is viewed as a fixed point of the RG transformations, thus the linearization of the RG equations around the fixed points yields asymptotic scaling laws with universal critical exponents and amplitudes for a universality class, i.e. systems in which the interactions depend on a dimensionality of space and of the order parameter. Fluids are classified as three-dimensional Ising systems, since the Hamiltonian is described by 3 dimensions in space and a scalar order parameter, namely the molar density. Nevertheless, the asymptotic behavior of fluids is valid only for regions close to the critical point, thus an appropriate model should incorporate the fluctuation-induced scaled thermodynamic be-

havior near the critical point and behave classically sufficiently far away from it.

Chen and coworkers [87, 100] were one of the first to provide a solution for this problem. They developed a procedure for modifying a series expansion of the classical Helmholtz energy into an equation that incorporates the non-analytical behavior of fluids near the critical point, and reduces to the classical expansion far from the critical point. This approach can be described by the following equation:

$$A = A_c + A_{bg} \tag{3.5}$$

where A_c represents the critical part of the free energy and takes into account the non-classical behavior of fluids in the critical region, and A_{bg} represents the regular behavior of fluids outside the critical region.

The Landau theory of critical phenomena is built upon the introduction of an order parameter $\Delta\eta$ which is zero in the more symmetric (disordered) phase and nonzero in the asymmetric (ordered) phase. Besides, the model's main assumption is that critical part of the Helmholtz energy (ΔA) can be expressed by a Taylor expansion in powers of the order parameter, as shown in the following equation:

$$\Delta\bar{A}\left(\tau, \Delta\eta\right) = \sum\sum a_{ij}\tau^i\Delta\eta^j \tag{3.6}$$

where $\Delta\eta = \frac{V}{V_c} - 1$, $\tau = \frac{T}{T_c} - 1$ and a_{ij} are system dependent constants. In the critical region, Equation (3.6) becomes:

$$\Delta\bar{A}\left(\tau, \Delta\eta\right) = a_{12}\tau\Delta\eta^2 + a_{04}\Delta\eta^4 \tag{3.7}$$

Equation (3.7) corresponds to the Landau theory of the critical phenomena. However, the Landau theory is valid only in the temperature region where the long-range fluctuations in the order parameter are negligible, which is given by the expression:

$$Gi \leq \tau \leq 1 \tag{3.8}$$

where the term Gi is the Ginzburg number, which is proportional to the average distance between the particles and inversely proportional to the effective average radius of the interaction between the molecules. Consequently, at temperatures less or equal to Gi, the intensity of the fluctuations diverges and the singular part of thermodynamic potential of a system becomes a non-

analytical scaling function of the temperature τ ($\tau = \frac{T}{T_c} - 1$) and the order parameter $\Delta\eta$ ($\Delta\eta = \frac{V}{V_c} - 1$).

The theoretical approach used by Chen et al. [87, 100], for constructing a crossover expression for thermodynamic potential of a system in the critical region, is based on the renormalization group theory. According to this procedure, the critical fluctuations close to the critical point renormalize Equation (3.7) into:

$$\Delta\bar{A}\left(\tau, \Delta\eta\right) = a_{12}\tau Y^{\left(-\alpha/2\Delta_1\right)}\Delta\eta^2 Y^{\left(\gamma-2\beta/2\Delta_1\right)} + a_{04}\Delta\eta^4 Y^{\left(\gamma-2\beta/\Delta_1\right)} - K\left(\tau\right) \quad (3.9)$$

where α, β, γ are universal critical exponents shown in Table 3.1 and Δ_1 is equal to 0.51, and is the product of ω, a correction-to-scaling exponent, with the exponent ν. The kernel term, K, is a function that provides the correct scaling behavior of the isochoric specific heat asymptotically close to the critical point, which has the form:

$$K\left(\tau^2\right) = {}^1\!/_2 a_{20}\tau^2\left[Y^{\left(-\alpha/\Delta_1\right)} - 1\right] \quad (3.10)$$

where Y is a crossover function. The crossover function modifies each term in Equation (3.9), then for dimensionless temperatures inferior to Gi the expression becomes non-analytic. while in the temperature region given by Equation (3.8), the expression for the free energy behaves classically.

The complete classical expression for the critical part of the free energy, $\Delta\bar{A}$, can be rewritten in terms of the renormalized terms $\bar{\tau} = \tau Y^{\left(-\alpha/2\Delta_1\right)}$ and $\Delta\bar{\eta} = \Delta\eta Y^{\left(\gamma-2\beta/4\Delta_1\right)}$ as the function:

$$\Delta\bar{A}\left(\tau, \Delta\eta\right) = \Delta\bar{A}\left(\bar{\tau}, \Delta\bar{\eta}\right) = \Delta\bar{A}\left(\tau Y^{\left(-\alpha/2\Delta_1\right)}, \Delta\eta Y^{\left(\gamma-2\beta/4\Delta_1\right)}\right) - K\left(\tau^2\right) \quad (3.11)$$

3.3.2 Kiselev's crossover approach

The difference between Kiselev's approach and the aforementioned crossover models based on the renormalized Landau expansions is that the critical part is also given by a mean-field model, instead of the Taylor expansion of the Hamiltonian close to the critical point. Additionally, the model reduces to ideal gas law in the limit of zero density and it was applied to different cubic EoS [48, 56] and non-cubic EoS [96, 101].

To apply Kiselev's method to an EoS, one must first rewrite the classical expression for the Helmholtz free energy in the dimensionless form:

$$\bar{A}\left(T,V\right)=\frac{A\left(T,V\right)}{RT}=\Delta\bar{A}\left(\tau,\Delta\eta\right)-\frac{V}{V_{0c}}\bar{P}_{0}\left(T\right)+\bar{\mu}_{0}\left(T\right) \tag{3.12}$$

where A is the Helmholtz energy, $\bar{P}_0$ is the dimensionless pressure at the critical isochore and μ_0 is analytic function of temperature. These functions are obtained from the classical EoS. The terms T_c, T_{0c}, V_c and V_{0c} are the experimental and classical critical temperature and volume.

The second step is to renormalize the temperature and volume in the critical part of $\Delta\bar{A}$, with the introduction of the terms $\bar{\tau}$ and $\Delta\bar{\eta}$. Since both terms are related to the real critical properties of a system and the classical EoS cannot correctly reproduce the surface of a fluid in the critical region, V_{0c} does not correspond to real critical volume of a fluid, so the author introduced additional terms to the renormalized parameters to take into account the differences between the classical and real critical parameters (T_{0c} and T_c, V_{0c} and V_c), using the expressions:

$$\bar{\tau}=\tau Y^{\left(-\alpha/2\Delta_1\right)}+\left(1+\tau\right)\tau_c Y^{\left(2(2-\alpha)/3\Delta_1\right)} \tag{3.13}$$

$$\Delta\bar{\eta}=\Delta\eta Y^{\left(\gamma-2\beta/4\Delta_1\right)}+\left(1+\Delta\eta\right)\Delta\eta_c Y^{\left(2-\alpha/2\Delta_1\right)} \tag{3.14}$$

where $\Delta\eta_c=\frac{V_{0c}-V_c}{V_c}$ and $\tau_c=\frac{T_{0c}-T_c}{T_c}$ are the dimensioless shifts of the critical temperature and volume.

One of the forms to describe the crossover function is to write it as a function of q, a parametric variable that corresponds to a renormalized measure of the distance from the critical point. One of the expressions for calculating Y is given by:

$$Y\left(q\right)=\left[q^2/R(q)\right]^{\Delta_1} \tag{3.15}$$

where $R\left(q\right)$ is given by:

$$R\left(q\right)=\left(1+\frac{q^2}{1+q}\right)^2 \tag{3.16}$$

and q is:

$$q = \frac{\tau}{Gi} + b_{LM}^2 \left(\frac{\Delta\eta + d_1\tau + d_2\tau^2}{Gi^\beta} \right)^2 Y^{\left(\frac{1-2\beta}{\Delta_1}\right)}(q) \tag{3.17}$$

where b_{LM}^2 is the universal linear-model parameter and it is equal to 1.359. The parameters d_1 and d_2 are the projection of the rectilinear diameter of the coexistence curve. Furthermore, there are several expressions for determining the value of the crossover function, Y [102].

The correction of the classical Helmholtz energy into the crossover form is completed by replacing the classical dimensionless temperature and volume with the renormalized values, and by adding the kernel term, yielding the expression:

$$\bar{A}(T,V) = \frac{A(T,V)}{RT} = \Delta\bar{A}(\bar{\tau}, \Delta\bar{\eta}) - \frac{V}{V_{0c}}\bar{P}_0(T) + \bar{\mu}_0(T) \tag{3.18}$$

The crossover EoS is attained from Equation (3.18) by differentiation with respect to volume:

$$P(T,V) = -\left(\frac{\partial A}{\partial V}\right)_T = \frac{RT}{V_{0c}}\left[-\frac{V_{0c}}{V_c}\left(\frac{\partial \Delta\bar{A}}{\partial \Delta\eta}\right) + \bar{P}_0(T) + \frac{V_{0c}}{V_c}\left(\frac{\partial K}{\partial \Delta\eta}\right)\right] \tag{3.19}$$

The approach developed by Kiselev and coworkers yields excellent representations of the non-analytical phase behavior of the critical region, besides different mean-field models can be applied in Equation (3.19). In the first papers, Kiselev [48] and Kiselev and Friend [56] applied the $PT\ EoS$ as the classical model for representing pure fluids and binary systems. Later, a simplified $SAFT$ [101] and $SAFT-VR$ [96, 103] models were used. More recently, crossover version using Kiselev's procedure were developed for traditional cubic EoS, like SRK [102].

It is important to note that a fixed expression is obtained with Kiselev's method, hence it does not increase much the computational time of the equilibrium and critical calculations. On the other hand, the crossover EoS has four additional parameters Gi, d_1, d_2 and $\Delta\eta_c$, which are strongly correlated and require a thorough evaluation for the determination of the optimum values of the parameters [102].

3.3.3 Recursive procedure for correcting the free energy density

A different method to take into account the fluctuations that arise close to the critical point was created by Wilson [57, 89]. In this method the fluctuations are incorporated using the phase-space cell approximation, which is schematically represented in Figure 3.4.

The procedure starts with the partition of the system's volume into several small subsets containing a few molecules. The total volume of a cell is defined as the sum over all density distributions in each cell; besides, due to the small size of the initial cell, it can be considered that the potential on a molecule is approximated by an average one given by a mean-field theory, since the extent of the fluctuations is constrained by the cell volume. In fact, as the mean-field model is used to calculate the free energy of the system, the second step only includes the lowest order of the wavelength fluctuations. Next, the size of the subsystem is increased, taking into account the neighboring cells; besides, the cell in the previous step is considered a "whole molecule". The calculation of the free energy is again done using the mean-field model, but now it accounts for longer wavelength fluctuations, as the system is composed of interacting cells with larger volumes. The procedure is repeated until the whole space, i.e. the total volume of the system, is covered. With this method the long wavelength contributions are incorporated in the calculation of the potential on all size scales, thus accounting for the long-range fluctuations that are crucial for the correct representation of the critical phenomena.

Although the theory developed by Wilson was able to correct the mean-field model close to the critical point, it couldn't be extended to the entire phase space. Therefore, White and co-workers created a set of recursive equations based on the phase-space cell approximation, including a renormalization of the variables that yield the non-analytical feature in the critical region, but reduces to the ideal gas law at low density [59]. This procedure enabled the expansion of the applicability of the method, and later the mean-field equation was changed so that the model would be reduced to different formulations.

In fact, the recursive term effectively corrects the representation of the critical region given by a mean-field model, but it does not greatly improve the performance of the underlying original equation far from this region, which is the reason that different crossover equations have been developed. Salvino and White [58] used the Percus-Yevick [104] equation, which describes the

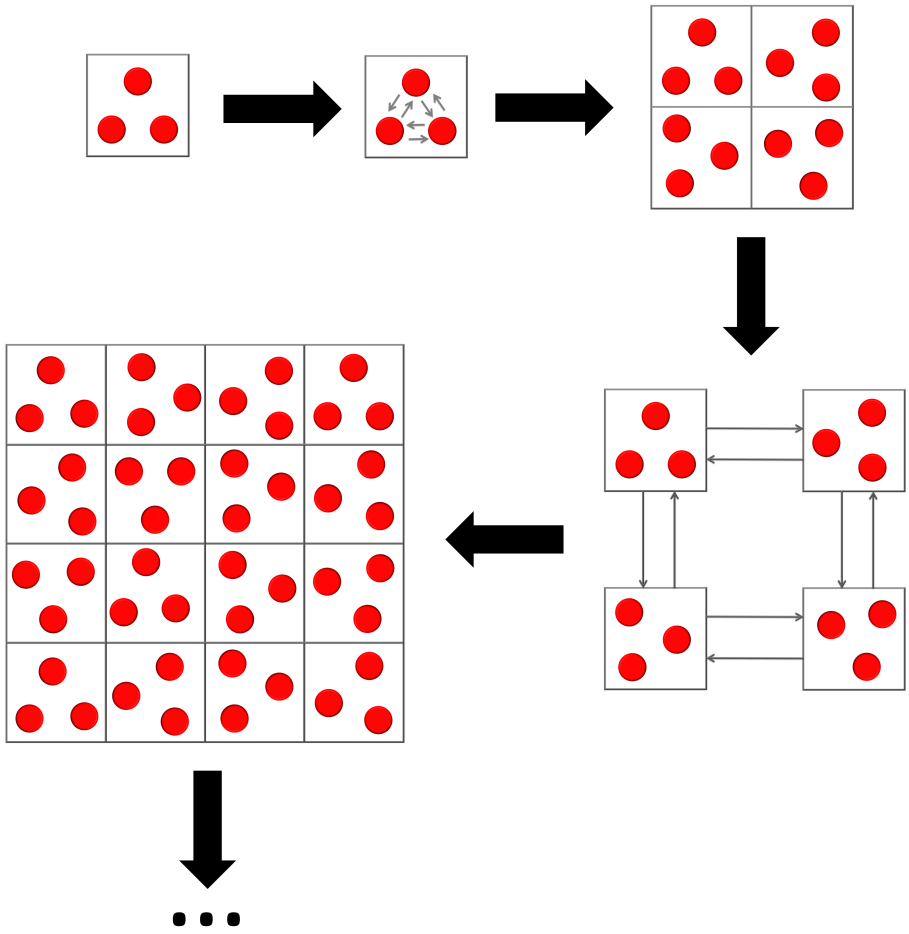

Figure 3.4: Schematic representation of the phase-space cell approximation. In the first step a small subset of the system is chosen and its behavior is described by a mean-field model. Then the interactions of the sub-system are calculated using a mean-field model. In the third step the size of the system is increased, following with the calculation of the properties of the new sub-system, where the interactions of each cell are given by the mean-field model. Finally, the size is again increased and the procedure repeated until the total size of the system is achieved.

repulsive interactions between the particles, as the basis for the iterative procedure. Lue and Prausnitz [97] replaced the hard-sphere model by the mean-spherical approximation, and Jiang and Prausnitz extended this work using an equation of state for chain fluids [105]. Several $SAFT\ EoS$ were applied as the mean-field model, e.g. $Soft-SAFT$ [54, 55, 106], $SAFT-VR$ [107, 108] and $PC-SAFT$ [109–111] EoS. Finally, implementations with the $SRK\ EoS$ [112, 113] and the $CPA\ EoS$ [98, 114] are also found in the literature. In the next subsection, the recursive procedure developed by White and co-workers is described, using the work of White and Salvino as a basis [58].

3.3.4 White's recursive procedure

The application of White's method is done by rewriting the mean-field equation of state for the Helmholtz free energy density as the sum of the free energy density for repulsive interactions and an additional term which takes into account all the attractive contributions, as shown by:

$$f_0\left(T,\rho\right) = f_{rep}\left(T, b\rho\right) - \alpha\left(T,\rho\right)\rho^2 \tag{3.20}$$

where the first term was originally represented by the hard sphere EoS [58], and depends on the density ρ and the hard sphere parameter b. The second term contains the information that is not present in the first term and may be approximated by analytic function far from the critical point.

Although an analytic representation of α may be correct far from the critical region, such equations are not useful in predicting the properties of a fluid in the asymptotic critical region. Near the critical point, the long wavelength density fluctuations must be taken into account in order to precisely predict the singular behavior of the systems.

To introduce the density fluctuation contributions into a classical EoS, the authors proposed a recursive procedure that produces the nth order approximation to the free energy density by means of mathematical operations on the preceding order approximation of the free energy density. This procedure is represented by the equations:

$$f_n = f_{n-1} + \delta f_n \tag{3.21}$$

$$\delta f_n = -K_n \ln\left(\Omega_{n,s}/\Omega_{n,l}\right) \tag{3.22}$$

where f_n is the nth order of the Helmholtz energy density, which is calculated from the precedent order (f_{n-1}) and the contribution of the actual order δf_n. The term δf_n is dependent on the ratio of the density fluctuations for the short-range attractive potential, $\Omega_{n,s}$, to the long-range attractive potential, $\Omega_{n,l}$.

The term K_n is evaluated by the equation:

$$K_n = {}^{k_B T}/_{2^{nd} L^d} \tag{3.23}$$

where k_B is the Boltzmann constant, d is the dimensionality, which is 3, and L is a system dependent parameter, that is related to an effective volume of cohesion surrounding the repulsive hard cores.

The contributions of the density fluctuations are calculated by the integral:

$$\Omega^{\lambda}_{n,i} = \int_0^{\min(\rho, \rho_{max}-\rho)} \exp\left({}^{-G^{\lambda}_{n,i}}/_{K_n}\right) dx \tag{3.24}$$

where λ indicates the type of interaction, i.e. short-ranged (s) or long-ranged (l), and the function G is calculated by the expression:

$$G_{n,i} = \frac{\bar{f}_{n,i}(\rho + x) + \bar{f}_{n,i}(\rho - x) - 2\bar{f}_{n,i}(\rho)}{2} \tag{3.25}$$

and the index i is related to the short and long wavelength contributions.

It should be noted that $\bar{f}_{n,i}$ functions are not the physical free energy density functions, but the free energy density with the attractive term corrected as described by the expressions:

$$\bar{f}_{n,l} = f_{n-1} + \alpha\rho^2 \tag{3.26}$$

$$\bar{f}_{n,s} = f_{n-1} + \frac{\alpha\rho^2\phi}{2^{2n}} \tag{3.27}$$

where ϕ is a parameter that corresponds to some multiple of the inverse square of the initial shortest wavelength of the density fluctuations.

One can see from the crossover EoS that $\Omega_{n,l}$ is initially calculated from the free energy without any contribution from the non-mean field term. From Equation (3.27) one observes that, at each iteration, smaller contributions of the attractive potential are added to the term $\Omega_{n,s}$, as the wavelength becomes increasingly longer than the range of the attractive potential. Thus, the term ${}^{\Omega_{n,l}}/_{\Omega_{n,s}}$, in the logarithm of Equation (3.22), is considered as the ratio of non-mean-field to mean field contributions at successive orders of the fluctuation

contributions (n).

In other words δf_n describes the effect of increasingly longer wavelength density fluctuations as the order is increased. The full free energy density is obtained in the infinite order limit. In this limit, the sum of all the fluctuation corrections incorporates density fluctuations on all wavelength scales and results in the full description of f at the critical point, as expressed by the following equation:

$$f = f_0 + \sum_{n=1}^{\infty} \delta f_n \tag{3.28}$$

In summary, the model proposed by White can be described by mathematical operations on a mean-field EoS. The mathematical operations map the initial mean field EoS into a non-mean-field equation by adding an infinite number of terms of density fluctuation contributions. Consequently, this EoS provides the correct description in the crossover region from the singular behavior close to the critical point to the analytic behavior far away from the critical region. The expression for calculating some thermodynamic properties using the renormalization group treatment proposed by White to correct a mean-field EoS is given in Appendix A.

As mentioned before the model has two additional parameters L and ϕ, besides the parameter from the classical EoS. These parameters permit a good fit to the critical compressibility factor, differently from the assumed initial mean-field equation which does not have the additional freedom to reproduce the experimental critical data. It is important to note that the improvement of the prediction of the critical compressibility is not only a result of the extra parameters, but a success of the renormalization group method, since the recursive procedure alters the mean field model into a non-analytical equation that can correctly describe the shape of the critical region. Moreover, the critical exponents calculated by the crossover EoS are much closer to the experimental universal values, in comparison to the ones calculated by a classical thermodynamic model.

A crossover EoS derived from White's procedure is computationally demanding because it requires the integration of Equation (3.24), which is done by discretizing the density range in equally distributed points, following by a trapezoid rule [60] or Simpson's rule [58] for the numerical integration. Additionally, the number of the recursive operations that take into account the density fluctuation contributions are approximated to a maximum of 5 or 7

[58]. Finally, the discretized Helmholtz energy density is interpolated with cubic splines. The details of the numerical implementations for the crossover EoS developed in this work are discussed in the next chapter. On the other hand, it is important to note that such model has a fewer number of parameters than the one obtained with Kiselev's approach and due to this feature, many authors have applied the procedure in cubic and non-cubic models, as mentioned previously.

3.3.5 Isomorphism assumption

The isomorphism assumption can be used in order to apply the crossover EoS to mixtures [62]. This corresponds to assuming that thermodynamic potential of a multicomponent system near its critical point has the same universal form of the pure fluid, which is valid if the chemical potentials are taken as independent variables [115]. This requirement increases the complexity of the calculations and poses an inconvenience, since most of the mean-field models use mole fractions as independent variables. Kiselev and Friend [56] modified the isomorphism assumption and utilized the mole fractions as independent variables obtaining a good approximation in the description of the properties of mixtures. Furthermore, several authors have adopted this method and applied it to different crossover EoS [56, 112, 116].

In the case of the crossover EoS using White's recursive procedure, the mixture's two additional parameters of the non-mean-field part are determined by:

$$L^3 = \sum_{i=1}^{n} x_i L_i^3 \tag{3.29}$$

$$\phi = \sum_{i=1}^{n} x_i \phi_i \tag{3.30}$$

Since the parameter L_i is the length of the three-dimensional space in which the mean-field model is assumed to correctly capture the density fluctuations of component i, then L^3, Equation (3.29), is just the volume characterizing the density fluctuations for the mixture weighted by the molar fraction of the species in the system. Moreover, the expression for determining ϕ, Equation (3.30), involves the mole fraction x_i and the initial shortest wavelength of the density fluctuations for each substance (ϕ_i).

In summary, the crossover EoS can be easily applied to mixtures by using

equation (3.29) and (3.30) for the recursive procedure parameters and the mixing and combining rules presented in the last chapter for the mean-field parameters.

Chapter 4

Results: Pure Fluids

In this chapter, the results for pure fluids obtained with different thermodynamic models are presented. First, the classical EoS were used to represent the phase equilibria and critical properties of pure compounds and the calculated properties were compared with experimental data. The motivation for this investigation was to compare the different mean-field models, both cubic (SRK, PR, SW and PT) and non-cubic (CPA), but especially to evaluate the advantages and shortcomings of rescaling the pure component parameters of CPA to improve the description of the critical pressures and temperatures. The following sections deal with the representation of the phase equilibrium and critical properties using non-mean-field EoS (Crossover SRK and CPA) and the comparison with experimental data and the classical models, in order to asses the improvements attained with the introduction of the fluctuations in the mean-field EoS.

4.1 Application of Classical EoS to Describe the Phase Behavior of Pure Fluids

Classical thermodynamic models, both cubic and non-cubic EoS, have been, for the last decades, extensively applied in the description of phase equilibria and critical properties of real fluids. There are also in the literature several comparisons of the CPA EoS with cubic and other non-cubic models in the representation of different systems [40, 46, 117–119]. Nevertheless, there are not many studies discussing in detail the critical pressure and tem-

perature over-estimation with this association thermodynamic model, and the comparison with other classical approaches, thus it is reasonable to perform an assessment of the capability of this model to predict the thermodynamic properties of pure fluids far away and close to the critical point, before pursuing more complex formulations.

4.1.1 Evaluation of pure component properties with classical EoS

Since the main focus of this study is related to substances important to the oil & gas industry, we have calculated the phase equilibrium and critical properties for n-alkanes (from methane to n-decane), alcohols (from methanol to n-octanol) and some other components (water, hydrogen sulfide, carbon dioxide and nitrogen). The list of the compounds is presented in Table 4.1, as well as the critical properties of the species and the literature values for the pure components properties of CPA, which were taken from [34]. Furthermore, these parameters were used in the calculations of the phase equilibria and critical properties and the results were compared to experimental data.

Table 4.2 exhibits the absolute average relative deviations (AAD) of the vapor pressure (ΔP_{sat}) and the volume of the saturated liquid and vapor phases (Δv_{liq} and Δv_{vap}, respectively) and the critical point temperatures, pressures and volumes (ΔT_c, ΔP_c and Δv_c, respectively). The AAD are calculated by the expression:

$$AAD = \frac{100}{N} \sum_{i=1}^{N} \left| \frac{X_i^{exp} - X^{calc}}{X_i^{exp}} \right| \tag{4.1}$$

where X is the property being evaluated, the superscripts exp and $calc$ represents the experimental and calculated values, while N is the number of points used in the calculation of the deviation.

The reduced temperature ($T_r = {}^{T}/_{T_c}$) range used in the determination of the AAD of the saturated properties was from a T_r of 0.5 to 1 for all components. This range was extended in relation to the typical one ($T_r = 0.5$ to $T_r = 0.9$ or 0.95) [38], in order to include the effects of the critical region in the overall deviations. From Table 4.2, it is possible to conclude that the two cubic models are similar in the representation of the vapor pressures and vapor phase volumes, but due to the additional constant, the $PT\ EoS$ has a superior description of the saturated liquid phase volumes as mentioned by the authors in the original paper [75]. The comparison of the cubic models with

Table 4.1: Experimental critical parameters of the pure species studied in this work, as well as the pure compound parameters for the $CPA\ EoS$. Experimental pure component properties were taken from the $DIPPR$ database, while CPA parameters were taken from [34].

$Comp.$	T_c (K)	P_c (bar)	v_c $\left(\frac{cm^3}{mol}\right)$	ω $(-)$	$10^{-5} \cdot a_0$ $\left(\frac{bar.mol^2}{cm^6}\right)$	b $\left(\frac{cm^3}{mol}\right)$	c_1 $(-)$	ε/R (K)	$10^3 \cdot \beta$ $(-)$
C_1	190.6	45.99	98.60	0.0116	23.2038	29.10	0.4472	-	-
C_2	305.3	48.72	145.5	0.0995	55.0926	42.90	0.5846	-	-
C_3	369.8	42.48	200.0	0.1523	91.1926	57.83	0.6307	-	-
C_4	425.1	37.96	255.0	0.2002	131.435	72.08	0.7077	-	-
C_5	469.7	33.70	313.0	0.2515	181.990	91.01	0.7986	-	-
C_6	507.6	30.25	371.0	0.3013	236.823	107.9	0.8313	-	-
C_7	540.2	27.40	428.0	0.3495	291.796	125.3	0.9137	-	-
C_8	568.7	24.90	486.0	0.3996	348.769	142.4	0.9942	-	-
C_9	594.6	22.90	551.0	0.4435	412.529	160.3	1.0463	-	-
C_{10}	617.7	21.10	617.0	0.4923	473.916	178.6	1.1324	-	-
C_1OH	512.5	80.84	117.0	0.5658	40.5332	30.98	0.4310	2958	16.1
C_2OH	514.0	61.37	168.0	0.6436	86.7208	49.11	0.7369	2590	8.00
C_3OH	536.8	51.69	219.0	0.6209	119.109	64.11	0.9171	2526	8.10
C_4OH	563.1	44.14	273.0	0.5883	156.958	79.70	0.9784	2526	8.20
C_5OH	588.1	38.97	326.0	0.5748	227.589	97.46	0.9358	2526	3.60
C_6OH	611.3	34.46	382.0	0.5586	271.785	110.8	0.9805	2526	3.30
C_7OH	632.3	30.85	444.0	0.5621	357.406	131.3	1.0110	3160	0.30
C_8OH	652.3	27.83	509.0	0.5697	415.845	148.5	1.1486	3219	0.14
H_2O	647.3	220.6	55.95	0.3449	12.2777	14.52	0.6736	2003	69.2
H_2S	373.5	89.63	98.50	0.0942	38.6049	29.20	0.5022	654.3	58.3
CO_2	304.2	73.83	94.00	0.2236	35.0814	27.20	0.7602	-	-
N_2	126.2	34.00	89.20	0.0377	13.7334	26.05	0.4986	-	-

CPA for the modeling of the saturated properties indicates that the non-cubic model is better than the other two and it is capable of precisely correlating the properties of fluids in sub-critical conditions. Nevertheless, in order to do so, it overestimates the critical point causing an incorrect prediction of the critical temperatures and pressures, although this has a stronger effect in the representations of the critical pressures. On the other hand, the errors in the critical volume predicted by CPA are smaller than the ones predicted by the other two models, yet a precise description of this property is not obtained, as the overall deviation is high (approximately 10%).

With the aim to evaluate the importance of the association term in the prediction of the saturated and critical properties of pure hydrogen bonding species, the deviations obtained for the alcohols and hydrocarbons were grouped in tables 4.3 and 4.4. As previously mentioned, CPA reduces to SRK for non-associating species, and the differences in the predictions of the thermodynamic properties are only due to the modification of the pure component parameters. The non-cubic model is superior to the cubic ones for the representation of the vapor pressures and saturated liquid volumes, especially for alcohols due to the extra term that takes into account the hydrogen bonding effect, on the other hand it deteriorates the representation of the critical temperatures and pressures. For hydrocarbons, the cubic EoS are superior with respect to with respect to the representation of the saturated vapor phase volume, particularly close to the critical point.

Figure 4.1 shows the experimental points and the calculated vapor pressure curves (Figure 4.1a and 4.1b), as well as the coexistence diagrams (Figure 4.1c and 4.1d) for selected n-alkanes (methane, propane, n-pentane and n-heptane) and alcohols (methanol, 1-propanol, 1-pentanol and 1-heptanol). The comparison of figures 4.1a and 4.1b shows that the overprediction of the critical point is higher for alcohols than for hydrocarbons. This is a consequence of the non-ideal behavior of associating compounds, which causes the contraction of the saturated liquid phase volume far away from the critical point [120], while in the critical region the long-range interactions become more important and the fluid possesses a universal behavior [39]. The difference between the regions makes it more difficult for classical models to represent the entire coexistence diagram. Furthermore, the plots indicate that the deviations reduce as the carbon number increases, in the case of alcohols, because the strength of the hydrogen bonding between the molecules decreases with the length of the carbon chain. The last two figures show that

Table 4.2: AAD of the saturated and critical properties for several pure species calculated with the SRK, PT and CPA EoS

$Comp.$	SRK				PT				CPA					
	ΔP_{sat} (%)	Δv_{liq} (%)	Δv_{vap} (%)	Δv_c (%)	ΔP_{sat} (%)	Δv_{liq} (%)	Δv_{vap} (%)	Δv_c (%)	ΔP_{sat} (%)	Δv_{liq} (%)	Δv_{vap} (%)	ΔT_c (%)	ΔP_c (%)	Δv_c (%)
C_1	2.0	5.6	2.5	16.3	1.3	4.7	1.3	14.6	0.9	3.1	3.09	1.4	4.0	13.5
C_2	1.6	8.6	1.9	19.4	0.8	4.3	0.7	15.2	0.4	2.5	3.90	1.6	6.9	13.4
C_3	1.3	10.2	1.6	20.6	0.8	4.1	0.8	15.0	2.2	2.3	6.0	2.40	11.0	11.3
C_4	1.5	11.7	1.7	21.6	0.6	4.0	0.8	14.8	0.5	3.7	5.5	2.6	14.9	8.8
C_5	1.5	14.0	1.9	23.3	0.5	3.9	0.9	15.2	0.4	1.8	5.0	2.1	12.6	11.9
C_6	1.5	16.0	2.4	25.2	0.7	3.8	1.4	15.8	2.0	1.4	8.4	2.9	14.6	11.9
C_7	1.3	17.5	2.5	27.7	0.9	3.3	2.1	16.7	0.8	1.3	7.30	2.6	16.6	12.7
C_8	1.4	19.4	2.0	30.2	1.2	3.4	1.8	17.9	0.8	1.2	5.7	2.3	18.0	12.8
C_9	1.6	21.1	1.9	30.6	1.3	3.4	1.9	17.2	0.8	1.3	6.1	2.6	20.1	12.0
C_{10}	2.0	22.1	3.1	31.3	1.5	3.0	2.8	16.9	2.6	1.2	4.4	2.3	22.5	12.2
C_1OH	7.2	37.8	13.2	50.2	5.0	13.2	11.5	31.7	1.0	1.5	8.1	4.5	31.4	5.5
C_2OH	3.3	26.5	5.6	38.2	2.8	5.3	3.8	19.5	2.2	1.1	8.2	4.8	35.0	7.3
C_3OH	3.4	20.4	4.7	31.3	6.5	6.8	6.9	14.1	1.0	1.3	3.7	2.8	26.8	7.4
C_4OH	7.5	17.8	8.2	29.3	10.4	6.8	8.9	13.1	2.5	1.8	4.4	2.0	24.7	6.9
C_5OH	8.2	16.9	12.0	28.1	11.7	7.0	14.6	12.3	0.7	1.4	4.8	2.8	19.7	10.8
C_6OH	12.8	18.5	22.1	28.5	16.2	6.1	23.7	13.0	2.8	2.6	3.0	3.0	23.1	8.0
C_7OH	9.7	13.8	17.6	27.8	11.7	7.8	18.6	12.3	2.9	3.7	0.7	3.2	17.1	12.8
C_8OH	15.7	18.5	15.4	27.5	19.6	5.5	15.8	11.9	2.9	1.2	1.1	2.5	17.0	11.8
H_2O	4.2	41.2	6.7	45.1	2.9	23.5	5.5	33.0	0.8	2.4	6.1	5.3	38.1	1.0
H_2S	0.5	7.4	2.0	17.5	1.4	3.2	1.5	13.7	0.5	1.1	5.5	2.6	13.0	7.4
CO_2	0.4	14.5	1.8	21.2	0.4	4.8	1.1	13.9	0.3	1.8	6.9	1.9	11.3	11.2
N_2	1.5	4.7	1.9	17.9	1.3	4.4	1.5	12.6	0.7	3.1	3.0	1.2	4.0	12.1
Average	**4.1**	**17.5**	**6.0**	**27.5**	**4.5**	**6.0**	**5.8**	**16.4**	**1.4**	**1.9**	**5.0**	**2.7**	**18.3**	**10.1**

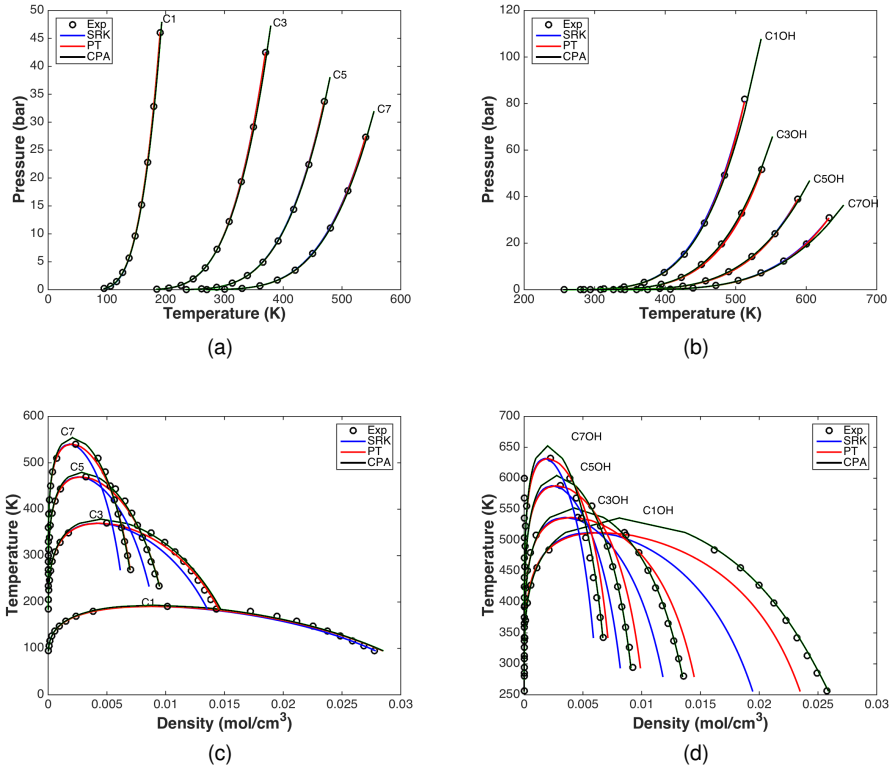

Figure 4.1: Saturated pressure as function of temperature for selected hydrocarbons (a) and alcohols (b), and the coexistence diagram for the hydrocarbons (c) and alcohols (d). Experimental data were taken from the $DIPPR$ database (open circles) and the curves were calculated with SRK (blue line), PT (red line) and CPA (black line).

the $PT\ EoS$ correctly correlates the saturated liquid phase volume for hydrocarbons, but it predicts a larger volume for alcohols, which means that the constant c needs to be refitted for these substances in order to give a better representation of this property. The CPA model is superior to both cubic equations, not only due to the association term that improves the description of the thermodynamic properties of alcohols, but also due to the modification of the critical point, which allows a better representation of the volume close to the critical region.

The deviations regarding the saturated properties for each group of components (normal hydrocarbons and alcohols) and the overall average errors are given in Table 4.3. As stated previously, the $CPA\ EoS$ is superior to

Table 4.3: AAD of the saturated properties for the pure n-alkanes (HC) and n-alcohols (Alc) studied in this work. The results were obtained with the SRK, PT and $CPA\ EoS$.

$Group$	ΔP_{sat} (%)			Δv_{liq} (%)			Δv_{vap} (%)		
	SRK	PT	CPA	SRK	PT	CPA	SRK	PT	CPA
HC	1.6	1.0	1.1	14.6	3.8	2.0	2.1	1.5	5.6
Alc	8.5	10.5	2.0	21.3	7.3	1.8	12.3	13.0	4.3
Avg	**5.0**	**5.7**	**1.6**	**18.0**	**5.5**	**1.9**	**7.2**	**7.2**	**4.9**

Table 4.4: AAD of the critical properties for the pure n-alkanes (HC) and n-alcohols (Alc) studied in this work. The results were obtained with the SRK, PT and $CPA\ EoS$.

$Group$	ΔT_c (%)	ΔP_c (%)	Δv_c (%)		
	CPA	CPA	SRK	PT	CPA
HC	2.3	14.1	24.6	15.9	12.0
Alc	3.2	24.4	32.6	16.0	8.8
Avg	**2.7**	**19.2**	**28.6**	**16.0**	**10.4**

the cubic models for the representation of the alcohols, due to the extra term that takes into account the hydrogen bonding effect. As for hydrocarbons, the better correlation of the properties is related to the parametrization of the association model [38]. With respect to the critical point representation of pure substances, it is seen that the classical CPA parametrization procedure leads to large deviations in the critical pressures and temperatures (Table 4.4).

Figure 4.2 shows the experimental and the calculated values with the $CPA\ EoS$ of the critical pressures (a) and temperatures (b) for the selected hydrocarbons and alcohols. For all substances, it is seen that the association model overpredicts the experimental values, however for hydrocarbons the relative deviations to the experimental critical properties slightly increase with the molecular weight, while for alcohols the behavior is the opposite, as the association effect decreases with the length of the hydrocarbon chain. Additionally, it is observed that the overprediction in terms of pressure is larger than in terms of temperature. Finally, since the cubic models are developed in order to match the critical pressures and temperatures of the pure components, they were not plotted in the figure; however, this is not the case for the critical volume.

The comparison of the calculated and experimental critical volumes is

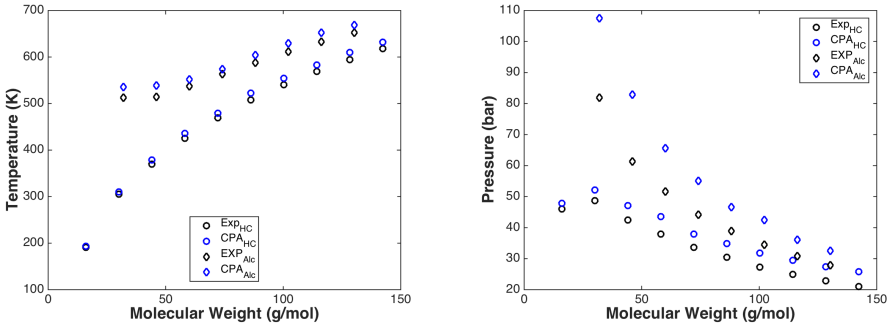

(a) (b)

Figure 4.2: Critical temperatures (a) and pressures (b) as a function of the molecular weight of normal alkanes (open circles) and alcohols (open diamonds). Experimental data were taken from the $DIPPR$ database (black), while the calculated points were obtained with CPA (blue).

shown in Figure 4.3. The first graph exhibits the results for hydrocarbons, while the second one shows the results for alcohols. Unlike the previous figures, we have plotted the density in g/cm^3 as a function of the molecular weight, because it allows the observation of a maximum that occurs for hydrocarbons. This behavior was studied by Tsonopoulos and Tan [121] with the Flory theory and the authors found a peak for the critical density around n-heptane, which was also corroborated by experimental data [122] and molecular simulations [123].

The calculations with the classical EoS indicate that this peak is obtained before the experimental one. Besides, the comparison of the results with the experimental data shows that aside from giving the highest deviations, SRK yields a qualitatively wrong description of the volumetric trend since the critical density decreases much strongly with respect to the carbon number than the predictions obtained with the other models. Furthermore, CPA is superior to PT, even though this cubic model has a third constant to correct the volume of the liquid phase. In fact, this characteristic is even more pronounced for alcohols. Since CPA has an association term that accounts for hydrogen bonding between the molecules, it is able to qualitatively describe the more or less monotonic descending trend in terms of the critical density, while the cubic models predict a behavior similar to one obtained for the n-alkanes.

The comparisons in this section indicated that the traditional CPA EoS, albeit superior to cubic models for the representation of saturated properties,

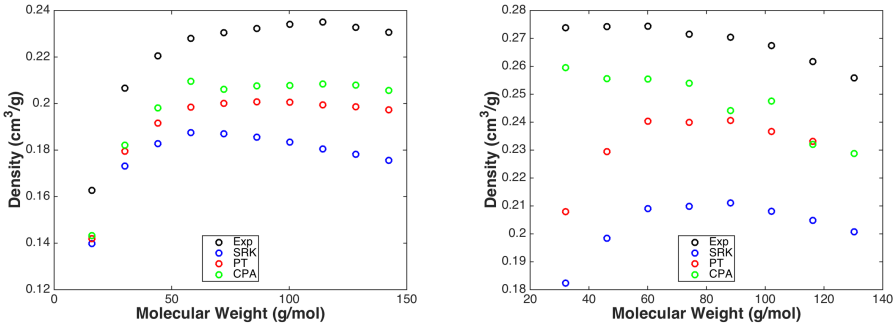

Figure 4.3: Critical density of normal alkanes (a) and alcohols (b) as a function of the molecular weight. Experimental data were taken from the $DIPPR$ database (black), while the calculated points were obtained with SRK (blue), PT (red) and CPA (green).

is unable to correctly represent the critical point of pure fluids. One way to improve the description of the critical properties with the association model without resorting to crossover approaches [48, 56, 58–61] is to rescale pure compound parameters to match the critical temperatures and pressures. This approach was applied to different $SAFT$ versions [124–126] and, in this work, a procedure for rescaling the pure component parameters of CPA was also developed, which is discussed in the following subsection.

4.1.2 Rescaling of the pure component parameters of the CPA EoS

In the original paper regarding the development of CPA, Kontogeorgis et al. [45] defined the following objective function (OF) for the evaluation of the pure components parameters of the model:

$$OF = \sum_{i=1}^{N} \left(\frac{P_{sat}^{exp} - P_{sat}^{calc}}{P_{sat}^{exp}} \right)^2 + \sum_{i=1}^{N} \left(\frac{v_{liq}^{exp} - v_{liq}^{calc}}{v_{liq}^{exp}} \right)^2 \tag{4.2}$$

where P_{sat} is the vapor pressure, v_{liq} is the saturated liquid densities and the superscripts exp and $calc$ correspond to the experimental and calculated values of the properties. No information of the critical properties is taken into account in the minimization process using Equation (4.2). Therefore, a differ-

ent objective function was defined and it is given by the expression:

$$OF = \frac{\theta_1}{N_{exp}} \sum_{i=1}^{N} \left| \frac{P_{sat}^{exp} - P_{sat}^{calc}}{P_{sat}^{exp}} \right| + \frac{\theta_2}{N_{exp}} \sum_{i=1}^{N} \left| \frac{v_{liq}^{exp} - v_{liq}^{calc}}{v_{liq}^{exp}} \right| + \theta_3 \sum_{i=1}^{N} \left| \frac{P_c^{exp} - P_c^{calc}}{P_c^{exp}} \right| + \theta_4 \sum_{i=1}^{N} \left| \frac{T_c^{exp} - T_c^{calc}}{T_c^{exp}} \right| \quad (4.3)$$

where θ_1 to θ_4 are parameter weights. In this work, the values of θ_1 to θ_4 were set to 1, thereby giving a bigger weight to the critical properties. The main difference between equations (4.2) and (4.3) is the inclusion of the critical properties in the search of the optimum parameters.

The pure substance parameters were determined with the application of the Particle Swarm Optimization (PSO) method to minimize Equation (4.3). Kennedy and Eberhart [127] elaborated the PSO algorithm based on the social behavior of flock animals. The method consists of a population of particles (swarm), containing randomly initialized pure component parameter sets, and it moves towards the minima along the iterations. Each particle has a position, i.e. a vector containing certain values for the pure species parameters, and a velocity, i.e. a vector that modifies the position of the particle, determined by the following equations:

$$x_{p,d}^{n+1} = x_{p,d}^{n} + v_{p,d}^{n+1} \quad (4.4)$$

$$v_{p,d}^{n+1} = \lambda v_{p,d}^{n} + \sigma_1 r_1 \left(x_{p,d}^{lb} - x_{p,d}^{n} \right) + \sigma_2 r_2 \left(x_{p,d}^{gb} - x_{p,d}^{n} \right) \quad (4.5)$$

where $x_{p,d}^{n+1}$ and $v_{p,d}^{n+1}$ is the position and velocity of the particle p in the search direction d at iteration $n+1$. The parameters of the PSO method are λ, inertial weight, σ_1 and σ_2, acceleration constants, these values should be carefully selected in order to cover the whole search space [128], while r_1 and r_2 are random vectors.

The PSO algorithm is useful for finding the optimal parameters of a EoS because it can search a broad region of the search-space without requiring gradient information that can be non-smooth for certain values of the parameters, thus hampering a regular gradient-based optimization procedure. It starts by randomly positioning the particles, i.e. a specific set of parameters of the model, which in the case of CPA is a_0, b, c_1,$\varepsilon^{A_iB_j}$ and $\beta^{A_iB_j}$. Thereafter, the vapor pressure, saturated liquid volume and critical pressure and tempera-

ture are calculated with the particles, yielding solutions to Equation (4.3). The position of each particle is changed using the velocity vector determined by Equation (4.5) and then the objective function is re-evaluated, Equation (4.3). If the result of the objective function is smaller than the solution obtained in the previous iteration, the modification of the position of the particle is accepted; otherwise the position is kept as in the previous step. The search is completed when a predetermined number of iterations is reached, or when the distance between the particles is smaller than a predefined value. To ensure that the particles are being directed towards the global minimum at a desired rate, the PSO parameters, i.e. λ, σ_1 and σ_2, can be modified. Nevertheless, the global minimum is not necessarily found, thus a procedure analogous to the one developed by Santos et al. [129, 130] is utilized for selecting the optimal parameters.

The optimization method begun with 100 particles randomly initialized around the literature parameters (Table 4.1). This strategy allows the evaluation of the changes in the parameters and the changes in the deviations of the saturated (ΔP_{sat} $(\%)$; Δv_{liq} $(\%)$) and critical (ΔP_c $(\%)$; ΔT_c $(\%)$) properties during the optimization procedure. At the end of the search, the final set of parameters was selected using LLE data. This approach was applied by Yakoumis et al. [118], which noticed that the several sets of pure component parameters for water can correctly represent the phase equilibria of the pure fluid and the VLE region; nonetheless, fewer parameters are capable of precisely representing LLE data.

For the selection of plausible sets of pure compound parameters, the experimental values of the critical properties obtained from the $DIPPR$ database were used. Since one of the goals of this investigation is to improve the critical region description with the $CPA\ EoS$, the PSO method was applied and all particles that returned deviations within the uncertainty range of the experimental critical point measurements were filtered. The optimal parameters were ultimately chosen with the use of LLE data.

As an example, Figure 4.4 shows the values of the parameters for methanol using two association sites ($2B$ scheme), at the final iteration of the optimization procedure. For all parameters, it is possible to observe that a region of minimum is found. Nevertheless, different sets return similar values of the objective function. This suggests, as pointed by Kontogeorgis and Folas [38], the necessity of VLE and principally LLE data to assess the quality of the pure compound parameters.

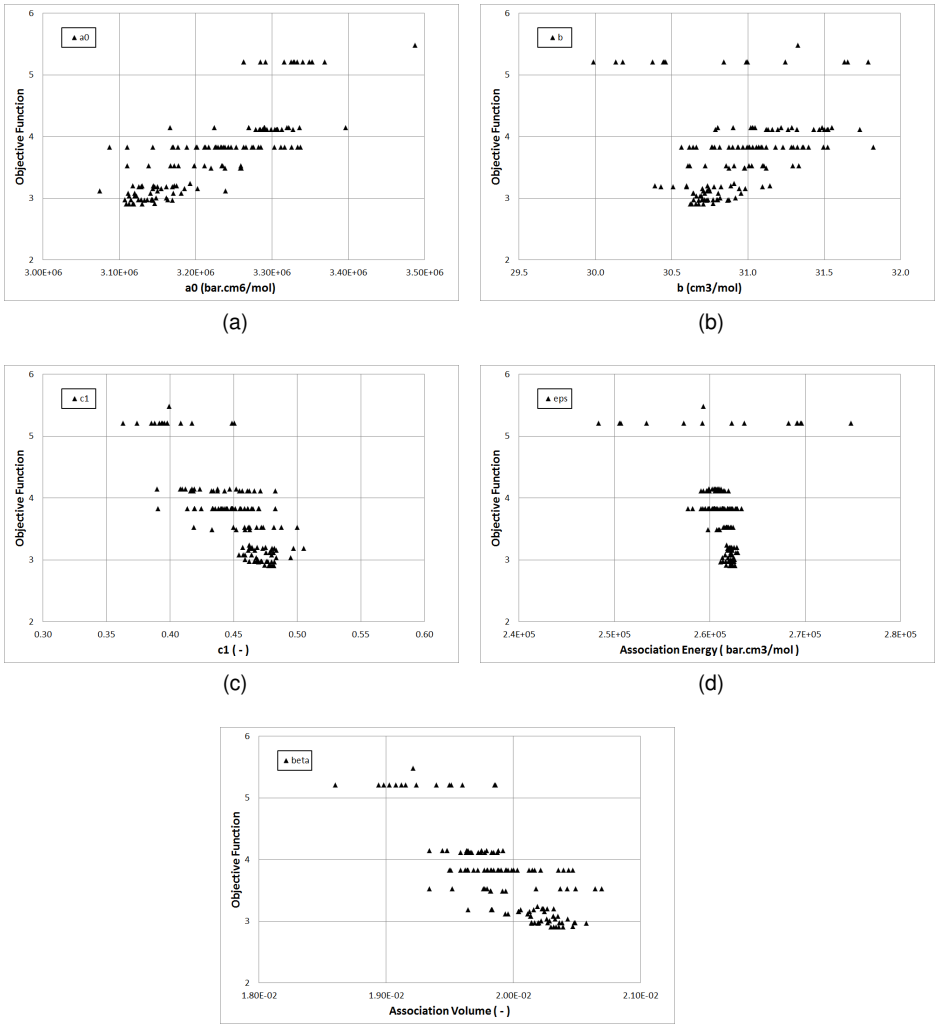

Figure 4.4: Values of the objective function given by Equation (4.3) as a function of the parameters of CPA: a_0 (a), b (b), c_1 (b), association energy (ε) (d) and association volume (β) (e) for methanol at the last iteration of the optimization process using the PSO algorithm. Figure taken from [3].

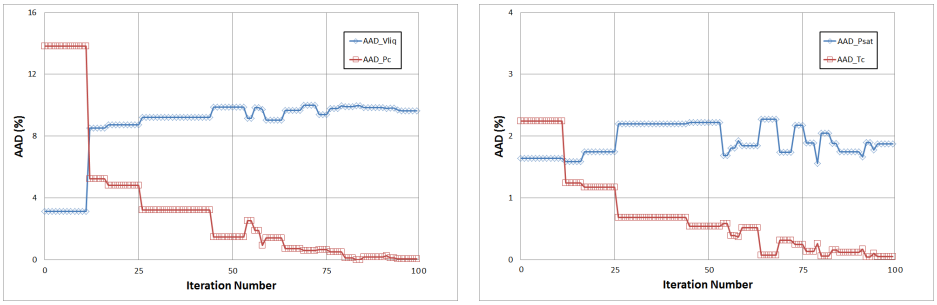

(a) (b)

Figure 4.5: AAD of the saturated liquid phase volume (Δv_{liq} $(\%)$) and critical pressure (ΔP_c $(\%)$) (a); and vapor pressure (ΔP_{sat} $(\%)$) and critical temperature (ΔT_c $(\%)$) (b) as a function of the iteration number for the global best particle in the optimization of the pure compound parameters of methanol using the PSO algorithm. Figure taken from [3].

Figure 4.5 indicates another important behavior of the parameters of the association model. It shows the values of the AAD of the saturated and critical properties for the particle with the global best position along the iterations of the optimization process. In the first iterations, the deviations for P_c and T_c are much higher than for v_{liq} and P_{sat}, which is related to the initialization around the original parameters. Throughout the search procedure, the deviations with respect to the critical properties reduce, while and the deviations regarding the saturated properties increase, particularly for the liquid phase volume. This is connected to the inability of any analytical EoS to correctly represent the shape of the coexistence diagram of real fluids [39]. Although, a volume translation technique can be used to reduce the errors with respect to density without changing the equilibrium [131], the use of rescaled parameters reduces the capacity of CPA to correlate the LLE of binary mixtures, as it will be shown in future chapters.

A different technique to overcome some of the weaknesses of the CPA EoS, like the overprediction of the critical point, was developed by Palma et al. [4]. The authors modified CPA by rescaling the pure compound parameters of the association model, hence matching the critical pressure and temperature. On the other hand, as noticed in their research, this modification deteriorated the representations of the vapor pressures and liquid phase densities. Therefore, they suggested the application of a temperature independent vol-

ume translation [131], as given by the equation:

$$v_t = v_0 - v_s \tag{4.6}$$

where v_t and v_0 are the final and initial volume of the system, and v_s is a constant estimated by fitting the liquid phase density at $T_r = 0.7$. Additionally, a more flexible temperature-dependent function, based on the Mathias-Copeman function [132], was proposed, with 3 or 5 parameters depending on the substance. The expression for the simpler α-function is given by:

$$a\left(T\right) = a_0 \left(1 + c_1 \left(1 - \sqrt{T_r}\right) + c_2 \left(1 - \sqrt{T_r}\right)^2 + c_3 \left(1 - \sqrt{T_r}\right)^3\right)^2 \tag{4.7}$$

where c_1 to c_3 are parameters determined for each component. Due to the increase in the number of parameters (from 4 to 6), a systematic procedure for the optimization of the parameters is required for obtaining a fair representation of the phase equilibria in a wide range of conditions. Still, some limitations are observed with this method.

Table 4.5 shows the parameters of methanol for the $CPA\ EoS$ using four different approaches. In the first case, the values were regressed from saturated data (CPA), while in the second (CPA_{crit}), they were rescaled using the methodology proposed in this work, i.e. using both saturated and critical properties in the procedure for the minimization of the objective function. The last two approaches, represented in the table by $Set\,C1$ and $Set\,C2$, are the parameters given by Palma et al. [4], with the application of a more flexible α-function and a volume translation method. For a better comparison of the models, a temperature-independent volume translation constant was also introduced in the CPA_{crit} for improving the predictions of the liquid phase density.

Figure 4.6a shows the experimental vapor pressures as a function of temperature and the calculated curves using the four aforementioned approaches. It is seen that the rescaling of the pure component parameters improves the description of the critical properties, and the overprediction of methanol's critical pressures and temperatures are corrected. Nevertheless, the limitations of the mean-field equation using rescaled parameters are seen in Figure 4.6b, which shows the experimental and calculated coexistence diagram for methanol. None of the models are capable of describing the coexistence curve correctly. The best approach in terms of the matching of the critical point ($Set\,C1$), has

Table 4.5: Pure component parameters of methanol using four different CPA approaches. In the first case (CPA) the parameters were regressed from saturated data, in the second (CPA_{crit}), the parameters were rescaled using experimental saturated and critical data, and the last two approaches ($Set\,C1$ and $Set\,C2$) were taken from [4].

EoS	$10^{-5} \cdot a_0$ $\left(\frac{bar.mol^2}{cm^6}\right)$	b $\left(\frac{cm^3}{mol}\right)$	c $(-)$	ε/R (K)	$10^3 \cdot \beta$ $(-)$	v_s $\left(\frac{cm^3}{mol}\right)$
CPA	40.5332	30.98	0.4310	2958	16.10	-
CPA_{crit}	31.6957	30.86	0.4696	3141	20.58	3.182
$Set\,C1$	20.0000	22.90	0.3500 -0.0400 1.8500	3237	37.60	-7.000
$Set\,C2$	68.0000	46.10	0.9000 -2.4700 3.2600	2996	4.600	18.60

Table 4.6: AAD of the saturated and critical properties calculated for methanol using CPA with the parameters were regressed from saturated data, CPA with the rescaled parameters using experimental saturated and critical data (CPA_{crit}), and CPA with the parameters from from [4] ($Set\,C1$ and $Set\,C2$).

EoS	ΔP_{sat} $(\%)$	Δv_{liq} $(\%)$	Δv_{vap} $(\%)$	ΔT_c $(\%)$	ΔP_c $(\%)$	Δv_c $(\%)$
CPA	1.0	1.5	8.1	4.5	31.4	5.5
CPA_{crit}	1.8	1.9	14.8	0.3	0.5	4.7
$Set\,C1$	5.7	0.8	19.6	0.5	1.5	0.2
$Set\,C2$	3.3	1.7	5.1	0.2	0.2	31.3

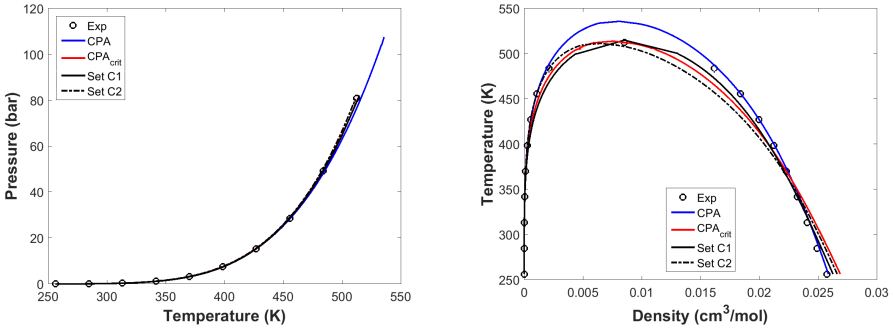

Figure 4.6: Saturated pressure as function of temperature (a) and the co-existence diagram (b) for methanol. Experimental data were taken from the $DIPPR$ database (open circles) and the curves were calculated with classical CPA (blue line), CPA using rescaled parameters obtained in this work (red line) and two different sets of parameters, $Set\,C1$ (black solid line) and $Set\,C2$ (black dash-dot line) taken from [4].

the worse representation of the vapor density, while the other two are inferior with respect to the fitting of the critical volume and saturated liquid phase density data.

The evaluation of the AAD of the saturated and critical properties (Table 4.6) indicates that the representation of all the saturated and critical properties was not achieved with the $CPA\ EoS$ and the different techniques. Moreover, Palma et. al [4], concluded that the VLE and LLE diagrams of binary mixtures containing methanol are not correctly described with $Set\,C1$. This behavior was also observed with CPA using the rescaled parameters estimated in this work. Better results for the binary phase equilibria were obtained with the second approach ($Set\,C2$), which, on the other hand, has the highest deviation of the critical volume. This might affect the correlations of the volumetric properties in the critical region.

In summary, the rescaling of the pure component parameters of mean-field models is an appealing method due to its simplicity. Nonetheless, such approach has inherent limitations, i.e. it does not take into account the fluctuations of the order parameter that become particularly important close to the critical point. Therefore, an accurate description of the different phase equilibria and critical properties over a wide range of conditions is only achieved with the application of crossover models, and, in the next section, the RG method

developed by White is used to correct the $SRK\ EoS$, yielding a global EoS.

4.2 Application of the Crossover SRK to Describe the Phase Behavior of Pure Fluids

The rescaling procedure can not change the mean-field character of a EoS, hence the correct representation of the properties of fluids far away and close to the critical point requires the utilization of a renormalization group theory method to correct the classical equation in the critical region. In this work, White's recursive procedure was chosen to take into account the density fluctuations in the mean-field model.

As presented in the last chapter, the first step of the recursive procedure requires the determination of the zero-order solution of the free energy density (f_0), given by Equation (3.28). This means that the method starts with a model including only short-wavelength density fluctuations, which can be represented by the repulsive term of the free energy (f_{rep}). If one uses a phenomenological EoS, e.g. SRK, then it is not possible to allocate which part of the model corresponds to the "true" repulsive and attractive terms [112]. This means that, in the case of the $SRK\ EoS$ using the pressure explicit equation as a function of density, Equation (4.8), the first term of the right-hand side of the following expression:

$$P = \frac{\rho RT}{1-\rho b} - \frac{a\rho^2}{1+b\rho} \tag{4.8}$$

is not only accounting for the repulsive interactions, while the second term is not only representing the attractive interactions. In Equation (4.8), P is pressure, R is the universal gas constant, T is temperature, ρ is the molar density which corresponds to the inverse molar volume (v^{-1}) and a and b are pure component constants calculated by equations (2.17) to (2.19).

The procedure for obtaining the correct terms that corresponds to the repulsive and attractive interactions from the $SRK\ EoS$ was proposed in [5], and they are defined by comparing the cubic model to the analytic expression for the hard spheres, namely the Carnahan-Starling EoS [133]:

$$Z = \frac{1+\eta+\eta^2-\eta^3}{(1-\eta)^3} \tag{4.9}$$

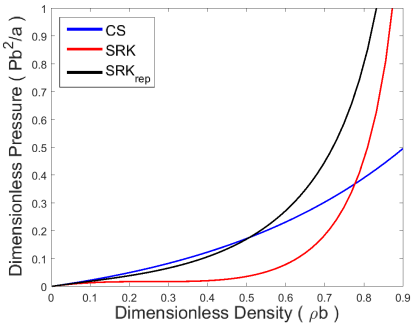

Figure 4.7: Dimensionless pressure ($^{b^2P}/_{a}$) as a function of the dimensionless density ($b\rho$) of methane calculated with the Carnahan-Starling EoS (CS), blue line, the $SRK\ EoS$, red line and the repulsive part of the cubic model (SRK_{rep}), which correspond to adding the term $-0.53a\rho^2$ to pressure calculated with SRK. Figure taken from [5].

where Z is the compressibility factor and η is equal to $^{b\rho}/_{4}$. The comparison of the two models is performed at the critical isotherm by subtracting the attractive part of the free energy, i.e. $-\alpha\rho^2$, until SRK matches the hard sphere equation. Similar to the work of Salvino and White [58], the comparison of the curves is done by plotting the dimensionless pressure ($^{b^2P}/_{a}$) as a function of the dimensionless density ($b\rho$) for methane (Figure 4.7). In this figure, the repulsive contribution for the $SRK\ EoS$, i.e. SRK_{rep}, was obtained by subtracting $-0.53a\rho^2$ from the classical cubic model.

The same procedure was applied to different normal alkanes, from ethane to n-decane, and similar curves to the one showed given by Figure 4.7 were obtained. The different terms were then averaged resulting in a value of approximately $-0.5a\rho^2$, hence the attractive term for the free energy density was set equal to:

$$\alpha\rho^2 = 0.5a\rho^2 \tag{4.10}$$

The initial free energy density for calculating the fluctuations using White's recursive procedure and the $SRK\ EoS$ is obtained by applying Equation (4.10) in (3.20), and also by integrating Equation (4.8), yielding:

$$f_0^{SRK} = \rho RT \ln\left(\frac{\rho}{1-\rho b}\right) - \rho\frac{a}{b}\ln\left(1+\rho b\right) + 0.5a\rho^2 \tag{4.11}$$

Another method of calculating the attractive part of the free energy density for the SRK EoS was proposed by Cai and Prausnitz [112]. The authors fitted

RG calculations to experimental data of different n-alkanes and obtained the same approximate result ($0.5a\rho^2$) for the attractive part of free energy, i.e. $-\alpha\rho^2$.

The application of the crossover SRK for the calculation of the properties of pure fluids, in this case n-alkanes (from methane to n-decane), requires the numerical integration of Equation (3.24). Additionally, it is needed an interpolation scheme to obtain a continuous function of the free energy density corrections. The scheme used in this work was the cubic spline. Following other works [54, 55, 98, 106, 112–114, 116], the density range, i.e. from a minimum value of $\rho = 10^{-12}b^{-1}$ to a maximum of $\rho^{max} = 0.999b^{-1}$ to avoid numerical issues, was divided into 500 steps, since it allows good accuracy for the calculations with the recursive procedure. Moreover, 5 summands ($n^{max} = 5$) were chosen to approximate $\sum_{n=1}^{\infty} \delta f_n$ in Equation (3.28), in order to include the density fluctuations in the mean-field model. Finally, the volume of each phase in equilibrium and other properties were determined with the procedures given in Appendix B.

4.2.1 Parametrization of the $CSRK\ EoS$ and description of the properties of pure fluids

In order to use the $CSRK\ EoS$ to quantitatively describe the properties of pure fluids far away and close to the critical point it is necessary to obtain the optimal pure components parameters, which are the virtual critical temperatures ($T_c^{'}$) and pressures ($P_c^{'}$) and acentric factors ($\omega^{'}$), and the recursive procedure parameters L and ϕ. The mean-field model parameters ($T_c^{'}$, $P_c^{'}$ and $\omega^{'}$) were obtained by fitting the experimental saturated pressure and liquid volume curves from a reduced temperature range of 0.5 to 0.75. This means that Equation (4.2) was minimized, within this T_r range, in order to yield the pure component parameters.

After the optimization of the SRK pure component parameters, L and ϕ were determined by fitting the experimental critical pressures, temperatures and volumes of the pure substances studied, along with the saturated liquid phase volumes and vapor pressures in conditions close to critical. Table 4.7 shows the parameters obtained for the n-alkanes (from methane to n-decane) studied in this work.

The reason for this approach is that the mean-field model essentially works well in regions far from the critical point, where density fluctuations do not af-

Table 4.7: Parameters of the crossover SRK for methane to n-decane. The parameters $T_c^{'}$, $P_c^{'}$ and $\omega^{'}$ represent the virtual critical parameters of the mean-field model.

$Comp.$	$T_c^{'}$ (K)	$P_c^{'}$ (bar)	ω $(-)$	L $\left(\mathring{A}\right)$	ϕ $(-)$
C_1	197.7	50.39	-0.0578	4.166	2.50
C_2	314.3	52.35	0.0392	5.264	1.20
C_3	382.2	46.74	0.0856	5.913	0.67
C_4	441.7	42.48	0.1204	6.452	0.60
C_5	489.1	38.53	0.1632	6.879	0.60
C_6	526.4	34.98	0.2247	7.207	0.60
C_7	561.4	32.46	0.2647	7.396	0.60
C_8	592.8	30.17	0.3044	7.597	0.60
C_9	620.7	28.09	0.3434	7.809	0.60
C_{10}	645.0	26.24	0.3882	8.041	0.60

fect the thermodynamic properties of the system. Therefore, the experimental critical parameters are changed in order to describe the correct behavior of the saturated properties far away from the critical point. Following the fitting of the mean-field parameters, the cutoff length and the initial wavelength of the short range interactions were optimized using near-critical data, i.e. saturation pressures and saturate liquid phase volume close to the critical point ($T_r = 0.95$ to 1.0). White's procedure has a strong effect on the free energy calculated from the classical EoS close to the critical point, changing the analytical character of the mean-field model, allowing it to capture the singularities that arise close to the critical point.

Figure 4.8 shows the isotherms for n-hexane at the critical temperature calculated with the traditional $SRK\ EoS$ using the experimental critical parameters and the $CPA\ EoS$, as well as the crossover SRK ($CSRK$). The plot indicates that the use of the EoS optimized to describe the behavior of the system at low reduced temperatures causes an overshoot of the critical point (CPA). The application of the recursive procedure corrects this behavior and matches the experimental critical pressure. Additionally, for pressures above the critical, the description of the density with the $CSRK\ EoS$ is superior to the $SRK\ EoS$. This is due to the fact that, far from the critical point, long-range fluctuations are no longer affecting the properties of the system and the use of parameters matching experimental saturated data enhances the description of the volume in the supercritical region [59].

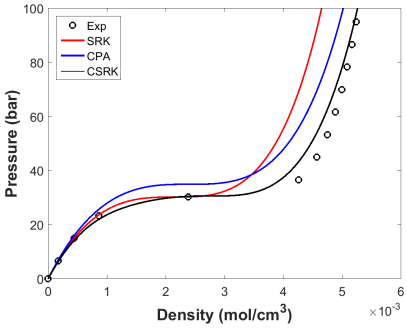

(a)

Figure 4.8: Critical isothermal experimental data (open circles) for n-hexane and the calculated curves using SRK (blue line), CPA (red line) and $CSRK$ (black line). Experimental data was taken from the $NIST$ database.

The three models were also applied in the calculation of the saturation properties of the n-alkanes studied in this work. Figure 4.9a shows the saturation pressure as a function of temperature and Figure 4.9b shows the temperature as a function of the density of the coexisting phases for selected normal alkanes (methane, propane, n-hexane, and n-decane).

The main improvements obtained with the application of the recursive procedure to introduce density fluctuations in the $SRK\ EoS$ can be observed in Figure 4.9. The crossover $SRK\ EoS$ ($CSRK$) corrects the overprediction, when the parameters are regressed using saturated pressures and liquid phase densities at conditions far from critical, matching the experimental critical temperatures and pressures for the selected hydrocarbons, as well as precisely describes the saturated liquid densities and vapor pressures. In addition to the qualitative comparison of the models, it is also important, for engineering applications, to evaluate the quantitative predictions of the saturated properties. Table 4.8 shows the AAD for the vapor pressure and the molar volume of the coexisting phases calculated with the $CSRK\ EoS$, as well as the deviations regarding the critical point. This table indicates that the crossover model is capable of precisely describing the saturated and critical properties for hydrocarbons. The comparison of the average errors from Table 4.8 with Table 4.3 shows that the $CPA\ EoS$ is slightly superior in the description of the vapor pressures and liquid phase densities. On the other hand, the $CSRK\ EoS$ yields lower deviations in terms of the representation of the saturated vapor phase densities. In addition, the comparison of the deviations with respect to

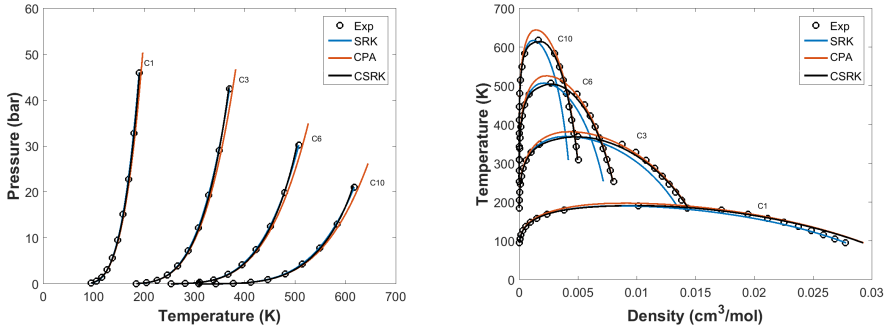

Figure 4.9: Saturation pressure as a function of temperature (a) and coexistence diagram (b) for selected hydrocarbons. Experimental data were taken from the $DIPPR$ database (open circles) and the curves were calculated with SRK (blue line), CPA (red line) and $CSRK$ (black line).

the critical properties show that, the model greatly improves the predictions of the critical point, especially for the critical pressures and volumes (tables 4.8 and 4.4). The $CPA\ EoS$ yields a large overprediction of T_c and P_c, while in the case of v_c, all the classical models tested are unable to correctly represent it.

The results obtained in the section with the $CSRK\ EoS$ have shown that this model is capable of correctly describing the thermodynamic properties of hydrocarbons far away from and close to the critical point. Nevertheless, in the case of associating species it is important, as mentioned in the second chapter, the use of a term that explicitly takes into account the effects of hydrogen bonding between the molecules, since the recursive procedure only corrects for the fluctuations that arise close to the critical point. Additionally, the $CPA\ EoS$ reduces to SRK if there are no associating molecules in the system, meaning that the application of the recursive procedure to CPA yields a model that behaves like the $CSRK\ EoS$, but also accounts for association. This is the topic of the next section.

Table 4.8: AAD of the saturation pressure and volumes of the saturated vapor and liquid phase, and of the critical properties for methane to n-decane and the average of all deviations calculated using the $CSRK\ EoS$.

$Comp.$	ΔP_{sat} (%)	Δv_{liq} (%)	Δv_{vap} (%)	ΔT_c (%)	ΔP_c (%)	Δv_c (%)
C_1	1.7	3.2	2.7	0.4	0.3	0.9
C_2	1.6	2.2	3.1	0.0	1.0	4.9
C_3	2.0	1.9	3.4	0.3	0.9	1.8
C_4	2.5	1.7	3.3	0.3	0.9	1.2
C_5	3.3	1.4	2.7	0.2	1.2	1.5
C_6	2.3	1.6	3.4	0.6	1.4	1.9
C_7	2.4	1.3	2.7	0.6	1.3	3.2
C_8	2.9	1.1	2.6	0.5	1.5	3.9
C_9	3.1	1.1	2.3	0.4	1.0	5.5
C_{10}	3.1	0.9	1.9	0.4	1.5	5.1
Average	**2.5**	**1.6**	**2.7**	**0.4**	**1.1**	**3.0**

4.3 Application of the Crossover CPA to Describe the Phase Behavior of Pure Fluids

Similar to the $CSRK\ EoS$, the calculation of the free energy corrections due to the fluctuations in the order parameter requires the use of an initial free energy expression that accounts for the short-range interactions only [58]. The zero-order solution of the Helmholtz energy density for CPA, i.e. f_0^{CPA} is given by the expression:

$$f_0^{CPA} = RT\rho \ln\left(\frac{\rho}{1-b\rho}\right) - \rho\frac{a}{b}\ln\left(1-b\rho\right) + \rho RT\sum_i x_i\left[\sum_{A_i}\ln\left(X_{A_i} - \frac{X_{A_i}}{2} + \frac{1}{2}\right)\right] + \alpha\rho^2 \quad (4.12)$$

where $\alpha\rho^2$ is the correction of the attractive part calculated by the expression:

$$\alpha\rho^2 = 0.5a\rho^2 \quad (4.13)$$

The constant a in the previous expression is calculated by Equation (2.49). This is the same expression used in the crossover approach for the SRK model, as explained in the previous section. In addition to the equations (3.21)

to (3.28), the application of the method requires the determination of the number of iterations in the mathematical procedure (n) and the the number of density steps ($\Delta\rho$), which were exactly the same as in the $CSRK\ EoS$.

The application of the $CCPA$ in the representation of the thermodynamic properties of pure fluids and mixtures require the estimation of the pure component parameters, i.e. a_0, b, c_1, $\varepsilon^{A_iB_j}$ and $\beta^{A_iB_j}$ for the mean-field equation and L, and ϕ for the recursive procedure, which are described in the following subsections.

Xu and Duan [98] also developed a crossover approach for CPA using White's recursive procedure. However, the authors used an extra parameter for correcting the contribution of the attractive term of the model depending on the association scheme. This additional constant was not considered here. Furthermore, they have derived a different expression for the initial free energy density, which is not equal to the expression used in this work, Equation (4.12).

4.3.1 Applying the pure component parameters of CPA in the crossover model

As discussed in the previous chapter, the pure component parameters of CPA are obtained by fitting the saturated pressure and liquid phase volume curves far away from the critical point. This is the same procedure used in the optimization of the $CSRK$ model, thus it is useful to test the whether the parameters are transferable to the crossover model, i.e. the fitting of the two additional parameters allows a quantitative description of the thermodynamic properties of real fluids.

Since the recursive procedure corrects the predicted critical point by the $CPA\ EoS$, then one way to evaluate the value of the parameters of the recursive part is to determine the distance between the calculated and the experimental critical point (d_c). This can be done with the expression:

$$d_c = \sqrt{\left(\frac{T_c^{exp} - T_c^{calc}}{T_c^{exp}}\right)^2 + \left(\frac{P_c^{exp} - P_c^{calc}}{P_c^{exp}}\right)^2 + \left(\frac{v_c^{exp} - v_c^{calc}}{v_c^{exp}}\right)^2} \qquad (4.14)$$

where the subscript c means the value of the property at the critical point and the superscripts $calc$ and exp are the calculated and experimental values of the properties.

The optimal values for L and ϕ can be found by plotting the value of Equa-

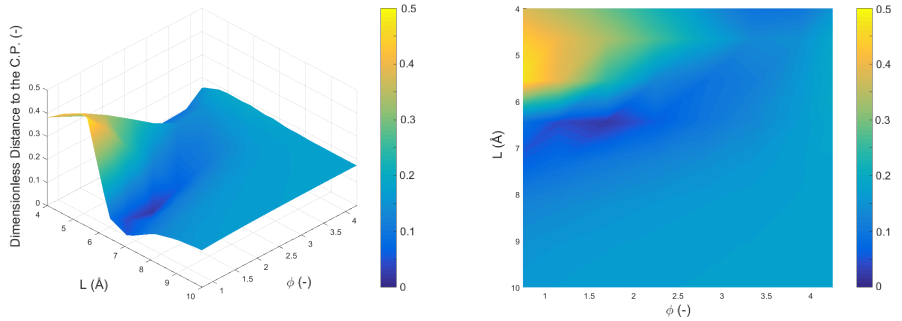

Figure 4.10: Dimensionless distance to the critical point as a function of the parameters of the recursive procedure in the $CCPA$ for n-pentane.

tion (4.14) as a function of the recursive parameters, and the best set should give a solution close to zero. Figure 4.10 shows the three-dimensional plot (a) and the color map (b) of the dimensionless distance to the critical point (d_c) as a function of the parameters L and ϕ for n-pentane. The figure indicates that a minimum distance to the critical point is achieved by the choice of the parameters, i.e. approximately 1.70 for ϕ and 6.44 for L. Additionally, it shows that the increase of both values deteriorates the improvements attained with the recursive procedure, as the d_c becomes close to the values obtained with the classical CPA. On the other hand the reduction of the values of the parameters values, especially L, cause an increasing in the distance to the critical point, by underpredicting the critical properties and making the predictions of the crossover model worse than classical.

After the graphical evaluation, the two optimal values of the crossover parameters were chosen and used in the calculation of the saturated and critical properties. The results were then compared to experimental data and to the mean-field CPA that was used as the basis for the recursive procedure. Figure 4.11a shows the vapor pressures divided by the critical pressure of n-pentane as a function of the reduced temperature, while Figure 4.11b shows the reduced temperature as a function of the saturated vapor and liquid densities divided by the critical density of n-pentane. The graphs plotted in terms of reduced variables allow the evaluation of the changes introduced in the model due to the incorporation of the density fluctuations for n-pentane to be extended to other n-alkanes, since the diagrams are very similar. With this

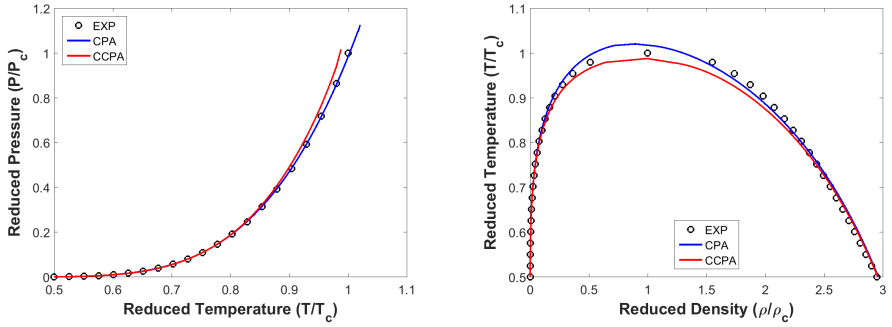

Figure 4.11: Reduced saturated pressures as a function of the reduced temperatures (a) and the reduced temperatures as a function of the reduced saturated vapor and liquid phase densities (b) for n-pentane. Experimental data were taken from the $DIPPR$ database (open circles) and the calculated curves were obtained with CPA (blue line) and $CCPA$ (red line).

approach, the main modification obtained with the recursive procedure is the displacement of the classical critical point to a position much closer to experimental values. Nevertheless, this causes an increase in the deviation of the saturated properties as the critical region is flattened.

The shift of the saturated pressure and densities curves caused by the crossover CPA can be evaluated with the comparison of the deviations from experimental data in different temperature ranges. This is shown in Figure 4.12 where the deviations in the saturated pressures and saturated liquid and vapor density are plotted as a function of the reduced temperature. Below $0.8T_r$, both models yield accurate representations of the saturated pressures and volumes (Figure 4.12), yet a small increase in the deviations of the vapor pressures is caused by the renormalization group procedure. According to Tang and Gross [111], the reason for this behavior is that the linear or cubic interpolation schemes are inadequate far from the critical region due to the nonlinear behavior caused by the contribution of the ideal gas free energy in the renormalization procedure. These numerical issues can be solved by the subtraction of the ideal gas contribution before the cubic-spline interpolation. However, since the improvements are marginal, they were not carried out in this work. From this point to $T_r < 1.0$, the errors obtained with the $CCPA\ EoS$ are much larger than the ones given by the classical model, suggesting that the flattening of the curves of the saturated properties are not in accordance

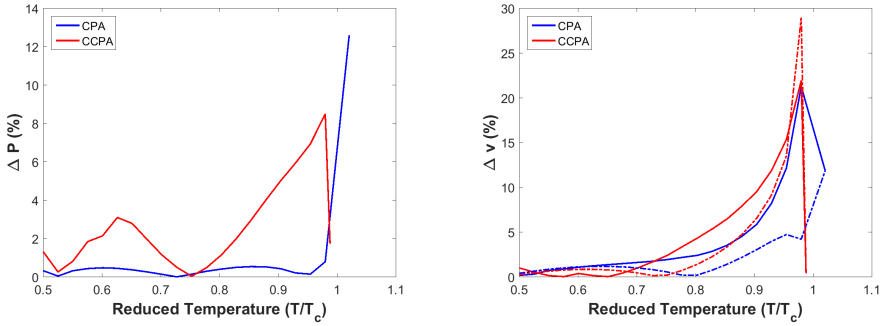

Figure 4.12: Deviations of the vapor pressures (a) and the saturated liquid (solid lines) and vapor (dashed lines) volumes (b) as a function of the reduced temperature of n-pentane.

to experimental data, and for a quantitative description of the data, a change in the mean-field parameters is necessary.

For a complete evaluation of the role of the two additional parameters, we have plotted the two previous graphs, but with different values for L while keeping ϕ constant and equal to the optimal value, and vice-versa. In the first case, the range of L values were: 4, 5, 6 and 7, represented in the figures 4.13a and 4.13c as $CCPA_1$ to $CCPA_4$, respectively, while ϕ was kept equal to 2.0. In the second case, the range of ϕ values were: 0.75, 1.75, 2.75 and 3.75, represented in the figures 4.13b and 4.13d as $CCPA_1$ to $CCPA_4$, respectively, and L was considered equal to 6.07. The plots show that the cutoff length has a stronger impact in the prediction of the properties in the critical region, since a reduction of approximately 40% of its value (from 6.07 to 4) causes a decrease of more than 20% in the critical pressure and 10% in the critical temperature, while using a ϕ of 60% (from 2.0 to 0.75) its optimal values, reduces the critical pressures and temperatures in less than 5%. Although the results with the two smaller L and ϕ values are worse than the ones given by classical model, the shape of the coexistence is closer to the real one, meaning that a change in the mean-field parameters is necessary for attaining quantitative values, as the qualitative picture is already described by the model. Finally, as seen before, the highest values for the recursive procedure parameters yield results that are similar to the mean-field EoS, meaning that the RG corrections become less important due to the greater size of the cut-off parameter.

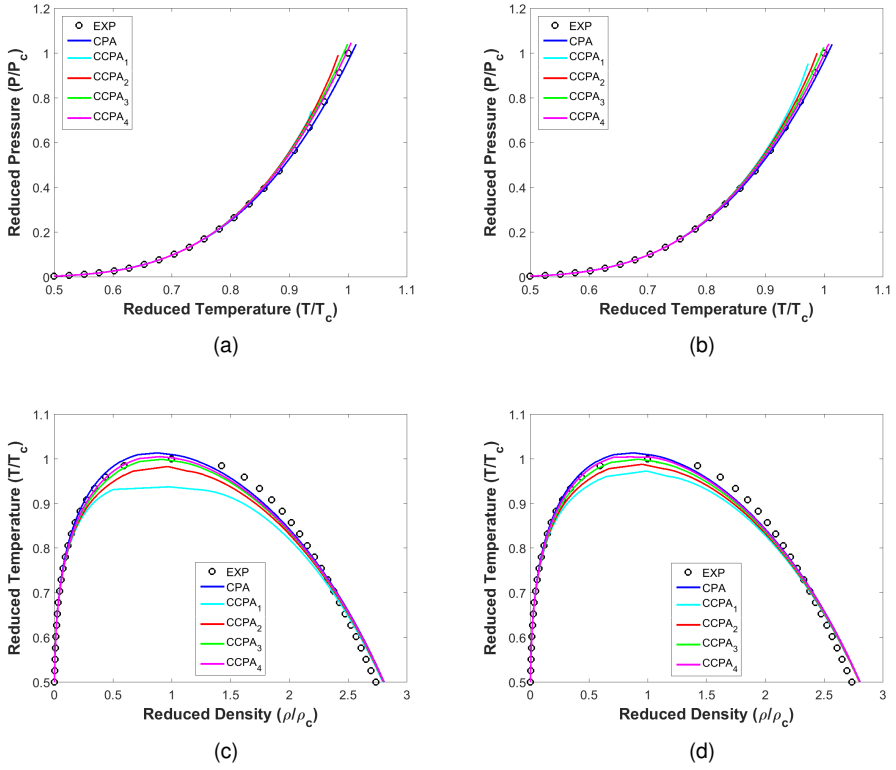

Figure 4.13: Reduced saturated pressures as a function of the reduced temperatures (a and b) and the reduced temperatures as a function of the reduced saturated vapor and liquid phase densities (c and d) for n-pentane using different values for the crossover term parameters. Experimental data were taken from the $DIPPR$ database (open circles) and the calculated curves were obtained with CPA (blue line) and $CCPA_1$ to $CCPA_4$.

4.3.2 Parametrization of the $CCPA\ EoS$ and description of the properties of pure fluids

The previous section proved that the change of the traditional pure component parameters of the $CPA\ EoS$, i.e. a_0, b, c_1, $\varepsilon^{A_iB_j}$ and $\beta^{A_iB_j}$, are necessary for quantitative descriptions of the pure fluid properties, along with the determination of the crossover term parameters. For hydrocarbons, the mean-field term parameters reduce to a_0, b and c_1. Furthermore, as aforementioned, the representation of the thermodynamic properties are more affected by the cutoff length, thus, in a first attempt, ϕ was kept constant and equal to 2, in

accordance to Salvino and White's approach [58].

The four adjustable parameters were estimated by fitting the experimental saturated data, vapor pressure and saturated liquid and vapor densities; as well as the critical temperature, pressure and volume of the compounds. The following equation shows the objective function used in the optimization procedure:

$$OF = \frac{1}{N_{exp}} \sum_{i=1}^{N_{exp}} \left| \frac{P_{sat}^{exp} - P_{sat}^{calc}}{P_{sat}^{exp}} \right| + \frac{1}{N_{exp}} \sum_{i=1}^{N_{exp}} \left| \frac{v_{liq}^{exp} - v_{liq}^{calc}}{v_{liq}^{exp}} \right| + \frac{1}{N_{exp}} \sum_{i=1}^{N_{exp}} \left| \frac{v_{vap}^{exp} - v_{vap}^{calc}}{v_{vap}^{exp}} \right| + \left| \frac{P_c^{exp} - P_c^{calc}}{P_c^{exp}} \right| + \left| \frac{T_c^{exp} - T_c^{calc}}{T_c^{exp}} \right| + \left| \frac{v_c^{exp} - v_c^{calc}}{v_c^{exp}} \right| \quad (4.15)$$

where the superscripts exp and $calc$ represent the experimental and calculated properties, respectively; while the subscripts P_{sat} is the saturated pressure, v_{liq} and v_{vap} is the saturated liquid and vapor densities, and the subscript c stands for the critical properties. The range of reduced temperatures used in the calculations were from 0.5 to 1.0. The difference between Equation (4.15) and Equation (4.3) is that the saturated vapor phase was used as an additional constrain, and it is useful for associating species in which the total number of parameters is 7.

Table 4.9: Parameters of the crossover CPA for methane to n-decane.

$Comp.$	$10^{-5} \cdot a_0$ $\left(\frac{bar.cm^6}{mol}\right)$	b $\left(\frac{cm^3}{mol}\right)$	c_1 $(-)$	L $\left(\mathring{A}\right)$
C_1	23.1977	28.19	0.3865	4.337
C_2	54.9617	41.70	0.5299	4.818
C_3	91.6517	57.31	0.6098	5.290
C_4	134.518	72.99	0.6762	5.666
C_5	182.123	89.13	0.7474	5.934
C_6	234.288	106.0	0.8189	6.211
C_7	291.425	123.8	0.8869	6.507
C_8	351.590	141.8	0.9612	6.732
C_9	414.549	159.7	1.0251	6.942
C_{10}	483.153	178.6	1.0779	7.176

Table 4.9 shows the optimum parameters obtained for the normal alkanes studied in this work, while Table 4.10 exhibits the deviations from experimental saturated and critical properties, where it is possible to see that all the proper-

Table 4.10: AAD of the saturated and critical properties calculated with the $CCPA\ EoS$ for for methane to n-decane.

$Comp.$	ΔP_{sat} (%)	Δv_{liq} (%)	Δv_{vap} (%)	ΔT_c (%)	ΔP_c (%)	Δv_c (%)
C_1	2.6	3.5	1.4	0.0	0.0	0.0
C_2	2.1	3.2	1.8	0.4	0.0	0.0
C_3	2.2	2.9	1.9	0.5	0.0	0.0
C_4	2.2	2.6	1.8	0.5	0.0	0.0
C_5	2.2	2.5	1.6	0.5	0.1	0.0
C_6	2.2	2.3	1.7	0.6	0.0	1.0
C_7	2.4	1.8	1.5	0.6	0.3	2.4
C_8	2.2	1.2	1.7	0.7	0.1	4.5
C_9	2.2	1.3	1.7	0.7	0.1	5.0
C_{10}	2.2	1.1	1.4	0.6	0.8	5.5
Average	**2.2**	**1.6**	**2.3**	**0.1**	**0.4**	**1.6**

ties are precisely described by the model. The comparison of the results with Table 4.8 indicates that both models have similar behavior, and that the better description of the vapor phase volumes are due to the addition of the property in the objective function, which also affects the prediction of the critical point. In fact, as CPA reduces to SRK when there are no association species in the system, the same is valid for $CCPA$ and $CSRK$.

Following the approach performed in the last subsection, we have plotted the experimental saturated properties of n-pentane and the calculated ones using the classical $CPA\ EoS$, the mean-field (CPA_{MF}) and $CCPA$ model using the parameters given in Table 4.9 (Figure 4.14). The figure shows that the saturated pressure curve calculated with the new parameters yields inferior representation of the saturated and critical properties in comparison to the classical CPA. Nevertheless, the application of the recursive procedure with new optimized values for L and ϕ allows the correct description of the coexistence curves and the critical point, except for the critical volumes of the heavier hydrocarbons (from C_6 to C_{10}). In order to improve the representation of this property, ϕ was used as an adjustable parameter in the optimization procedure, resulting in excellent matching of v_c, while maintaining the behavior of the other properties (Table 4.12). The phase equilibria calculations for mixtures (see next chapter) were done with the parameters from C_1 to C_5 taken from Table 4.9, and from C_6 to C_{10} using the values in Table 4.11.

In addition to the estimation of the pure compound parameter for n-alkanes,

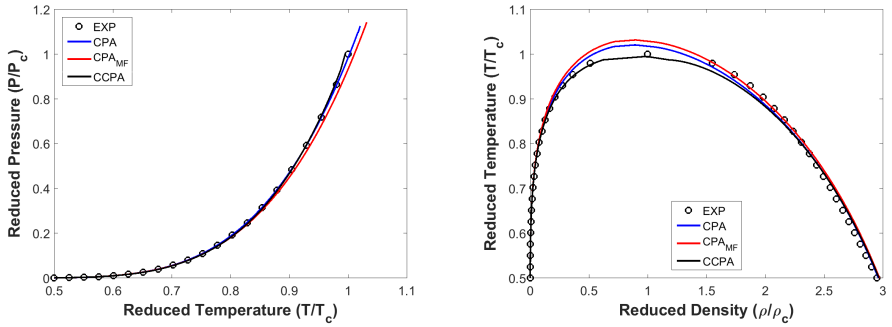

Figure 4.14: Reduced saturated pressures as a function of the reduced temperatures (a) and the reduced temperatures as a function of the reduced saturated vapor and liquid phase densities (b) for n-pentane. Experimental data were taken from the $DIPPR$ database, and the calculated curves were obtained with CPA (blue line), the mean-field term of $CCPA$ (red line) and $CCPA$ (green line).

Table 4.11: Parameters of the crossover CPA for n-hexane to n-decane using ϕ as an adjustable variable.

$Comp.$	a_0 $\left(\frac{bar.cm^6}{mol}\right)$	b $\left(\frac{cm^3}{mol}\right)$	c_1 $(-)$	L $\left(\mathring{A}\right)$	ϕ $(-)$
C_6	234.380	105.9	0.8164	6.2658	1.908
C_7	294.425	123.7	0.8869	6.664	1.746
C_8	352.788	141.6	0.9485	6.988	1.600
C_9	414.459	159.7	1.025	7.217	1.637
C_{10}	480.975	176.6	1.064	7.337	1.634

Table 4.12: AAD of the saturated and critical properties for n-hexane to n-decane using the $CCPA$ EoS with ϕ as an adjustable parameter.

$Comp.$	ΔP_{sat} $(\%)$	Δv_{liq} $(\%)$	Δv_{vap} $(\%)$	ΔT_c $(\%)$	ΔP_c $(\%)$	Δv_c $(\%)$
C_6	2.3	2.3	1.7	0.6	0.0	0.0
C_7	2.4	1.7	1.7	0.7	0.0	0.0
C_8	2.6	1.4	2.0	0.7	0.0	0.0
C_9	2.4	1.6	2.2	0.9	0.0	0.0
C_{10}	2.5	1.4	1.6	0.7	0.0	0.0

Table 4.13: $CCPA$ pure component parameters for carbon dioxide and nitrogen.

$Comp.$	a_0 $\left(\frac{bar.cm^6}{mol}\right)$	b $\left(\frac{cm^3}{mol}\right)$	c_1 $(-)$	L $\left(\mathring{A}\right)$	ϕ $(-)$
CO_2	35.797	26.91	0.6504	4.053	2.000
N_2	13.819	25.45	0.4356	4.246	2.000

Table 4.14: AAD of the saturated and critical properties for carbon dioxide and nitrogen calculated with the $CCPA\ EoS$.

$Comp.$	ΔP_{sat} $(\%)$	Δv_{liq} $(\%)$	Δv_{vap} $(\%)$	ΔT_c $(\%)$	ΔP_c $(\%)$	Δv_c $(\%)$
CO_2	2.2	1.7	0.7	0.0	0.0	0.0
N_2	2.8	3.6	1.8	0.1	0.0	0.0

other non-associating molecules, i.e. carbon dioxide and nitrogen, were evaluated with the $CCPA\ EoS$. These components are important for the correct representation of the phase behavior of natural gas, besides CO_2 is extensively used in industrial processes in near-critical and supercritical conditions. Table 4.13 shows the optimum the pure compound parameters for the species and the deviations of the critical and saturated properties are given in Table 4.14.

Figures 4.15a, 4.15b and 4.15c shows the plots of the parameters a_0, b and $c_1$for the hydrocarbons investigated in this work using CPA and $CCPA$. The comparison of the curves denotes that the trends obtained with the models are similar, and a difference in the magnitude of the values is only noticeable for c_1. Moreover, Figure 4.15c shows that the optimum values for L found for the n-alkanes follow a monotonically increasing trend. In all cases, simple linear or quadratic correlations can be used to correlate the parameters of the model.

The $CCPA\ EoS$ was also applied to normal alcohols (from methanol to n-octanol), but differently from the non-associating species, it has two additional mean-field parameters. Hence, the fitting of the saturated property curves and the critical point, as given in Equation (4.3), is done for 7 parameters, i.e. 5 from the underlying model and 2 for the recursive procedure. The values of the pure species parameters and the deviations from experimental data are shown in tables 4.15 and 4.16. The comparison of this table with Table 4.8 shows that although there is a small increase in the deviations related to

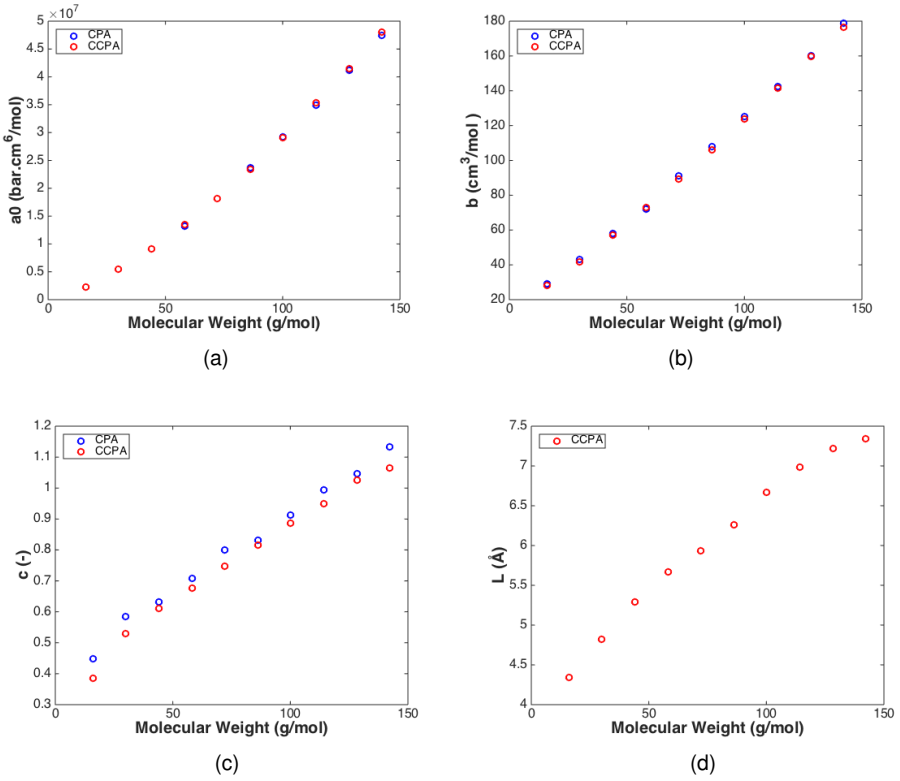

Figure 4.15: Plots of the parameters a_0 (a), b (b) and c_1 (c) as a function of the molecular weight of the hydrocarbons studied in this work using the CPA and $CCPA\ EoS$. The last figure (d), shows the trends in the cut-off length as a function of the molecular weight optimized for the n-alkanes using the $CCPA\ EoS$.

Table 4.15: Pure component parameters of the $CCPA\ EoS$ for methanol to n-octanol.

$Comp.$	a_0 $\left(\frac{bar.cm^6}{mol}\right)$	b $\left(\frac{cm^3}{mol}\right)$	c_1 $(-)$	$\varepsilon/_R$ (K)	$10^3 \cdot \beta$ $(-)$	L $\left(\mathring{A}\right)$	ϕ $(-)$
C_1OH	40.912	30.95	0.4430	2935	16.6	5.623	0.585
C_2OH	80.374	48.04	0.6820	2739	8.10	5.475	0.747
C_3OH	134.07	64.97	0.9485	2283	6.26	5.418	1.383
C_4OH	182.27	81.17	1.0243	2192	5.25	5.793	1.670
C_5OH	233.53	96.97	1.1028	2143	3.36	6.244	1.613
C_6OH	281.71	112.8	0.9944	2645	2.11	6.445	1.668
C_7OH	358.39	132.3	0.9705	3214	0.35	7.078	1.423
C_8OH	417.39	147.3	1.0730	3229	0.20	7.005	1.752

Table 4.16: AAD of the saturated and critical properties calculated with the $CCPA\ EoS$ for for methanol to n-octanol.

$Comp.$	ΔP_{sat} $(\%)$	Δv_{liq} $(\%)$	Δv_{vap} $(\%)$	ΔT_c $(\%)$	ΔP_c $(\%)$	Δv_c $(\%)$
C_1OH	1.7	1.1	3.7	0.0	0.2	0.0
C_2OH	1.0	1.0	1.1	0.8	0.1	0.4
C_3OH	1.3	1.7	1.3	0.0	0.9	0.0
C_4OH	2.7	1.7	2.0	1.2	0.9	0.4
C_5OH	2.3	2.3	2.8	0.0	1.4	0.0
C_6OH	3.5	2.3	0.5	0.0	1.2	0.0
C_7OH	2.5	1.6	1.1	0.0	0.5	0.0
C_8OH	3.4	1.5	1.5	0.0	0.4	0.0
Average	**2.3**	**1.7**	**1.8**	**0.2**	**0.7**	**0.1**

the liquid phase volume description, only the crossover model is capable of simultaneously representing the critical and phase equilibrium properties.

In addition to the calculations of the deviations of the critical and saturated properties, the parameters were used in the plot of the saturated pressure and the coexisting diagrams for the n-alkanes (Figure 4.16) and the alcohols (Figure 4.17). As previously discussed, the figures shows that both models are capable of representing the properties of the components far away from the critical point, nevertheless the introduction of the fluctuations in the mean-field model is necessary for correcting the overprediction of the critical point, as well as the coexistence curve in the vicinity of the critical point. The comparison of the two figures and the previous tables shows that the application of the recursive procedure is more important for associating components, since

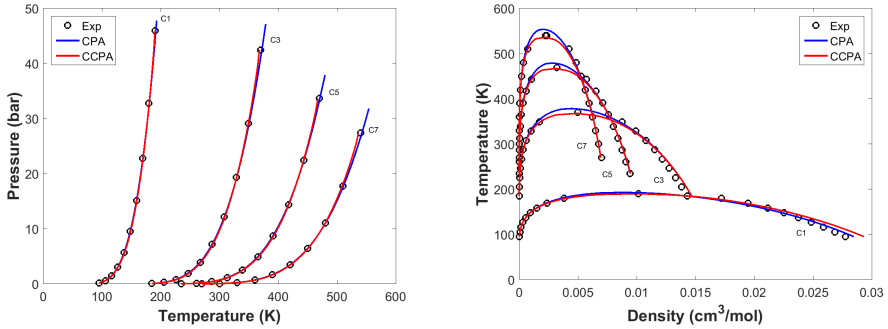

Figure 4.16: Saturation pressure as a function of temperature (a) and temperature as a function of the coexisting phases density (b) for selected n-alkanes (from methane to n-heptane). Experimental data (open circles) were taken from the $DIPPR$ database, while the blue line corresponds to the $CPA\ EoS$, the red line corresponds to the $CCPA\ EoS$.

the deviations from the mean-field are less pronounced in the non-associating species. As stated before, associating fluids have a non-ideal behavior far from the critical point, and the fitting of the saturated properties, in such conditions, with a mean-field equation results in larger deviations, for the universal, non-analytic part of the coexistence curve, i.e. the critical region.

The discrepancy in the prediction of the critical point with the classical model is better observed in Figure 4.18, which shows the critical temperatures, pressures and densities of the substances studied in this work as a function of the molecular weight. The comparison of the predictions obtained from both equations indicates that the introduction of the fluctuations in the classical EoS are especially useful for correcting the critical pressures and densities, since there is only slight overprediction of the experimental critical temperature data. Additionally, it is possible to observe that the association term deteriorates the description of the critical pressure, since the comparison of the calculated properties of alcohols and hydrocarbons with experimental data shows that the hydrogen bonding substances result in a much larger deviation in terms of P_c, and the deviations are reduced as the carbon chain length increases, due to the weakening effect of the association between molecules.

Due to the large number of pure component parameters for associating species in the $CCPA\ EoS$, two additional optimization procedures were performed. In the first one, the association volume (β) was considered constant

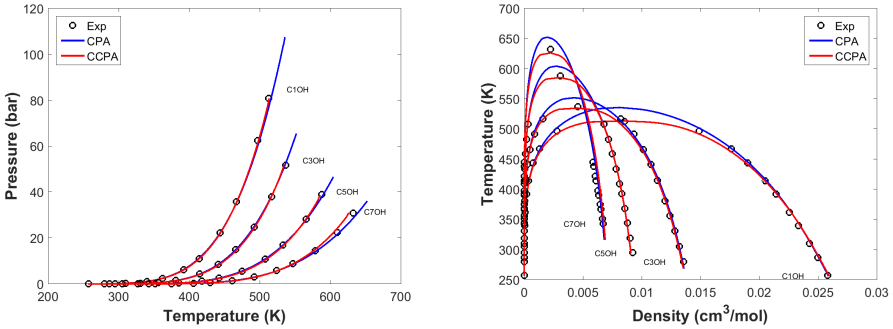

Figure 4.17: Saturation pressure as a function of temperature (a) and temperature as a function of the coexisting phases density (b) for selected alcohols (from methanol to 1-heptanol). Experimental data (open circles) were taken from the $DIPPR$ database, while the blue line corresponds to the $CPA\ EoS$, the red line corresponds to the $CCPA\ EoS$.

and equal to 0.006. In this case, the deviations in the saturated pressure and critical volumes were bigger than the ones obtained with the parameters from Table 4.15. In the second procedure, the association energy (ε/R) was set equal to 2586K, and although similar deviations were obtained in comparison to the approach using all parameters as adjustable values, non-smooth trends of the pure compound parameters were obtained, thus the values in Table 4.15 were used for the calculation of the phase behavior of mixtures.

Aside from the parametrization of n-alkanols, the determination of the pure component parameters of water and hydrogen sulfide were considered in this work. Table 4.17 shows the optimum values of the $CCPA$ pure component parameters, while Table 4.18 exhibits the deviations obtained for the different saturated and critical properties. It can be concluded from the comparison of tables 4.17 and 4.1 that the mean-field parameters for H_2S are nearly the same as the ones found in the literature for CPA; nevertheless, this is not the case for H_2O due to the highly non-ideal behavior of this substance. In fact, a major modification of the pure compound parameters was necessary for the correct representation of the critical and saturated properties with the $CCPA$ EoS, in comparison to the other associating molecules.

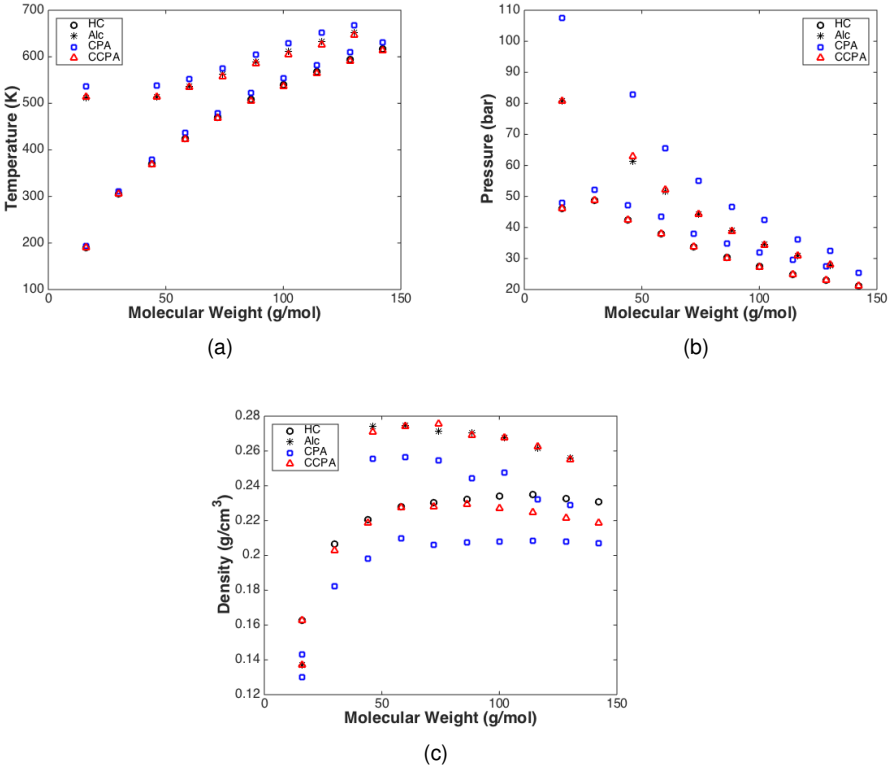

Figure 4.18: Experimental critical temperature (a), pressure (b) and density (c) as a function of the molecular weight of the n-alkanes (open circles) and n-alcohols (asterisk) studied in this work. The calculated critical properties were obtained with the CPA (blue squares) and the $CCPA$ (red triangles) EoS, while the experimental data were taken from the $DIPPR$ database.

Table 4.17: Pure component parameters of the $CCPA$ EoS for water and hydrogen sulfide.

$Comp.$	a_0 $\left(\frac{bar.cm^6}{mol}\right)$	b $\left(\frac{cm^3}{mol}\right)$	c_1 $(-)$	ε/R (K)	$10^3 \cdot \beta$ $(-)$	L $\left(\AA\right)$	ϕ $(-)$
H_2O	22.292	15.15	0.4387	1913	39.3	1.497	2.35
H_2S	41.981	29.32	0.4427	628.9	39.6	4.296	2.0

Table 4.18: AAD of the saturated and critical properties for water and hydrogen sulfide, calculated with the $CCPA\ EoS$.

$Comp.$	ΔP_{sat} (%)	Δv_{liq} (%)	Δv_{vap} (%)	ΔT_c (%)	ΔP_c (%)	Δv_c (%)
H_2O	2.4	2.8	2.2	3.8	0.0	0.1
H_2S	2.3	1.0	1.0	1.0	0.2	0.0

4.4 Calculation of the critical exponents with the $CCPA\ EoS$

The calculation of the critical exponents is another important test, in order to evaluate the capacity of the crossover model to describe the non-analytical behavior of the thermodynamic properties of real fluids in the vicinity of the critical point. Figure 4.19 shows the plots of the difference between the saturated liquid and vapor densities divided by the critical density as a function of the dimensionless distance to the critical temperature, as well as the dimensionless distance to the critical chemical potential as a function of the dimensionless distance to the critical density for 1-propanol. In the first case the slope of the curve represents the critical exponent β, while in the second case the slope represents the critical exponent δ. The classical values for these two exponents is 0.5 and 3.0, while the ones obtained in the calculations were 0.369 and 4.828, respectively, which are close to the universal values 0.326 and 4.8 [64]. Similar calculations were performed for other mean-field models and critical exponents [54, 58, 98], indicating that the recursive procedure developed by White yields the correct representation of the non-analytical/asymptotic behavior of fluids in the critical region; besides, it is independent on the underlying classical EoS.

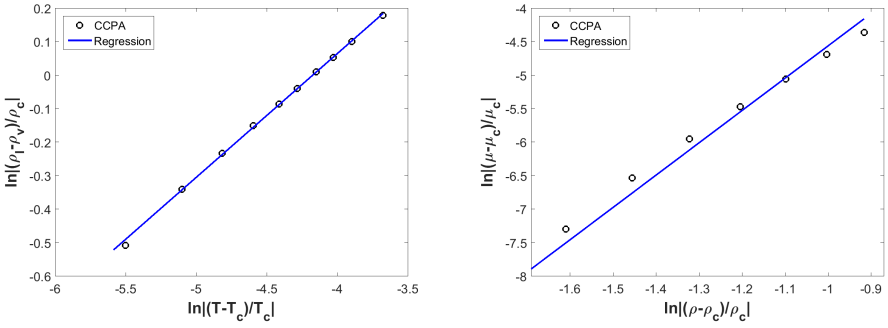

Figure 4.19: Critical exponents β (a) and δ (b) calculated for 1-propanol using the $CCPA\ EoS$ (open circles) and the regressed curve (blue line).

Chapter 5

Results: Mixtures

This chapter is dedicated to the evaluation of the thermodynamic models in the representation of mixtures studied in different regions of the phase diagram. The analysis is done by the comparison of the mean-field and crossover models with experimental data in an attempt to estimate their capacity to represent the phase behavior of the systems in regions close to and far away from the critical points.

The first section is divided into two parts, where the first one is concerned with the results for the VLE region for non-associating species and the second one is for mixtures with associating species. In both cases, we compare the representations obtained with the classical thermodynamic models, namely SRK and CPA, with its crossover versions using White's approach. Similarly, the following section shows the comparisons for mixtures containing associating species in the LLE region. Finally, the chapter ends with the results and the discussion of the results for the critical line calculations with systems containing non-associating and associating components.

5.1 Vapor-Liquid Equilibria

The results obtained in the previous chapter are interesting in a sense that they indicate the limitations of the classical models to describe the phase behavior of pure components, and how these limitations can be overcome with a procedure for including long-range interactions onto the traditional thermodynamic models. Nevertheless, pure compounds are rarely used as fluids in

industrial processes, and the behavior of a component in a mixture can be remarkably different from the pure species. In the next subsections, we show the results obtained with the models evaluated in this thesis for the VLE region, starting with mixtures of non-associating components, following with mixtures containing associating components.

5.1.1 Binary systems containing non-associating species

The evaluation of the models cited previously to describe the phase equilibrium of binary mixture starts with calculations in the VLE region of binary mixtures containing n-alkanes. It is usually assumed that the phase behavior of mixtures containing n-alkanes can be predicted by classical cubic EoS without the application of interaction parameters ($k_{ij} = 0$ and $l_{ij} = 0$) [134]. Still, the typical modeling approach in the oil & gas industry, for obtaining an improved representation of the properties of such mixtures, is to use a non-zero binary interaction parameter for the constant in the attractive term ($k_{ij} \neq 0$) and a linear mixing for the co-volume ($l_{ij} = 0$). Such assumptions are valid for mixtures containing components of similar size or energetic interactions. In fact, acceptable descriptions of experimental phase equilibrium data is observed for binary mixtures of methane or ethane with higher alkanes up to n-decane (C_{10}) [135].

In the case of very asymmetric mixtures, e.g. systems composed of methane and n-eicosene or heavier n-alkanes, equations of state like SRK with traditional mixing rules yield high deviations in the VLE region even with the use of an optimized k_{ij} [136]. Furthermore, RG corrections to the mean-field EoS only substantially modify the behavior of the model close to the critical point, meaning that the underlying model will keep its features for the computations far from the critical region [54]. Since the recursive procedure is not capable of improving the limitations of the mean-field equation far from the critical point, this work will focus on the calculations for systems where asymmetric interactions do not play a major role. Therefore, systems with a light component (methane, carbon dioxide and methanol) and n-alkanes heavier than C_{10} will not be considered.

An example of the predictive capability of the investigated models for ideal hydrocarbon mixtures far from the critical point is given in Figure 5.1. The plot shows the pressure-composition diagram of n-heptane/n-octane system at 313.15K, and the comparison of the results with experimental data indicates

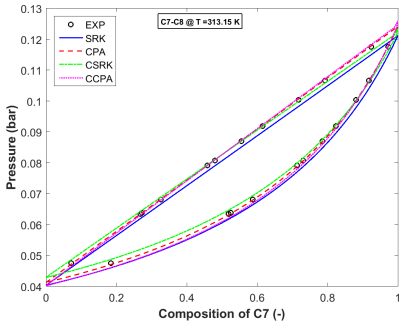

Figure 5.1: Pressure-composition diagram for the n-heptane/n-octane system. The experimental data were taken from [6] and the curves were calculated using the SRK, CPA, $CSRK$ and $CCPA$ EoS.

that the mean-field EoS, i.e. the SRK and CPA EoS, and their crossover versions are capable of correctly predicting the bubble point pressures and the compositions of the vapor phase, which were calculated with the algorithm given in Appendix B. Additionally, it was observed from this and other calculations that $CSRK$ behaves like $CCPA$ when no associating components are present. This is due to the fact that both models have the same number of parameters and that the recursive procedure is independent of the underlying model. Therefore, as CPA reduces to SRK when no hydrogen bonding molecules are in the system, the same is valid for $CCPA$ and $CSRK$. Since the two models are equivalent for the representation of inert species, as the input parameters are regressed from saturated pressure and density data, and $CCPA$ is capable of taking into account hydrogen bonding between the molecules in the systems, this work will only compare the latter equation with the mean-field models from now on. Additionally, the similarity of the results in this and other sections with the ones obtained in [5] is another indication of the equivalence of the models, as long as no associating components are present in the mixture.

The assessment of the models with respect to the representation of the VLE of binary mixtures of hydrocarbons was done by taking as reference the methane/n-alkane series. This approach is found in several works in the literature [91, 93, 106, 135, 136], since the accurate description of the properties of this series is more challenging than the one containing heavier hydrocarbons [136], besides it goes through several phase type behaviors according to van Konynenburg and Scott classification [2] (see section 5.3).

The first system in the VLE region studied in this work is the methane/ethane mixture. Figure 5.2 shows the predicted phase envelopes using the SRK, CPA and $CCPA\ EoS$, and the experimental data at three different temperatures: 200K, 250K, and 280K. For the lowest temperature, i.e. 200K, it is possible to conclude that the three models are capable of predicting the experimental saturation pressures and vapor compositions. With the increase of temperature, it can be seen that the two-phase region predicted by the CPA EoS is much larger than the experimental one, and the deviations increase substantially as the critical point is approached (Figure 5.2b). In order to correct this behavior, White's recursive procedure is applied to the mean-field model, which improves the representation in the critical region and allows a prediction similar to the one obtained with SRK (figures 5.2a and 5.2c). The results for the $C_1 - C_2$ system indicates that, as mentioned previously for the $C_7 - C_8$ system, far from the critical point, the mean-field and non-mean-field equations are equivalent; nonetheless, as the critical point is reached, the crossover model modifies the behavior of the CPA and reduces the overprediction of the critical points, which also affects the phase behavior in the critical region. This correction is more pronounced for the regions with a high content of the heavier component since the overestimation of T_c and P_c increases with the molecular weight of the pure n-alkane.

The increase in the asymmetry with respect to the molecular weight of the components in the system leads to more complex phase behaviors, which in turn deteriorate the performance of the classical models to predict the VLE data of the mixtures. An example is observed in Figure 5.3, where the phase envelopes were calculated with $k_{ij} = 0$ (solid lines) and interaction paramaters optimized with phase equilibrium data (dash-dot lines). The comparison of the results with the measured points indicates that the models predict a lower bubble point pressure when the k_{ij} are equal to zero. The application of non-zero k_{ij} improve the representation of this property, but an inferior description of the critical point is attained.

With the aim to further assess the performance of the EoS, phase equilibrium calculations were performed for several binary methane/n-alkane mixtures (methane/propane to methane/n-decane). The increase in the molecular weight of the second hydrocarbon, i.e. the increase in the asymmetry of the systems, creates difficulties for the correct modeling of the experimental data. This effect can be seen in Figure 5.4, which exhibits the VLE diagram for the methane/n-heptane system at 311K, 444K, and 510K. This plot shows that

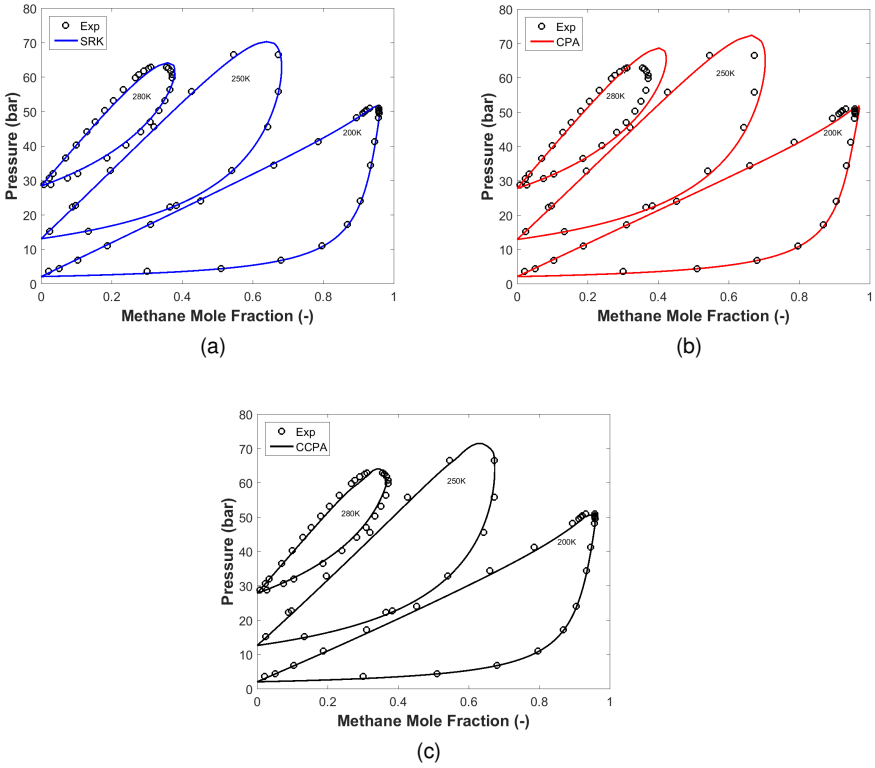

Figure 5.2: Experimental VLE diagram of the methane/ethane (open circles) and the predictions ($k_{ij} = 0$) using the $SRK\ EoS$ (a), the $CPA\ EoS$ (b) and the $CSRK\ EoS$ (c) for three different temperatures (200K, 250K and 280K). The experimental data were taken from [7] and [8].

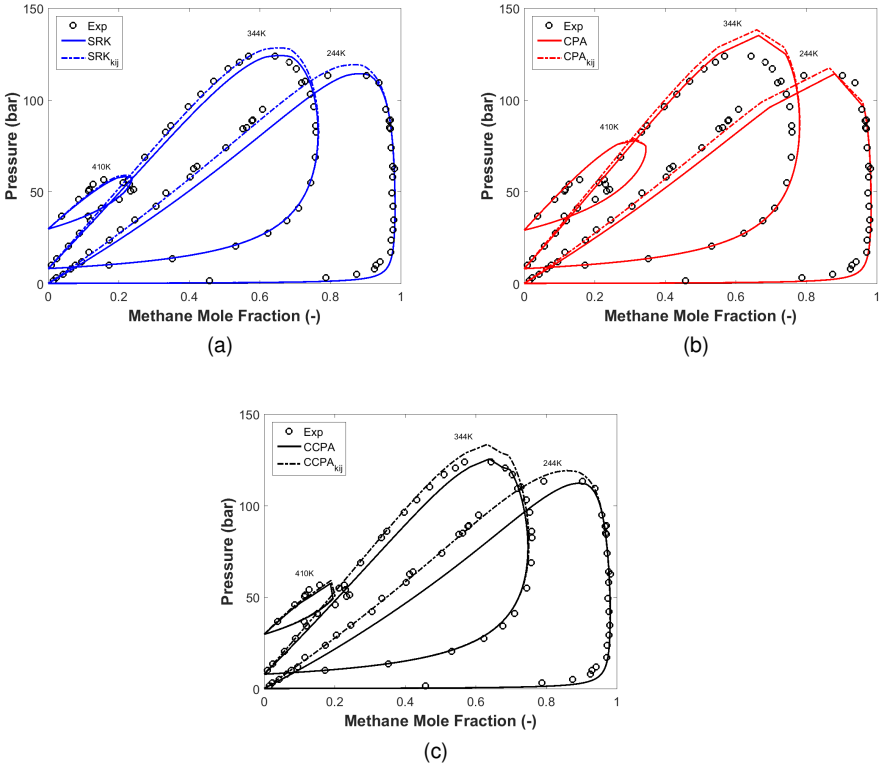

Figure 5.3: Experimental VLE diagram of the methane/n-butane (open circles) and the predicted (solid lines) and correlated (dash-dot lines) phase envelopes using the $SRK\ EoS$ (a), the $CPA\ EoS$ (b) and the $CCPA\ EoS$ (c) for three different temperatures. The experimental data were taken from [9, 10].

the increase in the asymmetry of the systems reduces the accuracy of the models, in comparison with the predictions for the $C_1 - C_2$ system. In fact, for quantitative description of the phase equilibrium properties, the use of k_{ij} is necessary.

The calculation of the interaction parameters was done by the minimization of the objective function represented by the following expression:

$$OF = \frac{1}{N}\sum_{i=1}^{N}\left|\frac{P_b^{calc} - P_b^{exp}}{P_b^{exp}}\right| + \frac{1}{N}\sum_{i=1}^{N}\left|\frac{y_1^{calc} - y_1^{exp}}{y_1^{exp}}\right| \tag{5.1}$$

where P_b is the bubble point pressure and y_1 is the composition of methane in the vapor phase, the subscripts $calc$ and exp represent calculated and experi-

mental values, respectively, and N is the number of experimental points.

Figure 5.4 shows the correlations for the system $C_1 - C_7$ with the SRK, CPA and $CCPA\ EoS$. Excellent descriptions of the experimental data are achieved far from the critical point; however, all the models show an over-prediction of the critical point, in particular for the $CPA\ EoS$ at higher temperatures (410K and 510K). In both cases, the $CCPA\ EoS$ presents a smaller phase envelope, yet at 510K negative deviations of the composition of methane in the vapor phase are observed close to the critical point. This is an indication that a modification of the linear mixing rules for the crossover parameters might be relevant for an improved representation of the phase behavior close to the critical point.

Table 5.1 shows the AAD for all the binary methane/n-alkane systems studied in this work at different temperatures and the overall average deviation. The calculation of the errors was done by comparing the bubble point pressures (ΔP_b) and the composition of methane in the vapor phase (Δy_1), computed with the optimum k_{ij}, with the experimental data given in the reference column. The results show that the three models correctly correlate the bubble point pressures and methane compositions, although the $CCPA\ EoS$ is slightly superior to the two approaches of the mean-field model. Since most of the experimental data used in the comparisons are far from the critical point, it is difficult to evaluate the improvement achieved with the introduction of the density fluctuations in the mean-field model. Anyhow, the similarity of the correlations attained with the crossover model, in comparison to the $SRK\ EoS$, denotes the importance of the RG corrections, if the CPA is used to model systems of hydrocarbons in a wide range of temperature conditions. Furthermore, the evaluation of the binary interaction coefficients in Table 5.1 shows that the k_{ij} values do not have a specific trend and that CPA requires smaller for correlating VLE data in comparison to the other equations, while $CCPA$ has the larger ones. However, it is important to note that the intention of this work was mainly to compare the thermodynamic models, but a careful analysis of the experimental data and the objective function can yield semi-predictive equations that correlate the binary interaction parameters and the properties of the series, e.g. the molecular weight of the hydrocarbon [136].

In spite of its seemingly simplicity, the phase behavior of the methane/n-alkane series can be remarkably challenging for the accurate representation over a wide range of temperatures, especially for very asymmetric systems in the high-pressure ranges. In fact, most of the articles in the literature, dealing

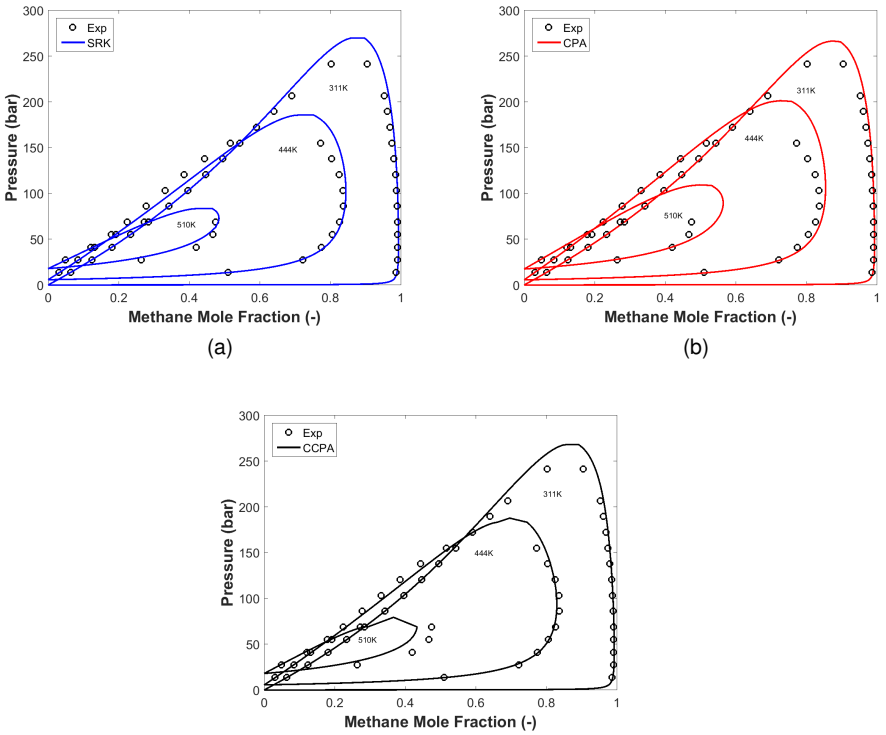

Figure 5.4: Experimental VLE diagram of the methane/n-heptane (open circles) and the correlated phase envelopes ($k_{ij} \neq 0$) using the $SRK\ EoS$ (a), the $CPA\ EoS$ (b) and the $CCPA\ EoS$ (c) for three different temperatures. The binary interaction parameters are given in Table 5.1 and the experimental data were taken from [11].

Table 5.1: Average AAD of the bubble point pressure and composition of methane in the vapor phases for binary methane/n-alkane systems (methane/ethane to methane/n-decane) for several temperatures calculated using the SRK, the CPA and $CCPA$ EoS.

System	ΔP_b (%)			Δy_1 (%)			k_{ij}			T (K)	$Ref.$
	SRK	CPA	$CCPA$	SRK	CPA	$CCPA$	SRK	CPA	$CCPA$		
$C_1 - C_2$	2.1	2.2	2.0	2.5	2.4	2.9	0.0028	0.0008	0.0119	200 250 280	[7, 8]
$C_1 - C_3$	1.5	1.3	2.0	7.7	4.5	7.9	0.0229	0.0113	0.0237	280 328 361	[137]
$C_1 - C_4$	3.2	3.5	2.8	6.4	9.5	6.6	0.0309	0.0221	0.0526	244 344 410	[9, 10]
$C_1 - C_5$	2.6	2.0	1.5	3.0	3.4	2.3	0.0252	0.0105	0.0379	278 378 411	[138]
$C_1 - C_6$	5.8	5.0	5.0	3.6	5.3	2.2	0.0252	0.0105	0.0281	311 378 444	[139]
$C_1 - C_7$	3.4	3.4	2.1	4.0	4.1	4.9	0.0222	0.0051	0.0332	311 444 510	[11]
$C_1 - C_8$	2.3	1.3	1.7	0.4	0.2	0.5	0.0409	0.0152	0.0500	298 348 423	[140]
$C_1 - C_9$	2.5	4.7	2.4	0.6	0.5	0.5	0.0363	0.0113	0.0383	298 348 423	[140]
$C_1 - C_{10}$	3.0	6.3	3.1	0.7	1.5	0.7	0.0395	0.0133	0.0372	311 444 510	[141]
Avg.	**2.9**	**3.3**	**2.5**	**3.2**	**3.5**	**3.2**	**-**	**-**	**-**	-	-

with mean-field equations, do not cover such ranges [136], and in the case of models that apply the RG treatment to correct mean-field EoS even fewer comparisons are found. Llovell and Vega [106] have investigated different n-alkane/n-alkane systems in the VLE and other equilibrium regions; however for the methane/n-alkane series the results were obtained only for the $C_1 - C_6$ system. The authors obtained an excellent description of the subcritical and critical properties, with the introduction of the density fluctuations in the $Soft - SAFT\ EoS$, and similar conclusions were achieved, regarding the importance of the RG corrections for models that overpredict the critical properties of the pure components, which in this work is CPA. This is an important result, nevertheless further investigations for systems with heavy n-alkanes, e.g. C_{20} to C_{36}, are fundamental for the understanding of the limitations of the crossover models.

In addition to the calculations of the phase equilibrium in the VLE region of methane/n-alkane systems, this work also contains the evaluation of the models for binary mixtures composed of carbon dioxide. The understanding and modeling of the phase behavior of systems containing carbon dioxide are fundamental for the rational design and operation of many processes [142]. Therefore, in addition to the evaluation of the methane/n-alkane series, this thesis also comprises the study of the CO_2/n-alkane homologous series. From the academic point of view, this is series is sometimes taken as reference in the analysis of other mixtures containing non-alkanes and carbon dioxide [143]. In the case of technological applications, CO_2 is used in several industries, e.g. as a method for enhanced oil recovery, in which supercritical CO_2 is injected in order to increase the oil recovery in depleted oil wells [144]. In the chemical industry, supercritical fluid extraction is a promising method for substituting traditional methods like distillation and liquid-liquid extraction, e.g. the recovery of alcohols [145] and the removal of compounds like phenols [146] from aqueous solutions.

Apart from the importance of mixtures containing carbon dioxide, the accurate modeling of such systems is challenging and it is a not fully solved problem of physical chemistry [143]. In the case of the CO_2/n-alkane series, it is important to mention that carbon dioxide has a large quadrupolar moment [147], while n-alkanes are non-polar. Besides, the complexity of the phase behavior increases with the molecular weight of the hydrocarbon. Hence, the correct simulation of processes containing such mixtures requires models that are able to account for the non-idealities, i.e. asymmetry in molecular weight

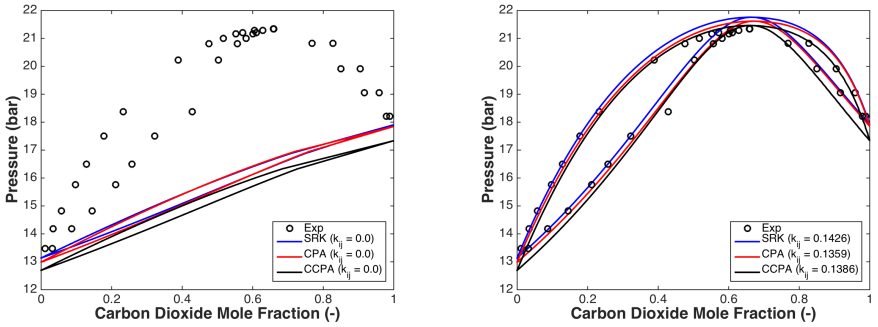

Figure 5.5: Experimental VLE diagram of the $CO_2 - C_2$ at 250K (open circles) and the predicted ($k_{ij} = 0$) curves (a) calculated with the SRK EoS (blue line), the CPA EoS (red line) and the $CCPA$ EoS (black line) and the correlated curves (b) using the same models. The experimental data were taken from [12].

and energetic interactions.

The comparison of the models evaluated in this work starts with the calculations in the VLE region. Due to the reasons mentioned previously, the prediction ($k_{ij} = 0$) of the phase equilibrium properties of CO_2/n-alkane systems is difficult for cubic and non-cubic EoS. As observed by other authors [142, 148], large k_{ij} are necessary for equations like the SRK and CPA EoS for the qualitative and quantitative representation of the VLE of such mixtures. Figure 5.5 shows the calculated $P - x$ diagram of CO_2 and ethane at 250K using SRK, CPA and $CCPA$, along with the experimental data. It can be concluded from the first plot (Figure 5.5a) that the models are incapable of predicting the azeotropic behavior of the system. Additionally, the introduction of density fluctuations in the mean-field model only modifies the near-critical behavior, thus $CCPA$ is not qualitatively different from CPA far from the critical region, and the differences in the curves are due to the change of the pure component parameters as specified in the previous chapter.

On the hand, the application of a temperature independent k_{ij}, obtained by minimizing Equation (5.1) for different conditions given in Table 5.2, allows the accurate representation of the VLE and the description of the azeotrope pressure and composition (Figure 5.5b). As indicated in the table, the values for the interaction are large, but in accordance with the magnitude (around 0.12 to 0.15) estimated in other works [142]. In fact, the prediction of the

properties of this system can only be achieved if a term that explicitly takes into account the quadrupolar moment is added to the model [148]. Nevertheless, except for the difference in the interaction parameter, the representations of the VLE for this and other systems in the series with the quadrupolar CPA ($qCPA$) are similar to the classical one.

The evaluation of the series continues in Figure 5.6, where the calculated and experimental phase equilibrium properties of the $CO_2 - C_1$ system are plotted. Similar to the previous representation, large k_{ij} values, obtained from the minimization of Equation (5.1), were needed for the precise description of the bubble point pressure and vapor phase compositions. The comparison of the curves with the measured data indicates that the three models are equally capable of describing the phase behavior of this system for the different temperature conditions (230K, 250K and 270K). The main difference is that the $CPA\ EoS$ (Figure 5.6b) predicts a larger two-phase region than the other two models. This effect is corrected by the non-mean-field model (Figure 5.6c), and it can be seen from the graphs especially close to the region of the minimum composition of CO_2 in the liquid phase. Nonetheless, these corrections are not substantial for this mixture because the overprediction of the pure components critical point with the $CPA\ EoS$ is small and the interaction parameters have a major role in the correlation of the properties.

The importance of introducing long-range interactions to the $CPA\ EoS$ can be seen in Figure 5.7. The comparison of figures 5.7b and 5.7c point out the modification of the phase envelopes, especially close to the critical point. It can also be seen that as the temperature increases the two-phase region becomes smaller, thus increasing the deviations with respect to the $CPA\,EoS$. The correlations obtained from SRK and $CCPA$ are similar, except for the highest temperature, i.e. 411K, in which the crossover model yields a smaller phase equilibrium region in comparison to the measured points. Nevertheless, the overall deviations are similar, as shown in Table 5.2.

The complexity of the description of the phase behavior increase with the asymmetry between the molecules. In fact, a LLE region appears from n-decane to heavier alkanes [149], and this behavior is believed to be due to the quadrupolar moment of CO_2 [148]. The calculations for the mixture of CO_2 and C_{10} in the VLE region indicates that the three models are able to reproduce the experimental data, (Figure 5.8) at least for the temperatures investigated, i.e. 373K and 444K. In these cases, the crossover CPA and the classical one, figures 5.8b and 5.8c, are equivalent and the improvement

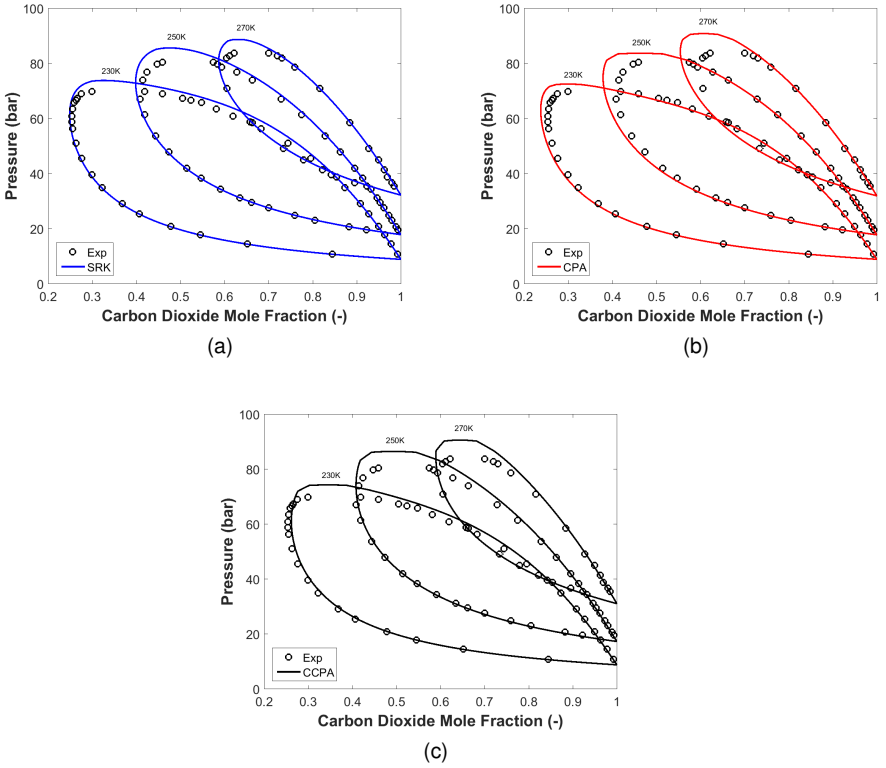

Figure 5.6: Experimental VLE diagram of the $CO_2 - C_1$ (open circles) at 230K, 250K and 270K, and the correlated curves (k_{ij} given in Table 5.2) using the $SRK\ EoS$ (a), the $CPA\ EoS$ (b) and the $CCPA\ EoS$ (c). The experimental data were taken from [12].

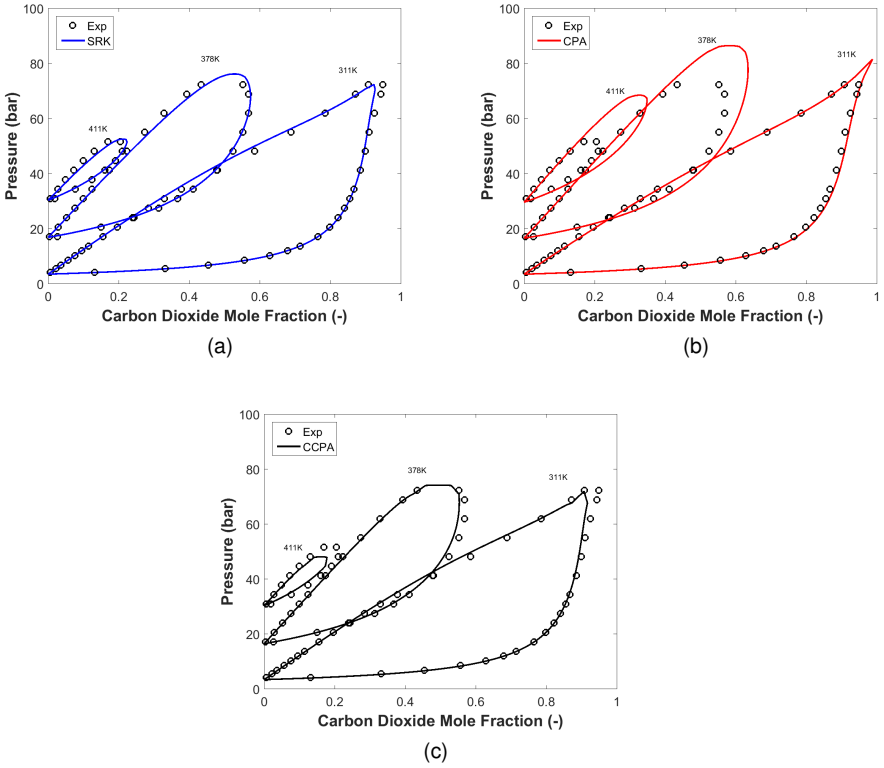

Figure 5.7: Experimental VLE diagram of the $CO_2 - C_4$ (open circles) at 311K, 378K and 411K, and the correlated curves (k_{ij} given in Table 5.2) using the $SRK\ EoS$ (a), the $CPA\ EoS$ (b) and the $CCPA\ EoS$ (c). The experimental data were taken from [13].

of the application of the RG procedure is not observed. As it will be discussed in the section related to the evaluation of critical lines, the $CCPA$ corrects the behavior of the mean-field model, improving the results when the k_{ij} is zero; however, the use of interaction parameters obtained from the region of high concentration of CO_2 and low temperatures, as done in this work, increase the deviation of the critical points with respect to the experimental measurements. The same behavior is observed for the other two equations and it is an evidence that the behavior of such asymmetric system is different in the two limits of infinite dilution [150]. The accurate prediction of the VLE along with other types of phase equilibria (LLE and $VLLE$), in the entire range of carbon dioxide composition, can be achieved, for example, with the use of more complex mixing rules [151].

The AAD of the CO_2/n-alkane series investigated in this work is summarized in Table5.2. This table shows the deviations with respect to the bubble pressure (ΔP_b) and the composition of CO_2 in the vapor phase (Δy_1). In addition, it gives the values of the temperature independent binary interaction parameters optimized for the different phase envelopes in the VLE region. The comparison of the average deviations shows that the models are similar in terms of the correlation of both properties, although SRK is slightly superior to the two models. The reason for this similarity is that most of the data found are in conditions far from critical, where the three models are equivalent, since they reduce to the same expression, being the only exception the pure component parameters. Besides, in all cases, CO_2 is treated as an inert component, which means that the main correction for the quantitative representation of the data is related to the use of large k_{ij}. Indeed, the comparison of the values of the interaction parameters show that they are in the same range, although the optimum values for the $CPA\ EoS$ are marginally smaller, plus further analysis should be carried out for the development of correlations of the k_{ij} with respect to the carbon number of the n-alkane.

In addition to the comparison of the bubble pressure and composition of the CO_2 in the vapor phase of the series in the VLE region, this work contains the evaluation the density of the phases in equilibrium for the systems $CO_2 - C_4$ at the temperatures given in Table 5.2 and the mixture $CO_2 - C_{10}$ at $377K$. As discussed in [143], a limited amount of published density data is available in the literature, in comparison to compositional data. Nevertheless, these two systems can be used to infer the ability of the models to predict the density of the phases in equilibrium. The word prediction is used here as density data

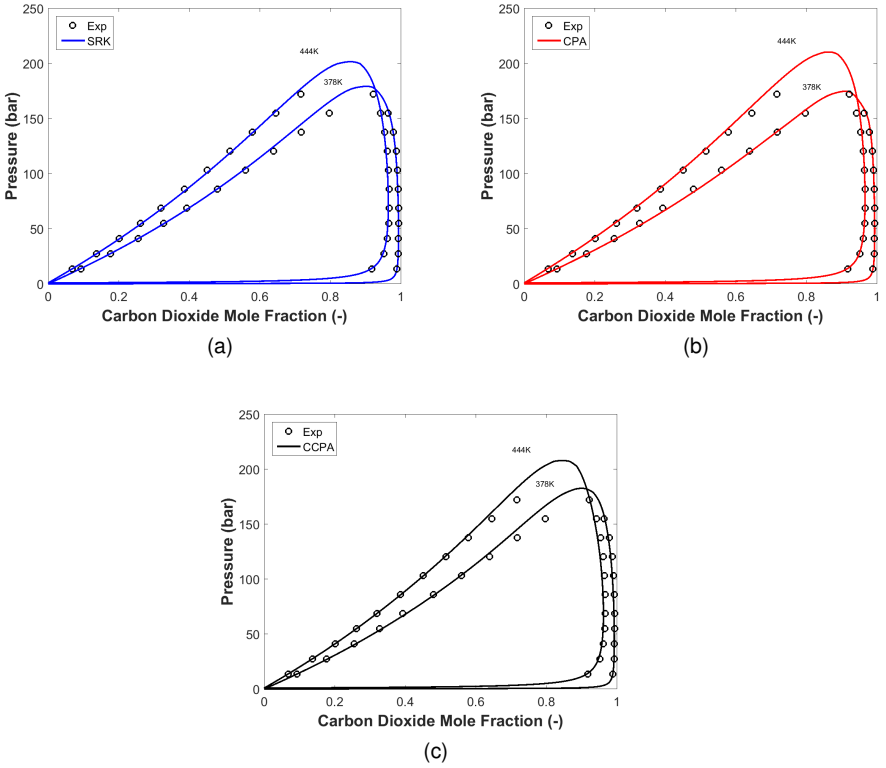

Figure 5.8: Experimental VLE diagram of the $CO_2 - C_{10}$ (open circles) at 378K and 444K, and the correlated curves (k_{ij} given in Table 5.2) using the $SRK\ EoS$ (a), the $CPA\ EoS$ (b) and the $CCPA\ EoS$ (c). The experimental data were taken from [13].

Table 5.2: Performance of the SRK, CPA and $CCPA$ EoS for the correlation of the CO_2/n-alkane binary systems in the VLE region and the optimized k_{ij} from VLE experimental data. The experimental data used for the calculation of the deviations are given in reference column.

System	ΔP_b (%)			Δy_1 (%)			k_{ij}			T (K)	$Ref.$
	SRK	CPA	$CCPA$	SRK	CPA	$CCPA$	SRK	CPA	$CCPA$		
$CO_2 - C_1$	1.7	1.1	2.6	2.2	4.8	2.2	0.1055	0.0854	0.1056	230 250 270	[12]
$CO_2 - C_2$	1.2	1.0	1.4	2.7	2.5	2.8	0.1426	0.1359	0.1386	230 250 270	[12]
$CO_2 - C_3$	4.7	4.6	4.6	2.5	2.9	2.2	0.1474	0.1413	0.1521	230 270	[152]
$CO_2 - C_4$	2.1	1.9	2.1	5.7	7.8	5.7	0.1455	0.1199	0.1460	311 411 459	[13]
$CO_2 - C_5$	1.4	1.5	3.1	4.5	3.4	5.1	0.1391	0.1144	0.1381	394 458	[153]
$CO_2 - C_6$	2.2	2.3	2.4	0.8	1.3	0.9	0.1420	0.1229	0.1375	313 393	[154]
$CO_2 - C_7$	1.0	3.9	2.1	3.5	1.4	4.2	0.1128	0.0944	0.1149	353 477	[155]
$CO_2 - C_8$	6.3	4.4	6.1	0.4	0.4	0.2	0.1473	0.1255	0.1397	322 372	[156]
$CO_2 - C_9$	1.9	3.8	2.9	0.3	0.3	0.6	0.1135	0.0844	0.1150	344 419	[157]
$CO_2 - C_{10}$	1.8	2.4	2.1	0.2	0.1	0.5	0.1257	0.0919	0.1162	378 444	[14]
Avg.	**2.4**	**2.7**	**2.9**	**2.3**	**2.5**	**2.4**	**-**	-	-	-	-

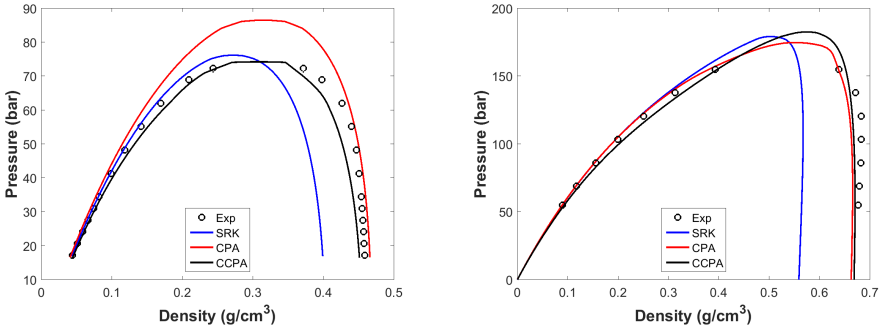

Figure 5.9: Pressure-density diagram at 337K for the $CO_2 - C_4$ (a) and $CO_2 - C_{10}$ systems. The curves were calculated with the SRK (blue line), CPA (red line) and $CCPA$ (black line) EoS, using k_{ij} given in Table 5.2, and the experimental data (open circles) was taken from [13] and [14], respectively.

was not used in the correlation of the interaction parameters.

Figure 5.9 show isothermal liquid-vapor equilibrium density curves for the systems $CO_2 - C_4$ and $CO_2 - C_{10}$ at 377K. It can be seen that the SRK EoS cannot correlate the liquid densities, a similar behavior to one observed in the calculations of the pure components. On the other hand, both CPA and $CCPA$ are capable of describing this property. Additionally, it can be concluded from Figure 5.9a that the crossover procedure corrects the overestimation of the two-phase region predicted by CPA; however, due to the reasons aforementioned, this change is not seen in the second plot. The AAD for all the systems studied in the prediction of the densities is 9.5% for SRK, 7.3% for CPA and 6.2% for $CCPA$. This shows that the non-mean-field model is slightly superior to the CPA EoS for the systems studied, but since most of the data is far from the critical region, a better improvement is not observed. A wider comparison of the volumetric properties will be presented in the next section regarding the calculation of the critical lines, where it shows the comparison of the models for the representation of the critical volume.

In summary, the modeling of the VLE region for mixtures containing carbon dioxide and a n-alkane (from $CO_2 - C_1$ to $CO_2 - C_{10}$) have shown that the SRK and CPA EoS, as well the crossover version of the last model, are capable of precisely describing the phase equilibrium properties of the systems studied, as long as a non-zero k_{ij} is applied in the calculations. It was also seen that the incorporation of the density fluctuations in the mean-field

model is important for correcting the size of the phase envelope yielded by the $CPA\ EoS$, especially for the cases in which the composition of the hydrocarbon is high. The comparison of the results with experimental data points out that the difficulty of modeling the phase behavior increases with the asymmetry between the molecules of the system. This phenomenon has been extensively discussed in the literature, and the accurate representation of the CO_2/n-alkane mixtures, especially with n-tetradecane or heavier n-alkanes, is a major challenge regarding the representation of the different phase behavior (VLE, $VLLE$ and LLE) and critical lines in a wide range of conditions. Polishuk et al. [94] used a four parameter EoS with temperature dependent binary repulsive (l_{ij}) and attractive (k_{ij}) parameters, and, although a good representation of the liquid-vapor part of the critical lines was attained, an overestimation of the size of the liquid-liquid region was observed. Additionally, it yielded an overestimation of the mole fractions of CO_2 in the liquid phase of the $VLLE$ region. Vitu et al. [158] used a group-contribution function for temperature-dependent k_{ij} and obtained good results for mixtures with n-alkanes with low to moderate molecular weight; nonetheless, the model failed to quantitatively describe the behavior of systems containing heavy n-alkanes (C_{14} or heavier). Fu et al. [159] presented satisfactory correlations using $PC-SAFT$ for CO_2 with light and heavy hydrocarbons, but only for low temperatures. Cismondi et al. [143] managed to obtain quantitative representations of different phase equilibria and critical lines of the series containing the CO_2-C_1 system to CO_2-C_{36} using the $RKPR\ EoS$ [76] and a cubic mixing rule with 8 additional interaction parameters. Due to the flexibility of the model, a systematic procedure for the estimation of the parameters is necessary. In conclusion, these works show that the phase behavior of the series is remarkably complex and, although the application of the RG procedure is useful for improving some imperfections of the classical models, other approaches are necessary for the accurate representation of different phase behavior in a wide range of conditions for the entire series.

5.1.2 Binary systems containing associating species

The accurate description of the phase behavior of systems containing associating components using EoS was a challenge until the mid-1980s and the beginning of the 1990s when terms for explicitly taking into account the hydrogen bond between molecules were incorporated into equations of state [43].

Without the use of an association term or local composition mixing rules [38], the thermodynamic models are unable to correlate the experimental data of systems containing molecules like methanol.

Figure 5.10 shows the VLE diagrams of the methanol/n-hexane and methanol/n-heptane systems far from the critical point, i.e. at T equal to 333.15K and 298.15K, respectively. In the first figure, the classical $SRK\ EoS$ and CPA were used to describe the experimental data. In both cases, a binary interaction parameter, obtained with the minimization of Equation (5.1), was used to improve the accuracy of the computations. Nevertheless, as Figure 5.10a shows, the cubic thermodynamic model is not only quantitative incorrect, as well it gives qualitative wrong descriptions, since incorrect phase behavior is obtained and the equilibrium pressures and compositions of the vapor phase calculated with the cubic model strongly deviate from the experimental points. This behavior is observed for all the systems in VLE region evaluated in this work, therefore future figures in this work will not contain the results yielded by the cubic models. On the other hand, the $CPA\ EoS$ yields a precise description of the experimental data with the use of a k_{ij}, thus indicating the importance of the hydrogen bonding term for such representations.

In addition to the use of the traditional $CPA\ EoS$ for describing the VLE diagram of the $C_1OH - C_6$ system, CPA with the rescaled parameters to match the critical point of the pure components was also applied for representing the same mixture (Figure 5.10a). As mentioned in the previous chapter, this approach is useful for correcting the description of the model in the critical region without resorting to models based on RG theory. However, precise correlations were only obtained for the VLE region, and, as it will be shown in the next section, the model fails to accurately describe the LLE diagram [3], which was one of the reasons for the application of the crossover procedure to the $CPA\ EoS$. Figure 5.10b shows experimental data of the $C_1OH - C_7$ at 298.15K and the calculated phase diagrams with both versions of CPA and similar conclusions are obtained. In fact, the main difference between the approaches is that CPA with literature parameters needs smaller k_{ij} for fitting the bubble point pressures and the composition of methanol in the vapor phase.

Unlike the computations of the methane/n-alkane and carbon dioxide/n-alkane series, the methanol/n-alkane mixtures evaluated in this work contained hydrocarbons from C_6 to C_{10}. This choice was done in order to compare the crossover CPA developed in this research with the model proposed

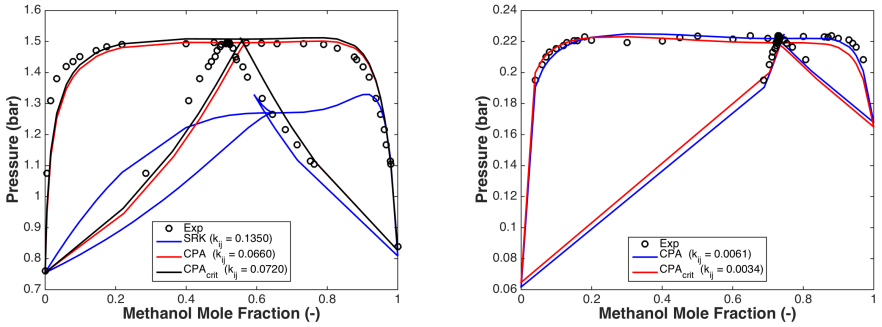

Figure 5.10: VLE diagrams for the methanol/n-hexane system at 333.15K (a) calculated with SRK (blue line), and CPA with the literature (red line) and rescaled (black line) pure compound parameters, and methanol/n-heptane system at 298.15K (b) calculated with the two approaches for the association model. In the methanol/n-hexane system, the binary interaction parameters were optimized for the cubic and association models using VLE data taken from [15], while in the methanol/n-heptane mixture data was taken from [16].

by Xu and Duan [114]. Nevertheless, as the authors did not carry out the calculations in sub-critical conditions, the comparisons are done only for the thermodynamic models studied in this work. Table 5.3 shows the deviations between the calculated and experimental data, as well as the regressed k_{ij} used in each model. For all cases tested, the performance of CPA is superior to the cubic EoS, especially for the composition of the vapor phase. The comparison between each approach for the association model, i.e. the literature and the rescaled pure component parameters, shows that CPA with the literature parameters gives a slightly superior representation of the compositions of the vapor phase; nevertheless, similar results in the representation of the bubble pressure are obtained (Table 5.3). This indicates that the change of the pure component parameters does not affect the representation of the VLE, as long as a new k_{ij} is regressed from experimental data. This conclusion is the same as the one obtained from Figure 5.10. Additionally, it is seen that the crossover model behaves like the mean-field one, which is expected as the systems are far away from the critical point.

Although the evaluation of the models for correlating LLE data will be shown in the next section, the k_{ij} estimated from this region was also applied in the VLE calculations. This approach was employed in order to ob-

Table 5.3: Performance of the SRK and CPA EoS with the literature and rescaled parameters for the correlation of methanol/n-alkane binary systems in the VLE region and the optimized k_{ij} from VLE experimental data.

System	EoS	ΔP_b (%)	Δy_1 (%)	k_{ij}	$Ref.$
$C_1OH - C_6$	SRK	16.1	24.6	0.1350	[15, 160]
	CPA	3.2	5.5	0.0660	
	CPA_{crit}	2.7	6.2	0.0720	
	$CCPA$	2.5	2.6	0.0700	
$C_1OH - C_7$	SRK	22.1	18.0	0.0022	[16]
	CPA	1.0	1.1	0.0061	
	CPA_{crit}	1.9	1.5	0.0034	
	$CCPA$	2.9	1.6	0.0072	
$C_1OH - C_8$	SRK	8.3	-	0.1164	[31]
	CPA	2.4	-	0.0393	
	CPA_{crit}	2.1	-	0.0418	
	$CCPA$	1.2	-	0.0423	
$C_1OH - C_9$	SRK	4.9	-	0.0664	[31]
	CPA	0.9	-	0.0064	
	CPA_{crit}	0.8	-	0.0295	
	$CCPA$	3.4	-	0.0083	
$C_1OH - C_{10}$	SRK	2.2	-	0.0366	[31]
	CPA	0.3	-	0.0105	
	CPA_{crit}	0.3	-	0.0333	
	$CCPA$	2.3	-	0.0161	
Avg.	SRK	**10.7**	**21.3**	-	**-**
	CPA	**1.6**	**3.3**		
	CPA_{crit}	**1.6**	**3.8**		
	$CCPA$	**2.5**	**2.1**		

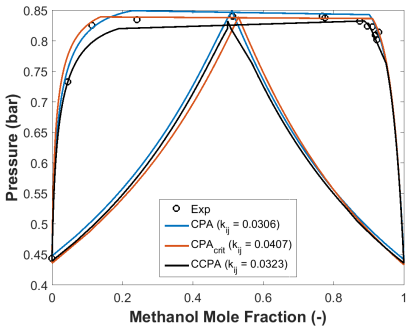

Figure 5.11: Methanol/n-hexane VLE diagram at 318.15K. Experimental data were taken from [15], while the calculated curves were obtained using the CPA with literature and rescaled pure component parameters (blue and red lines, respectively) and the $CCPA$ EoS (black line).

serve whether reasonable correlations for the methanol/n-alkane systems are obtained with the application of a single temperature independent binary interaction parameter [3]. As it can be seen from Figure 5.11, where the bubble point pressure is plotted as a function of the composition of methanol in the phase in equilibrium at 318.15K, the VLE is not much affected by the change of the k_{ij}. Still, the comparison of tables 5.3 and 5.4 points out that improved correlations need distinct k_{ij} for different regions of the phase diagram. This behavior was also seen in the literature for the CPA EoS. Palma et al. [4] used two k_{ij} for modeling the $C_1OH - C_6$ mixture in the VLE and LLE regions. The authors used a modified version of the CPA EoS to improve the critical point description and obtained interaction parameter of similar magnitude: 0.052 and 0.036. Kontogeorgis et al. [40] used the traditional CPA to represent the methanol/n-pentane system in the VLE and LLE regions. For the first case, an optimum k_{ij} of 0.051 was obtained, while for the second case the value was 0.0132. It is important to note that in both cases the values of the interaction parameters are similar to the ones estimated in this work.

As it was observed for the evaluations of the models regarding the representation of non-associating fluid mixtures, the main improvements achieved with the introduction of the density fluctuations onto the mean-field model are observed in the critical region. Indeed, as the critical point is approached, the introduction of the RG corrections become important for the accurate representation of the phase equilibrium properties of mixtures. Figure 5.12a shows the calculated and experimental data of the VLE diagram of ethanol/n-hexane

Table 5.4: Performance of the $CPA\ EoS$ with the literature and rescaled pure component parameters for the correlation of methanol/n-alkane binary systems in the VLE region and the optimized k_{ij} from LLE experimental data.

System	EoS	ΔP_b (%)	Δy_1 (%)	k_{ij}	$Ref.$
$C_1OH - C_6$	CPA	6.7	8.1	0.0091	[18]
	CPA_{crit}	7.7	8.2	0.0085	
	$CCPA$	4.2	5.0	0.0099	
$C_1OH - C_7$	CPA	1.6	0.9	0.0045	[19]
	CPA_{crit}	2.0	1.5	0.0060	
	$CCPA$	3.2	1.6	0.0045	
$C_1OH - C_8$	CPA	6.5	-	-0.0007	[19]
	CPA_{crit}	6.8	-	-0.0054	
	$CCPA$	2.1	-	-0.0046	
$C_1OH - C_9$	CPA	3.5	-	-0.0062	[19]
	CPA_{crit}	4.0	-	-0.0117	
	$CCPA$	4.3	-	-0.0056	
$C_1OH - C_{10}$	CPA	2.8	-	-0.0129	[19]
	CPA_{crit}	3.8	-	-0.0210	
	$CCPA$	2.7	-	-0.0128	
Avg.	CPA	**4.2**	**4.5**	-	-
	CPA_{crit}	**4.8**	**4.9**		
	$CCPA$	**3.3**	**3.3**		

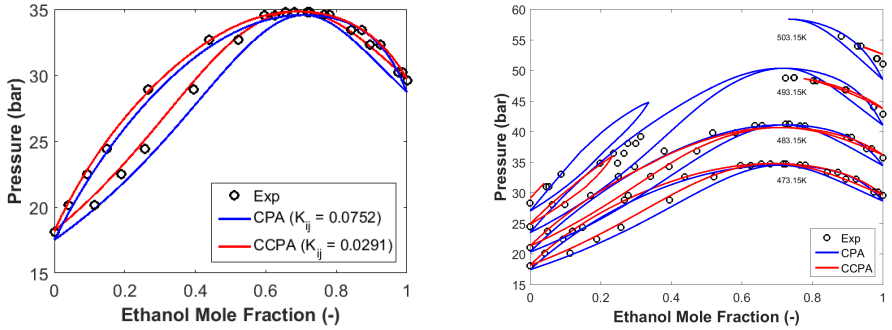

Figure 5.12: VLE diagrams of the system ethanol/n-hexane at 473.15K (a) and for other temperatures near the critical line. Experimental data were taken from [17], and the curves were calculated using the CPA and $CCPA$ EoS.

at 473.13K. It is possible to conclude from the figure that the mean-field model needs a much higher binary interaction parameter to correctly correlate experimental the vapor compositions and bubble point pressures. Additionally, the comparison of the results with experimental data shows that $CCPA$ is superior to CPA in the correlation of these properties. Furthermore, with the increase of the temperature (Figure 5.12b), it is seen that the traditional CPA cannot match the bubble point pressures and vapor compositions simultaneously, which is the reason why this model correlates a much larger two-phase region than what is observed with the measured points. Conversely, the $CCPA$ is capable of accurately describing the phase behavior of this system as the temperature approximates the critical, indicating the importance of the crossover equation and the inclusion of the density fluctuations in the mean-field model. In fact, these corrections are more important for the association models than the cubic ones, due to the overprediction of the pure component critical pressures and temperatures.

5.2 Liquid-Liquid Equilibria

As mentioned in the previous section, some of the calculations in the VLE region for methanol/n-alkane systems were done using the binary interaction parameters optimized with LLE data. This procedure was applied as an attempt to evaluate the representation of the phase diagrams of such mixtures

with the classical and non-mean-field models using a single temperature independent k_{ij}. These values were obtained with the minimization of the objective function given by the expression:

$$OF = \frac{1}{N}\sum_{i=1}^{N}\left|\frac{x_1^{hc,calc} - x_1^{hc,exp}}{x_1^{hc,exp}}\right| + \frac{1}{N}\sum_{i=1}^{N}\left|\frac{x_1^{alc,calc} - x_1^{alc,exp}}{x_1^{alc,exp}}\right| \tag{5.2}$$

where x_1 represents the composition of methanol, and the superscripts alc and hc refer to the alcohol-rich and hydrocarbon-rich phases, respectively, while the superscripts $calc$ and exp represent the calculated and experimental compositions, respectively. The calculated compositions were computed with the flash algorithm described in Appendix B. Finally, the optimized k_{ij} values were used in the phase equilibrium calculations and the calculated curves were compared to experimental data.

Prior to the assessment of the crossover association model for representing the measured points in the LLE region, a comparison is given regarding different results yielded by the mean-field equations, i.e. the $SRK\ EoS$ and CPA with the pure component parameters estimated by the fitting of the saturated pressure and liquid phase density curves, as well as the rescaled parameters to match the critical pressures and temperatures of the pure compounds. Figure 5.13a shows the experimental LLE data for the $C_1OH - C_6$ system and the results obtained with the mean-field models, i.e. the SRK and the $CPA\ EoS$ with the literature and rescaled parameters, respectively. From the graph, it is possible to conclude that the cubic equation overestimates the composition of methanol in the alcohol-rich phase, while the $CPA\ EoS$ with both sets of pure component parameters quantitatively correlates this phase. Moreover, SRK cannot predict the trend in the data, since the composition of methanol in the oil-rich phase increases in a non-linear way as the temperature rises, while the cubic model yields an approximately linear increase. On the other hand, the association model with the rescaled pure component parameters is inferior to the traditional one in the description of the composition of methanol in the hydrocarbon-rich phase, although this feature is more noticeable for the mixture containing the heavier n-alkane, e.g. $C_1OH - C_8$ (Figure 5.13b).

The comparison of the plots 5.13a and 5.13b indicates that the differences between CPA and CPA_{crit} for representing the hydrocarbon-rich phase enlarge as the molecular weight of the hydrocarbon increases. In fact, the sec-

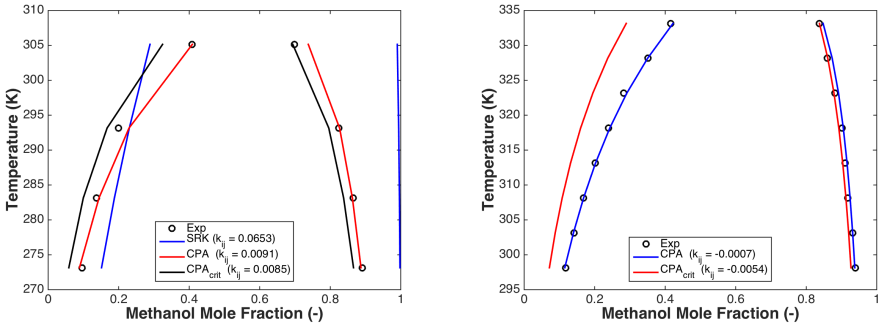

Figure 5.13: LLE diagrams at 1.01325bar for the methanol/n-hexane (a) system calculated with SRK (blue line) and CPA with the literature (red line) and rescaled (black line) parameters, and methanol/n-octane (b) mixture calculated with the two approaches for the association model. The binary interaction parameters were optimized with experimental LLE from [18] and [19], respectively.

ond version of the association model becomes inferior to the $SRK\ EoS$ for describing this property. These results indicate that, the modification of the pure component parameters to match the pure component critical temperatures and pressures have little effect on the representation of the properties of the VLE region, as shown in the previous section; nonetheless, these changes reduce the capacity of the association model to describe the LLE region of the methanol/n-alkane systems. As discussed in [3], this flaw in the rescaled version of CPA, along with the incapacity of mean-field models to correctly represent the critical behavior of real fluids, was on of the motivations for the investigation performed in this work, i.e. to apply the recursive procedure developed by White in order to introduce density fluctuations in the association EoS.

Figure 5.14a shows the experimental LLE data for the $C_1OH - C_6$ system, but instead of the correlations with the cubic model, it contains the representation of the phase diagram with the $CCPA\ EoS$. The comparison of the crossover with the classical CPA denotes that the two models behave similarly, indicating that the fluctuations are negligible and that $CCPA$ reduces to CPA, as seen for the VLE region. As for Figure 5.14b, which shows the phase behavior of the $C_1OH - C_{10}$ system, it can be concluded that differently from the rescaled CPA, the RG corrections to the mean-field model do

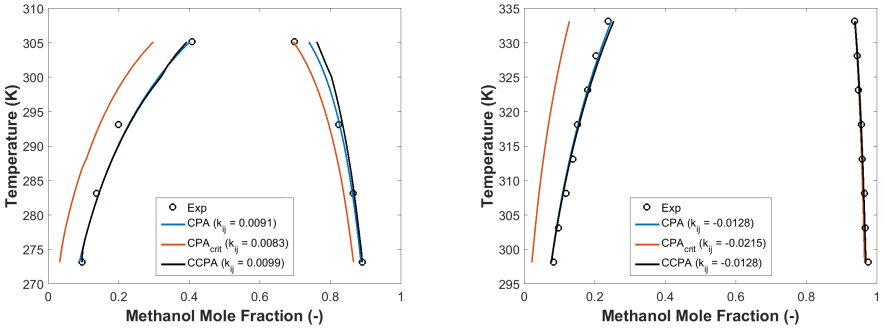

Figure 5.14: LLE diagrams for the methanol/n-hexane (a) and methanol/n-decane (b) systems at 1.01325bar. The curves were calculated using CPA with the literature (blue line) and rescaled (red line) parameters and $CCPA$ EoS (black line). The binary interaction parameters were optimized with experimental LLE data taken from [18] and [19], respectively.

not hamper the correlation of the composition of methanol in the hydrocarbon-rich phase. This is a clear advantage of the $CCPA$ EoS, because it allows the same representations of the phase behavior far from the critical point, but it improves the description in the near-critical and critical regions. This feature was seen in Figure 5.12 and will be further discussed in the next section, dealing with the calculation of the critical lines.

Table 5.5 shows the AAD for the different systems studied in the LLE region, as well as the average overall deviation calculated with the aforementioned models. As observed in Figure 5.13, the cubic model is incapable of correctly describing the composition of both phases, although as the molecular weight of the hydrocarbon increases, the oil-rich phase becomes purer, thus decreasing the deviations in comparison to the systems with lighter alkanes. The results for the CPA_{crit} EoS indicates that the rescaling of the pure component parameters deteriorates the capacity of the model to describe the alcohol-rich phase and, as seen before, the deviations become higher than the ones obtained with the SRK EoS. Finally, it is seen that the traditional and crossover CPA EoS are able to describe the experimental data of the systems studied; although the deviations with the non-mean-field equation are almost twice as big as the traditional model. This is an indication that the pure component parameters obtained for the $CCPA$ EoS are not optimum and LLE data should be used as a final test for the selection of the parameters as done

Table 5.5: Performance of the SRK, CPA with the literature and rescaled parameters, and $CCPA$ EoS for the correlation of the composition of methane in the hydrocarbon (x_1^{hc}) and alcohol (x_1^{alc}) rich phases for several methanol/n-alkane binary systems in the LLE region.

System	EoS	Δx_1^{hc} (%)	Δx_1^{alc} (%)	k_{ij}	$Ref.$
$C_1OH - C_6$	SRK	22.8	18.6	0.0653	[18]
	CPA	1.6	7.0	0.0091	
	CPA_{crit}	2.2	26.3	0.0085	
	$CCPA$	2.2	7.7	0.0099	
$C_1OH - C_7$	SRK	16.8	16.3	0.0572	[19]
	CPA	0.3	2.0	0.0045	
	CPA_{crit}	0.7	34.3	0.0060	
	$CCPA$	2.5	10.2	0.0045	
$C_1OH - C_8$	SRK	11.5	16.3	0.0789	[19]
	CPA	0.6	1.7	-0.0007	
	CPA_{crit}	0.7	34.3	-0.0054	
	$CCPA$	0.3	7.6	-0.0046	
$C_1OH - C_9$	SRK	6.2	11.5	0.1000	[19]
	CPA	0.4	3.4	-0.0062	
	CPA_{crit}	0.5	43.2	-0.0117	
	$CCPA$	0.4	3.9	-0.0056	
$C_1OH - C_{10}$	SRK	4.5	9.1	0.1117	[19]
	CPA	0.2	4.4	-0.0129	
	CPA_{crit}	0.3	44.0	-0.0210	
	$CCPA$	0.2	5.0	-0.0128	
Avg.	SRK	**12.4**	**14.4**	-	-
	CPA	**0.6**	**3.73**		
	CPA_{crit}	**0.9**	**36.4**		
	$CCPA$	**1.1**	**6.9**		

in other works with CPA [129, 130].

It is important to note that other authors managed to obtain a precise description of the LLE and VLE regions of mixtures containing associating components with a modified version of CPA to improve the description of the critical point [4, 161]. Both representations were achieved with the use of a more flexible alpha function [132], thus introducing 4 additional pure component parameters. Furthermore, they used a temperature independent volume shift [131] to correct the liquid phase density underpredictions. Hence, for applying the model in various temperature conditions, they developed a systematic parametrization procedure in order to contain the flexibility of the equation. Despite these improvements, this approach is still unable to describe the asymp-

totic behavior of real fluids near the critical point like any mean-field EoS.

5.3 Critical Lines

This section is dedicated to the modeling of the critical behavior of mixtures using the models investigated in this work. The results obtained with the different approaches were compared to experimental data, in order to evaluate the performance of the equations. Furthermore, this section is organized similar to the one concerning VLE descriptions, i.e. it is divided into two parts, where the first is contains the calculations for mixtures of inert species and the second one for systems with associating components, with an additional section regarding the calculation of a ternary system.

5.3.1 Binary systems containing non-associating species

The representation of the critical behavior of mixtures is important for academic and technological reasons. First of all, measurements in this region are very difficult and significant differences between the data found in the literature is observed for the same systems. Second, it gives important information about the topology of the phase behavior [91]. As showed by van Konynenburg and Scott [2], mixtures can be classified according to six classes.

The first systems in critical condition studied in this work were the homologous series of methane/n-alkanes (from ethane to n-decane). This series shows a continuous transition of phase behavior that is representative of hydrocarbon family. It has been found that for mixtures with n-alkanes up to n-pentane, the systems possess a type I behavior in accordance with van Konyneburg and Scott classification, i.e. a continuous vapor-liquid critical curve connects the critical points of the pure components. However, there are some indications that the $C_1 - C_5$ system is close to the tricritical point [162], at which the liquid splits into two phases and starts to have a type V phase behavior [163]. In spite of these results, the methane/n-pentane system probably belongs to the type I class. The next mixture, i.e. $C_1 - C_6$, shows a type V behavior, while systems with n-heptane or heavier hydrocarbons are classified as type III [93]. Due to these complex changes in phase behavior, the performance of a model is subjected to its capacity to describe the transition seen for this series.

Figure 5.15 shows the critical pressures as a function of the critical temperatures for the systems: methane/ethane, methane/propane, and methane/n-butane. As mentioned previously, the three mixtures possess a type I behavior, which is predicted ($k_{ij} = 0$) by the three models (SRK, CPA and $CCPA$). The graph also indicates that the curves obtained with SRK correctly describe the experimental data, while CPA overpredicts almost all the measured critical points. Furthermore, the deviations increase as the composition of the heavier hydrocarbon increases in the mixture. This happens because of the pure component parameters used in the model, which are obtained from the matching of saturated data instead of the pure fluid's critical point, cause an overprediction of the critical temperatures and pressures, which, as shown previously, becomes larger as the molecular weight of the compound increases. The introduction of density fluctuations in the second mean-field approach allows a better representation of the experimental data.

The increase in the molecular weight of the hydrocarbon changes the behavior of the critical lines in comparison with the previous systems. For the methane/n-pentane system, Figure 5.16a shows that all the models, except for SRK, predict a type I behavior. The $SRK\ EoS$ yields a type V behavior, which means that the two critical pure critical points are no longer connected by a line. In fact, the critical line going from the heavier component ends on a lower critical endpoint ($LCEP$), due to a split of the liquid phase into two liquids. This three-phase line is connected to an upper critical endpoint ($UCEP$), which is linked to the critical point of the light species [93]. This behavior can be modified with the use of a small negative interaction parameter. Polishuk et al. [91] estimated a $k_{ij} = -0.05$ for correcting the phase diagram and improving the correlation of the experimental point; however, this value is different in terms of magnitude and sign to the one optimized with VLE data (Table 5.1). This points out that a single temperature independent interaction parameter is not enough for describing such systems in different conditions. In fact, other authors used temperature-dependent k_{ij} and l_{ij} for the correlation of the experimental data in different equilibrium conditions [136]. For the other systems containing heavier hydrocarbons (C_6 to C_{10}), SRK and the other two models predicted a type V behavior.

The comparison of the calculated critical lines with the experimental critical data in Figure 5.16a shows that $CCPA$ is similar to the $SRK\ EoS$ near the critical point of the pure n-pentane. Additionally, the crossover model correctly describes the phase type of the system. The $CPA\ EoS$ overpredicts

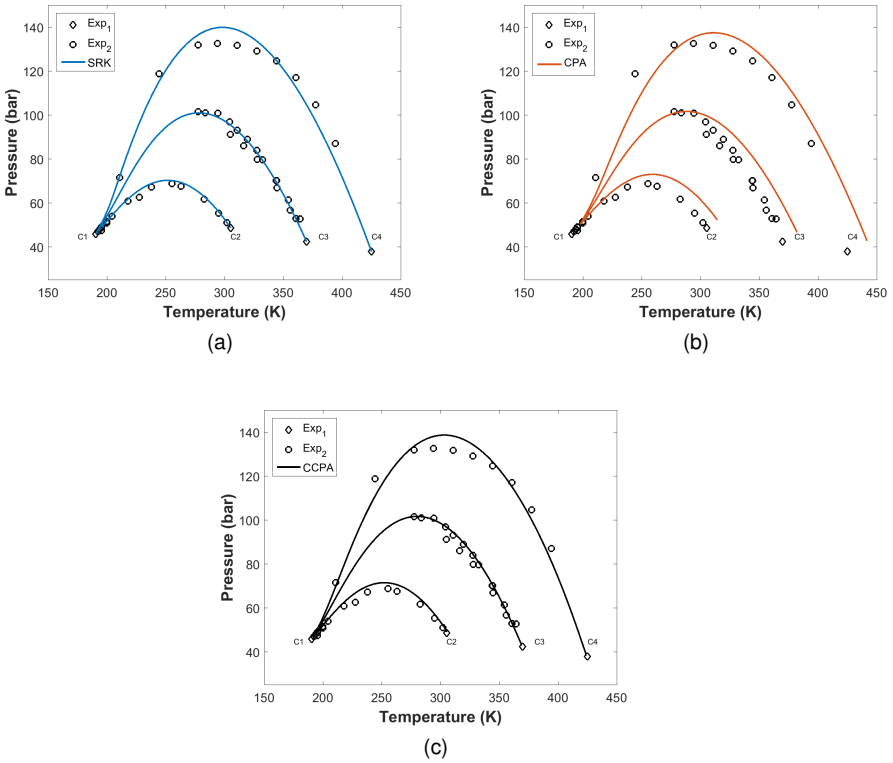

Figure 5.15: Experimental critical temperature as function of the critical pressure for the systems methane/ethane, methane/propane and methane/n-butane (open circles and diamonds) and the predicted critical lines ($k_{ij} = 0$) using the $SRK\ EoS$ (a), the $CPA\ EoS$ (b) and the $CCPA\ EoS$ (c) for three different temperatures. Pure component experimental data (Exp_1) were taken from the $DIPPR$ database, while the measurements for the mixtures (Exp_2) were taken from [20].

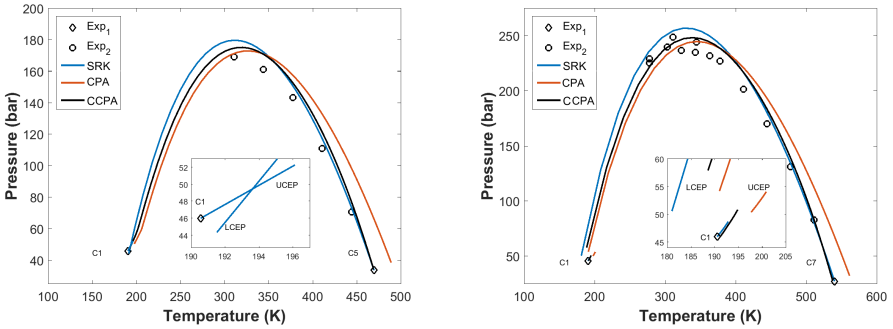

Figure 5.16: Experimental critical temperature as function of the critical pressure for the systems methane/n-pentane (a), methane/n-heptane (b) (open circles and diamonds) and the predicted critical lines ($k_{ij} = 0$) using the $SRK\ EoS$ (blue line), the $CPA\ EoS$ (red line) and the $CCPA\ EoS$ (black line). Pure component experimental data (Exp_1) were taken from the $DIPPR$ database, while the measurements for the mixtures (Exp_2) were taken from [20].

both the critical temperatures and pressures of the system. As the composition of methane increases the system reaches its maximum pressure, which is overpredicted by the models; however CPA and $CCPA$ yield the best representation of this property. Figure 5.16b shows the vapor-liquid critical behavior of the $C_1 - C_7$ mixture. Similar to the first figure, the cubic equation overpredicts the maximum pressure, while CPA underpredicts it. On the other hand, $CCPA$ is the model that gives the best descriptions the maximum critical pressure and the critical points close to the region of a high content of the heavier hydrocarbon, suggesting the importance of the introduction of the density fluctuations to CPA.

The evaluation of the predictions of the models regarding the experimental critical pressures, for both the methane/n-pentane and methane/n-heptane systems, can also be considered from the pressure-composition diagrams (Figure 5.17). From the figures, it is possible to observe that the $CCPA\ EoS$ is superior to the other models, as it corrects the description given by CPA, especially in regions with high concentration of the heavier hydrocarbons, besides it has a lower maximum critical pressure in comparison to the $SRK\ EoS$, as mentioned before. The diagram also shows the discontinuity in the critical line, characteristic of a type V behavior, predicted by the $SRK\ EoS$ for the methane/n-pentane system (Figure 5.17a), while the other models predict a

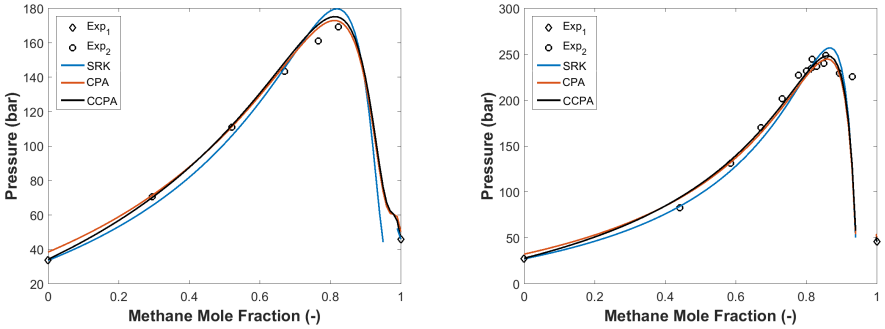

Figure 5.17: Experimental critical temperature as function of the critical pressure for the systems methane/n-pentane (a), methane/n-heptane (b) (open circles and diamonds) and the predicted critical lines ($k_{ij} = 0$) using the $CPA\ EoS$ (blue line), the $CPA\ EoS$ (red line) and the $CCPA\ EoS$ (black line). Pure component experimental data (Exp_1) were taken from the $DIPPR$ database, while the measurements for the mixtures (Exp_2) were taken from [20].

type I behavior with a sharp variation in composition close to pure methane, as discussed in [91]. For the methane/n-heptane system, the three equations have similar features (Figure 5.17b), since a type V behavior is predicted by all models. Moreover, due to the appearance of a second liquid, the system is no longer represented by the fluctuations in density. As a matter of fact, the order parameter becomes the composition of one of the components, thus a different method should be applied in order to incorporate the fluctuations into to the mean-field model [164].

In addition to the plots of the critical pressure as a function of composition, it was also evaluated the relationship between the critical volume and the mole fraction of the light component (Figure 5.18). In the figures, it is possible to see that the predictions are similar in the region of high concentration of methane; nonetheless, the increase of the mole fraction of heavier n-alkane in the mixture results in a higher deviation of the critical molar volume by the mean-field models. On the other hand, the $CCPA\ EoS$ gives an accurate description of the densities for the two systems in the entire range of methane composition.

The AAD between the calculated and measured critical points is presented in two tables, the first containing the systems belonging to the type I phase behavior (Table 5.6) and the second with the $C_1 - C_6$ to $C_1 - C_{10}$ mixtures (Table 5.7). This makes the evaluation of the performance of the models

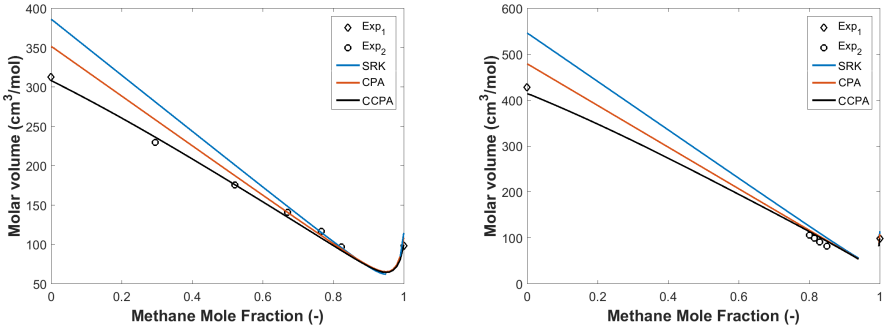

Figure 5.18: Experimental critical molar volume as function of the methane mole fraction for the systems methane/n-pentane (a), methane/n-heptane (b) (open circles and diamonds) and the predicted critical lines ($k_{ij} = 0$) using the $SRK\ EoS$ (blue line), the $CPA\ EoS$ (red line) and the $CCPA\ EoS$ (black line). Pure component experimental data (Exp_1) were taken from the $DIPPR$ database, while the measurements for the mixtures (Exp_2) were taken from [20].

easier since it allows the comparison of the models for the case in which the asymmetry between the molecules does not play a major role for the representation of the critical properties of the systems, and the other one in which it does.

Table 5.6 shows the AAD of the more symmetric systems with respect to the critical temperatures, pressures and volumes. It can be concluded from the results that SRK and CPA are able to correctly describe the critical temperature, while CPA has a higher deviation, around 4.5%. In the case of the critical pressure, it is seen that the $CCPA$ is superior to the cubic model, showing the importance of the RG corrections to the mean-field model. Finally, the analysis of the deviations regarding the critical volume indicates that the SRK is incapable of describing this property. Furthermore, as the pure component parameters are changed to match the saturated data, an improvement in the performance of the representation of the critical volume is seen; nonetheless, the crossover model is superior to both models, due to the incorporation of the density fluctuations. For the asymmetric mixtures, it can be concluded from Table 5.7 that, although $CCPA$ is superior to CPA, the difference in size between the molecules has a strong effect in the predictions since all the models are incapable of precisely describing the critical properties of the mixtures.

Table 5.6: Average AAD of the critical temperature, pressure and volume for binary methane/n-alkane systems (methane/ethane to methane/n-decane) calculated using the SRK, the CPA and the $CCPA$ EoS. No binary interaction coefficients were used in the calculations ($k_{ij} = 0$). The experimental data were taken from [20].

System	ΔT_c (%)		
	SRK	CPA	$CCPA$
$C_1 - C_2$	0.7	3.9	1.0
$C_1 - C_3$	1.0	3.7	0.8
$C_1 - C_4$	3.0	6.7	3.8
$C_1 - C_5$	1.2	3.9	1.0
Avg.	**1.5**	**4.5**	**1.7**
System	ΔP_c (%)		
	SRK	CPA	$CCPA$
$C_1 - C_2$	1.4	8.8	2.9
$C_1 - C_3$	2.5	2.5	1.5
$C_1 - C_4$	7.9	6.8	7.5
$C_1 - C_5$	5.3	2.1	2.9
Avg.	**4.2**	**6.1**	**3.5**
System	Δv_c (%)		
	SRK	CPA	$CCPA$
$C_1 - C_2$	-	-	-
$C_1 - C_3$	12.9	9.0	5.6
$C_1 - C_4$	17.7	12.5	6.6
$C_1 - C_5$	8.9	5.3	3.9
Avg.	**13.2**	**9.0**	**5.4**

Table 5.7: Average AAD of the critical temperature, pressure and volume for binary methane/n-alkane systems (methane/ethane to methane/n-decane) calculated using the SRK, the CPA and the $CCPA$ EoS. No binary interaction coefficients were used in the calculations ($k_{ij} = 0$). The experimental data were taken from [20].

System	ΔT_c (%)		
	SRK	CPA	$CCPA$
$C_1 - C_6$	14.4	16.0	13.8
$C_1 - C_7$	9.9	11.2	9.13
$C_1 - C_8$	41.5	42.9	39.4
$C_1 - C_9$	24.1	23.7	21.5
$C_1 - C_{10}$	13.9	13.1	10.9
Avg.	**20.8**	**21.4**	**18.9**
System	ΔP_c (%)		
	SRK	CPA	$CCPA$
$C_1 - C_6$	4.4	4.6	3.7
$C_1 - C_7$	7.5	6.6	6.2
$C_1 - C_8$	14.1	12.0	10.6
$C_1 - C_9$	1.8	3.8	2.6
$C_1 - C_{10}$	4.5	4.4	4.2
Avg.	**6.5**	**6.3**	**5.5**
System	Δv_c (%)		
	SRK	CPA	$CCPA$
$C_1 - C_6$	-	-	-
$C_1 - C_7$	19.6	12.0	9.6
$C_1 - C_8$	72.7	56.2	51.6
$C_1 - C_9$	34.3	22.3	20.4
$C_1 - C_{10}$	23.9	10.2	8.4
Avg.	**37.6**	**25.2**	**22.5**

In addition to the calculations of the deviations using k_{ij} equal to zero, the AAD of the methane/n-alkane homologous series was also computed with the interaction parameters optimized with the experimental VLE data (Table 5.1). This was done in order to observe the dependence of the representation on the energy interaction parameters. Table 5.8 shows that the deviations in terms of critical pressures and temperatures increase for most of the systems when the k_{ij} obtained from VLE data is used in the model. As a matter of fact, Polishuk et al. [91] used several types of classical thermodynamic models with an interaction parameter correlated with experimental critical data to represent the $C_1 - C_2$ to $C_1 - C_8$ systems, still quantitative descriptions were only achieved for systems belonging to the type I phase behavior, while for the more asymmetric ones, i.e. from $C_1 - C_6$ to $C_1 - C_8$, the models were incapable to describe the $UCEP$, pressure-composition diagrams and compositions of the critical LLE. In a different paper [93], precise representations of the mixtures containing methane and a n-alkane (from C_2 to C_{10}) were attained with a near to cubic model and temperature dependent k_{ij} and l_{ij}. In the case of non-mean-field models, a detailed investigation of the behavior of the series was not found in the literature. Llovell and Vega [106] proved that the crossover $Soft - SAFT\ EoS$ with a single k_{ij} is capable of capturing the transition in the phase behavior that occurs at the $C_1 - C_6$ system, besides the model can accurately represent the critical endpoints and phase equilibrium data; nevertheless, the authors did not compare the phase behavior yielded by the model with experimental data of the more asymmetric systems.

In summary, the results for the methane/n-alkane homologous series showed that models can qualitatively describe the type of phase diagram for the methane/n-alkane binary mixtures, i.e. the transition in the phase behavior types. However, a quantitative representation was obtained with SRK and $CCPA$ for the symmetric systems, while all models failed to correctly describe the experimental data of the more asymmetric mixtures of methane with n-hexane or heavier hydrocarbons. It is important to note that the application of White's recursive procedure to the mean-field models is useful, since it improves the predictions of the critical lines, especially in the case of the critical volume of the mixtures; nonetheless, the accurate representation of the entire series might only be achieved with the use of more complex mixing rules [151], which take into account the difference in the behavior of the systems in both limits of composition, or temperature dependent k_{ij} and l_{ij} [135, 136], both of which are not in the scope of this thesis.

Table 5.8: Average AAD of the critical temperature, pressure and volume for binary methane/n-alkane systems (methane/ethane to methane/n-decane) calculated using the SRK, the CPA and the $CCPA$ EoS. Binary interaction coefficients regressed from VLE data were used in the calculations (Table 5.1). The experimental data were taken from [20].

System	ΔT_c (%)		
	SRK	CPA	$CCPA$
$C_1 - C_2$	0.7	3.2	0.6
$C_1 - C_3$	1.0	3.1	0.9
$C_1 - C_4$	1.9	3.8	1.6
$C_1 - C_5$	1.7	3.3	1.7
$C_1 - C_6$	15.3	18.9	15.8
$C_1 - C_7$	16.9	38.2	22.2
$C_1 - C_8$	41.6	42.3	39.4
$C_1 - C_9$	21.8	18.6	17.5
$C_1 - C_{10}$	12.4	11.0	8.8
Avg.	**12.6**	**15.8**	**12.1**
System	ΔP_c (%)		
	SRK	CPA	$CCPA$
$C_1 - C_2$	1.3	7.2	2.2
$C_1 - C_3$	1.9	5.1	4.0
$C_1 - C_4$	7.1	5.2	5.9
$C_1 - C_5$	7.0	6.9	8.4
$C_1 - C_6$	6.7	12.2	8.6
$C_1 - C_7$	29.0	49.1	28.8
$C_1 - C_8$	8.3	4.3	3.0
$C_1 - C_9$	8.8	9.0	10.0
$C_1 - C_{10}$	6.2	4.1	6.2
Avg.	**8.5**	**11.5**	**8.5**
System	Δv_c (%)		
	SRK	CPA	$CCPA$
$C_1 - C_2$	-	-	-
$C_1 - C_3$	12.1	8.1	6.6
$C_1 - C_4$	14.8	8.7	5.0
$C_1 - C_5$	9.7	7.9	7.02
$C_1 - C_6$	-	-	-
$C_1 - C_7$	16.3	5.6	4.2
$C_1 - C_8$	67.9	49.7	45.9
$C_1 - C_9$	26.7	11.5	11.2
$C_1 - C_{10}$	17.7	5.2	4.1
Avg.	**23.6**	**13.8**	**12.0**

The second group of non-associating mixtures studied in this work was the carbon dioxide/n-alkane systems. The critical behavior of binary CO_2/n-alkane mixtures has been investigated by several authors [94, 103, 143, 150], due to the importance of this series.

The first systems of the series investigated in this work were composed of methane to n-pentane and carbon dioxide. Figure 5.19 shows the experimental critical temperatures as a function of the critical pressures of the $CO_2 - C_1$ to $CO_2 - C_5$ systems and the predicted critical lines using the SRK, CPA and $CCPA\ EoS$. In the three calculations, no binary interaction parameters were used and it is possible to observe that the models yield similar results for the first mixtures, although CPA predicts a higher maximum pressure. Additionally, the larger overprediction of the pure component critical temperature and pressure, observed for the heavier hydrocarbons, affects the computations of the critical lines and increases the deviations with respect to the experimental data. On the other hand, the crossover model ($CCPA$) and the cubic one (SRK) give similar predictions for the remaining systems.

It is also important to observe that none of the models is capable of capturing the trend of the experimental data as the mixture becomes richer in CO_2 when the k_{ij} are equal to zero. Figure 5.20 denotes that a minimum in temperature is reached (around 290K) for the mixture of carbon dioxide and ethane; however, the model that gives a lower T_c is the $CCPA\ EoS$, corresponding to 302K. This observation leads to the conclusion that the use of optimum k_{ij} are important for the precise prediction of the minimum temperature and the correct trends of the critical lines.

Another important comparison between the models is given in Figure 5.21. This plot exhibits the critical volume lines as a function of the mole fraction of CO_2 for the systems aforementioned. Unfortunately, critical volumetric data is scarce in the literature and only a few points for the $CO_2 - C_3$ and $CO_2 - C_4$ mixtures were found. Nonetheless, interesting behaviors can be seen in the figure. First, it is possible to observe that the three models have similar trends, although the cubic model, which can yield good estimation for the critical pressures and temperatures, is the worst model for predicting the critical volumetric data. Besides, it is seen that the $CCPA\ EoS$ can accurately represent the experimental points, although the deviation increases close the pure CO_2 critical point, this can also be improved with the application of k_{ij}.

Following the procedure applied to the methane/n-alkane mixtures, the calculations of the critical lines were applied with the utilization of binary inter-

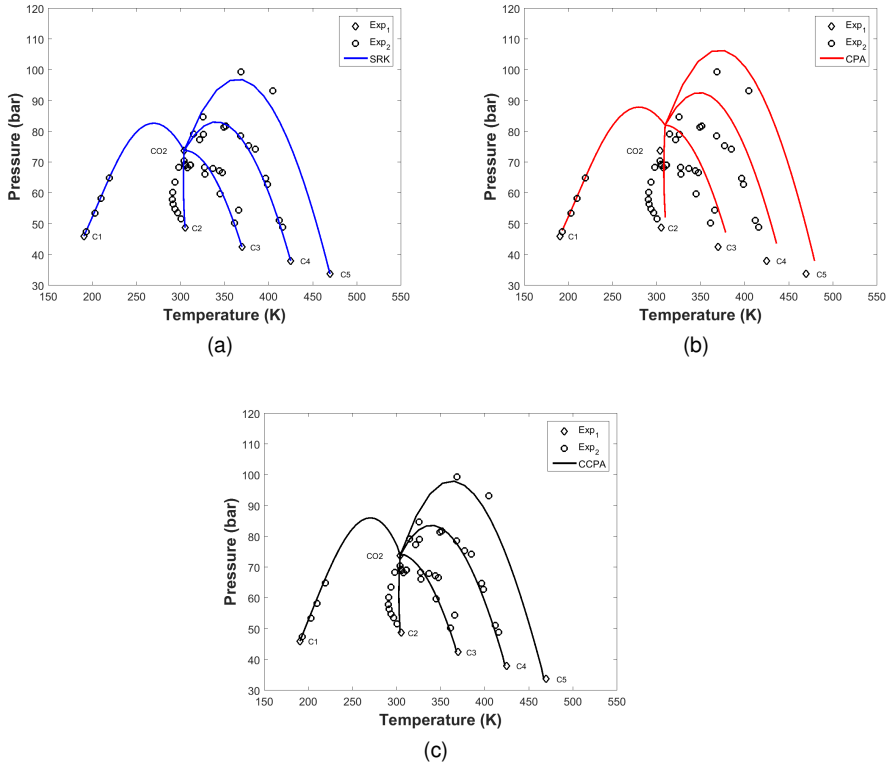

Figure 5.19: Experimental critical pressure as a function of the critical temperature for the systems $CO_2 - C_1$ to $CO_2 - C_5$ (open circles and diamonds) and the predicted critical lines ($k_{ij} = 0$) using the $SRK\ EoS$ (a), the $CPA\ EoS$ (b) and the $CCPA\ EoS$ (c). Pure component experimental data (Exp_1) were taken from the $DIPPR$ database, while the measurements for the mixtures (Exp_2) were taken from [13, 21–25].

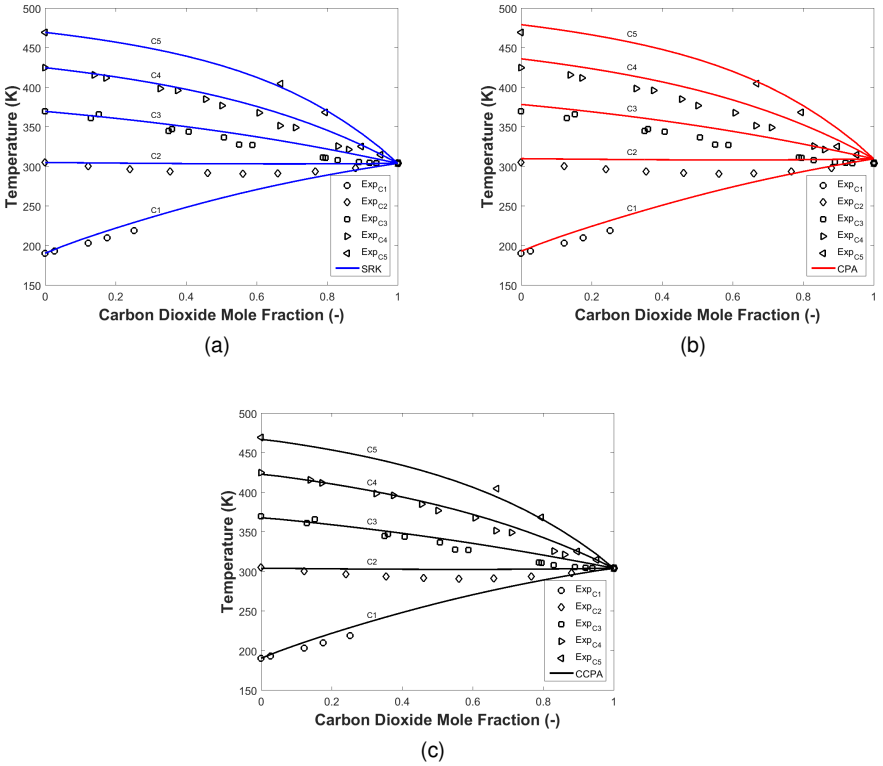

Figure 5.20: Experimental critical temperature as a function of the mole fraction of carbon dioxide for the systems $CO_2 - C_1$ to $CO_2 - C_5$ (open circles and diamonds) and the predicted critical lines ($k_{ij} = 0$) using the $SRK\ EoS$ (a), the $CPA\ EoS$ (b) and the $CCPA\ EoS$ (c) for three different temperatures. Pure component experimental data (Exp_1) were taken from the $DIPPR$ database, while the measurements for the mixtures were taken from [13, 21–25].

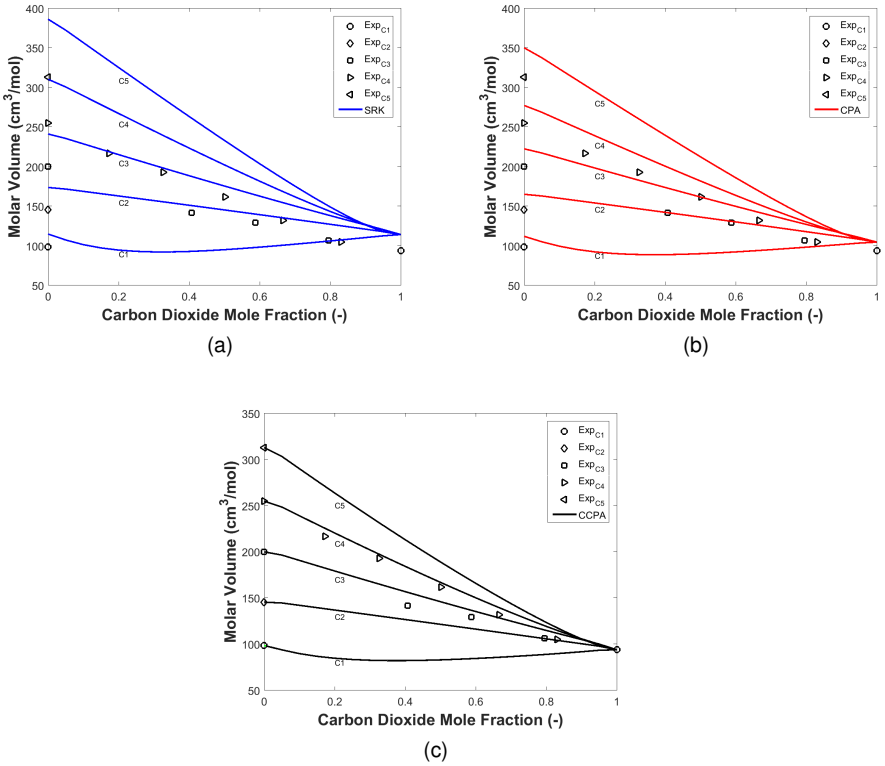

Figure 5.21: Experimental critical volume as a function of the mole fraction of carbon dioxide for the systems $CO_2 - C_1$ to $CO_2 - C_5$ (open circles and diamonds) and the predicted critical lines ($k_{ij} = 0$) using the $SRK\ EoS$ (a), the $CPA\ EoS$ (b) and the $CCPA\ EoS$ (c) for three different temperatures. Pure component experimental data (Exp_1) were taken from the $DIPPR$ database, while the measurements for the mixtures were taken from [13, 21–25].

action parameters optimized with VLE. Figure 5.22 shows the experimental critical points and the correlated critical pressures as a function of temperature computed with the models evaluated in this work. From the graph it is possible to observe that the correct trend for the critical lines is attained, especially for the systems $CO_2 - C_1$ to $CO_2 - C_3$. The comparison of the results with the experimental data indicates that SRK and $CCPA$ behave similarly and are able of precisely representing the critical behavior of the systems, while the CPA EoS overpredicts the measured points. This behavior is similar to the one seen for the hydrocarbon mixtures, and it can be concluded that the RG corrections to the mean-field model are important for improving the calculations in the critical region of mixtures containing CO_2 and a n-alkane.

Tables 5.9 and 5.10 show the AAD calculated from the comparison of the results with experimental data using $k_{ij} = 0$ and optimum k_{ij} estimated with VLE data, respectively. For the first case, it can be concluded the models are capable of predicting P_c better than T_c, and as seen from the figures 5.19 to 5.21, the CPA EoS is the worst model, while $CCPA$ is the best, although similar to SRK. The comparison of the deviations in terms of the critical volume obtained from the three models indicate that the inclusion of the density fluctuations is important for the description of this property, since the crossover model yields smaller errors compared with the two mean-field EoS, especially for the cubic one.

In addition to mixtures containing CO_2 and n-alkanes with low molecular weight, i.e. from C_1 to C_5, this study also contains the calculations and comparison with experimental data for systems with heavier n-alkanes, from C_6 to C_{10}. Systems with CO_2 and C_7 up to C_{12} are classified as type II according to van Konynenburg and Scott classification [2]. This transition in the series is also accompanied by an increase in the complexity of the phase behavior, since a second critical locus appears.

The experimental critical temperatures of the $CO_2 - C_6$ to $CO_2 - C_{10}$ systems are plotted in Figure 5.23, as a function of the critical pressures along with the predicted critical lines using the SRK, CPA and $CCPA$ EoS. The comparison of the predicted lines with experimental data shows that while CPA overpredicts the experimental critical temperatures and pressures, the two other models underpredict them. It can also be seen that the crossover model is marginally superior to the classical cubic EoS.

The diagrams of the critical temperature versus the mole fraction of CO_2 show a similar problem observed with the lighter hydrocarbons (Figure 5.24).

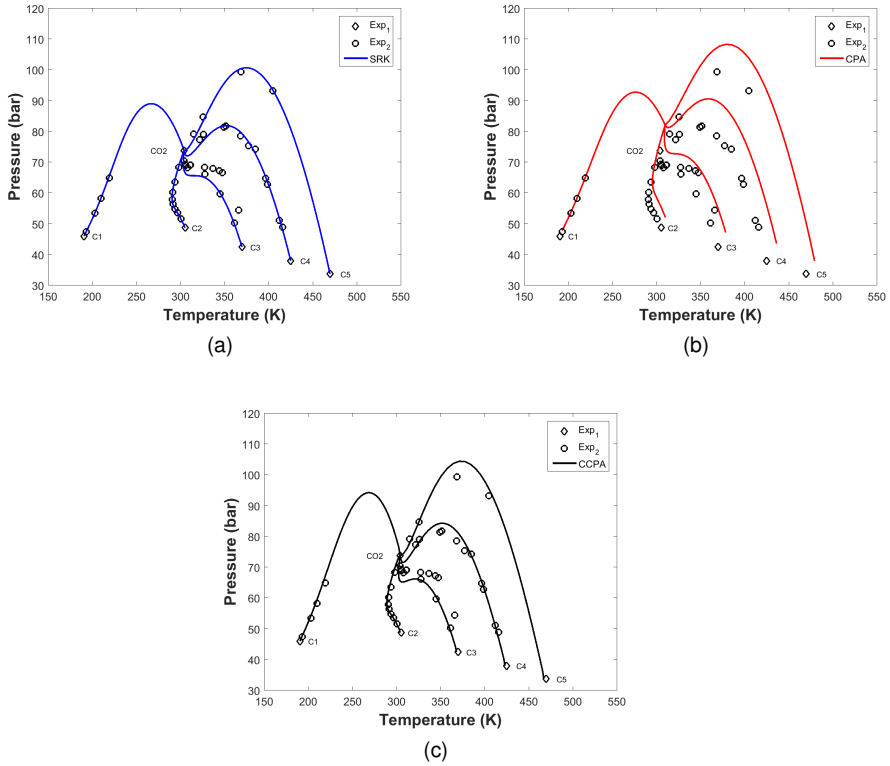

Figure 5.22: Experimental critical pressure as a function of the critical temperature for the systems $CO_2 - C_1$ to $CO_2 - C_5$ (open circles and diamonds) and the calculated critical lines with k_{ij} optimized from VLE data using the $SRK\ EoS$ (a), the $CPA\ EoS$ (b) and the $CCPA\ EoS$ (c). Pure component experimental data (Exp_1) were taken from the $DIPPR$ database, while the measurements for the mixtures (Exp_2) were taken from [13, 21–25].

Table 5.9: Average AAD of the critical temperature, pressure and volume for binary carbon dioxide/n-alkane systems ($CO_2 - C_1$ to $CO_2 - C_5$) calculated using the SRK, the CPA and the $CCPA$ EoS. No binary interaction parameters were used in the calculations ($k_{ij} = 0$). The experimental data are shown in the reference column.

System	ΔT_c (%)			$Ref.$
	SRK	CPA	$CCPA$	
$CO_2 - C_1$	2.2	2.6	2.2	[21]
$CO_2 - C_3$	2.5	4.2	2.4	[22]
$CO_2 - C_3$	2.2	4.2	1.9	[23–25]
$CO_2 - C_4$	2.0	4.3	1.4	[13, 24]
$CO_2 - C_5$	1.6	3.2	1.6	[24]
Avg.	**2.1**	**3.7**	**1.9**	-
System	ΔP_c (%)			$Ref.$
	SRK	CPA	$CCPA$	
$CO_2 - C_1$	5.8	10.4	7.0	[21]
$CO_2 - C_3$	2.3	11.0	2.6	[22]
$CO_2 - C_3$	6.2	9.6	5.9	[23–25]
$CO_2 - C_4$	5.6	8.7	4.5	[13, 24]
$CO_2 - C_5$	4.4	12.9	3.9	[24]
Avg.	**4.8**	**10.5**	**4.8**	-
System	Δv_c (%)			$Ref.$
	SRK	CPA	$CCPA$	
$CO_2 - C_1$	-	-	-	[21]
$CO_2 - C_3$	-	-	-	[22]
$CO_2 - C_3$	26.3	16.2	4.8	[23–25]
$CO_2 - C_4$	25.3	13.0	3.5	[13, 24]
$CO_2 - C_5$	-	-	-	[24]
Avg.	**25.8**	**14.6**	**4.1**	-

Table 5.10: Average AAD of the critical temperature, pressure and volume for binary carbon dioxide/n-alkane systems ($CO_2 - C_1$ to $CO_2 - C_5$) calculated using the SRK, the CPA and the $CCPA$ EoS. Binary interaction parameters regressed from VLE data were used in the calculations (Table 5.2). The experimental data are shown in the reference column.

System	ΔT_c (%)			$Ref.$
	SRK	CPA	$CCPA$	
$CO_2 - C_1$	0.4	2.1	0.3	[21]
$CO_2 - C_3$	0.1	1.7	0.4	[22]
$CO_2 - C_3$	0.5	1.7	1.0	[23–25]
$CO_2 - C_4$	0.4	2.7	0.7	[13, 24]
$CO_2 - C_5$	1.2	1.8	1.8	[24]
Avg.	**0.5**	**2.0**	**0.8**	-
System	ΔP_c (%)			$Ref.$
	SRK	CPA	$CCPA$	
$CO_2 - C_1$	1.5	6.7	2.2	[21]
$CO_2 - C_3$	0.2	8.6	0.4	[22]
$CO_2 - C_3$	3.9	6.7	3.2	[23–25]
$CO_2 - C_4$	1.6	10.7	2.5	[13, 24]
$CO_2 - C_5$	1.6	10.9	2.7	[24]
Avg.	**1.8**	**8.7**	**2.2**	-
System	Δv_c (%)			$Ref.$
	SRK	CPA	$CCPA$	
$CO_2 - C_1$	-	-	-	[21]
$CO_2 - C_3$	-	-	-	[22]
$CO_2 - C_3$	24.5	14.6	3.2	[23–25]
$CO_2 - C_4$	21.7	10.4	2.1	[13, 24]
$CO_2 - C_5$	-	-	-	[24]
Avg.	**23.1**	**12.5**	**2.6**	-

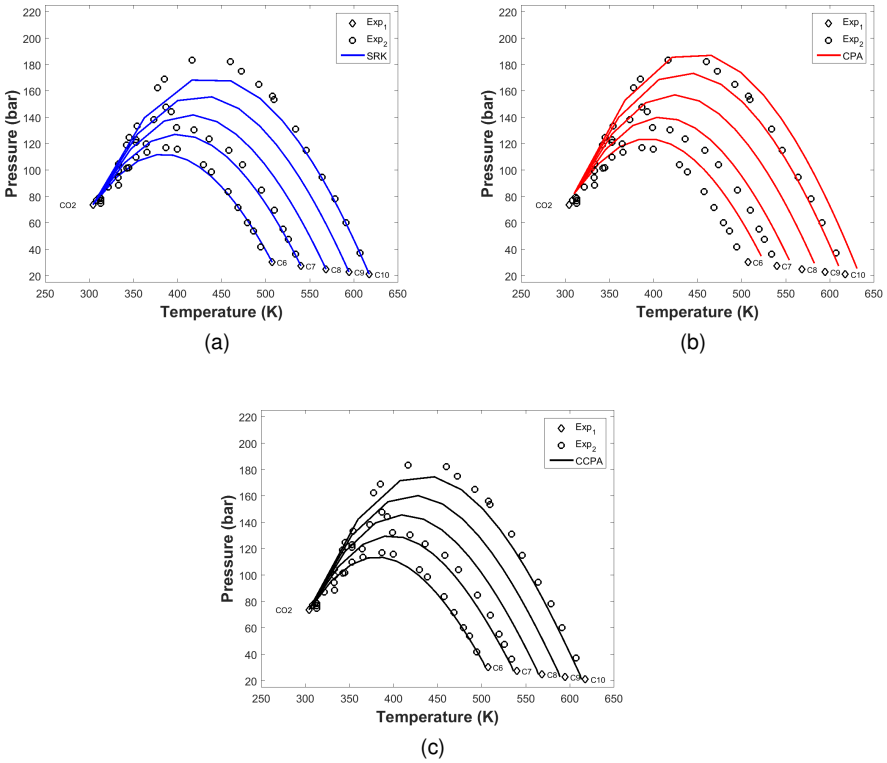

Figure 5.23: Experimental critical pressure as a function of the critical temperature for the systems $CO_2 - C_6$ to $CO_2 - C_{10}$ (open circles and diamonds) and the predicted critical lines ($k_{ij} = 0$) using the $SRK\ EoS$ (a), the $CPA\ EoS$ (b) and the $CCPA\ EoS$ (c) for three different temperatures. Pure component experimental data (Exp_1) were taken from the $DIPPR$ database, while the measurements for the mixtures (Exp_2) were taken from [26–30].

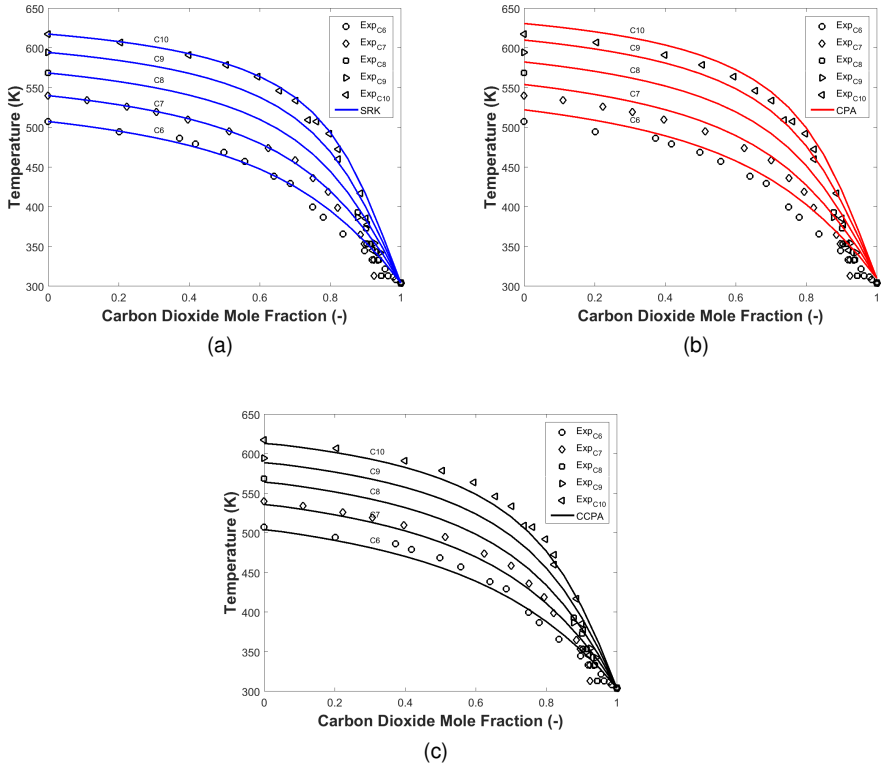

Figure 5.24: Experimental critical temperature as a function of the mole fraction of carbon dioxide for the systems CO_2-C_6 to CO_2-C_{10} (open circles and diamonds) and the predicted critical lines ($k_{ij}=0$) using the $SRK\ EoS$ (a), the $CPA\ EoS$ (b) and the $CCPA\ EoS$ (c) for three different temperatures. Pure component experimental data (Exp_1) were taken from the $DIPPR$ database, while the measurements for the mixtures were taken from [26–30].

As the concentration of CO_2 increases, the models are unable to describe the trends in the experimental data. This behavior indicates the need for using k_{ij} for improving the representation of the critical data, but also for the qualitative behavior of the system as the pure CO_2 critical point is approached.

Similar to the previous calculations, only a few data point for the critical volume was obtained in the literature (Figure 5.25). In the case of the CO_2-C_6 to CO_2-C_{10} mixtures, the measurements found were only in the region of high concentration of CO_2. For such concentrations, it is difficult to compare the ability of the models to represent experimental points; nonetheless, for the CO_2-C_{10} system, it is possible to observe that the introduction of the density

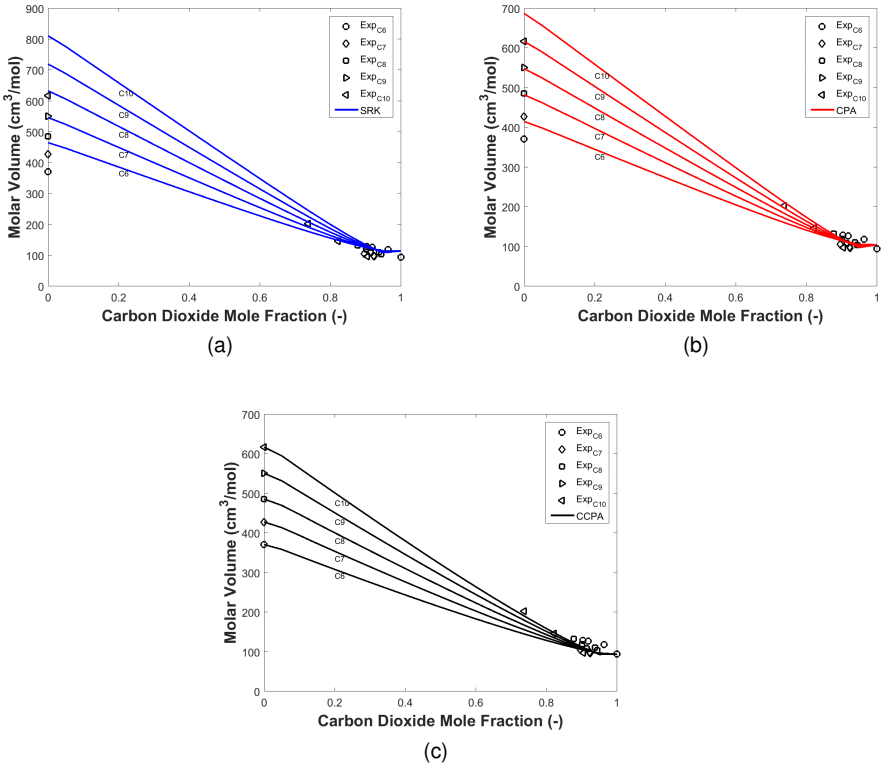

Figure 5.25: Experimental critical volume as a function of the mole fraction of carbon dioxide for the systems $CO_2 - C_6$ to $CO_2 - C_{10}$ (open circles and diamonds) and the predicted critical lines ($k_{ij} = 0$) using the $SRK\ EoS$ (a), the $CPA\ EoS$ (b) and the $CCPA\ EoS$ (c) for three different temperatures. Pure component experimental data (Exp_1) were taken from the $DIPPR$ database, while the measurements for the mixtures were taken from [26–30].

fluctuations improve the representation of the experimental critical volume of the mixture, as both mean-field equations predict a much higher value for the mixture's property.

The use of the binary interaction parameters optimized with VLE data increases the maximum pressure represented by all models, hence it causes an overestimation of the critical points by all models. It is clear from the comparison of the figures 5.23 and 5.26 that a k_{ij} is important for improving the representation of asymmetric systems with carbon dioxide and a n-alkane. As the magnitude of the interaction parameter is different if regressed from the sub-critical or critical regions, it is necessary to introduce a temperature

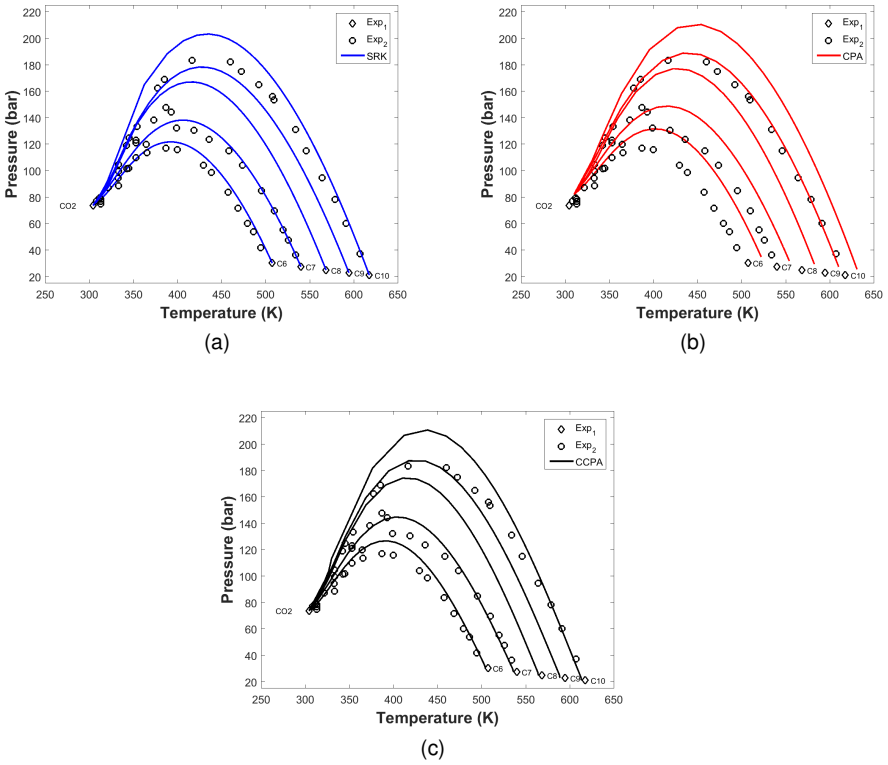

Figure 5.26: Experimental critical pressure as a function of the critical temperature for the systems $CO_2 - C_6$ to $CO_2 - C_{10}$ (open circles and diamonds) and the calculated critical lines with k_{ij} obtained from VLE data using the $SRK\ EoS$ (a), the $CPA\ EoS$ (b) and the $CCPA\ EoS$ (c). Pure component experimental data (Exp_1) were taken from the $DIPPR$ database, while the measurements for the mixtures (Exp_2) were taken from [26–30].

function in the estimation of the k_{ij}.

The deviations of the critical properties shown in Table 5.11 indicate that the crossover and the cubic equations yield similar predictions in terms of temperatures and pressures, and that they are superior to CPA. Nevertheless, the comparison with Table 5.9 shows that the increase of the molecular weight of the hydrocarbon is a challenge for the models, since the representations are not much improved even with the use of k_{ij} obtained from the fitting of the VLE region (Table 5.12). A thorough evaluation of the representation of CO_2 and n-alkane systems with crossover models was not found in the literature. Sun et al. [103] applied the crossover $SAFT - VR$ to represent the critical

lines of $CO_2 - C_2$ to $CO_2 - C_5$ mixtures. Precise match of the critical lines and the experimental points were obtained; however, no calculations for more asymmetric systems were applied by the authors. Additionally, for improving the descriptions, a temperature-independent k_{ij} was applied.

Finally, as mentioned before, the further increase in the molecular weight of the n-alkane increases the complexity in the phase behavior representation. Cismondi et al. [143] used cubic mixing rules for increasing the flexibility of the model in terms of the composition, allowing a precise representation of the critical properties for the homologous series of carbon and a n-alkane (from C_1 to C_{32}). Since the scope of the thesis is to evaluate the RG corrections to mean-field models, such approach for dealing with very asymmetric systems, where the difference in size and energy between the molecules play a major role in the phase behavior of the mixture, was not investigated.

5.3.2 Binary systems containing associating species

This part is concerned with the evaluation of the models to describe the critical behavior of binary mixtures containing associating species, using mean-field and non-mean-field models. Before analyzing the results obtained with the crossover models, it is important to compare the mean-field models, in order to asses the importance of the association term in CPA to represent the critical properties.

The first system evaluated in this part was the methanol/n-hexane mixture, in which the SRK and $CPA\ EoS$, using the original and rescaled parameters, were applied in the prediction of the experimental critical data. Figure 5.27 shows the critical temperature and pressure curves obtained by each model and the experimental points [27]. The graphs indicate that the use of the rescaled parameters is crucial for the correct representation of the critical curve of the system, as the original CPA overpredicts all the experimental points. It is also possible to conclude that the hydrogen bonding term is fundamental for the representation of the trend in data, because, when the binary interaction parameters are set to zero, the cubic model is only precise in the region close to the pure component limits. Furthermore, the trend of the critical pressure as a function of the composition of methanol (Figure 5.27b) is incorrectly predicted with the cubic model. The $SRK\ EoS$ is incapable of qualitatively describing the points of inflection that are observed in experimental data, a behavior which is captured by the CPA with the different approaches

Table 5.11: Average AAD of the critical temperature, pressure and volume for binary carbon dioxide/n-alkane systems ($CO_2 - C_6$ to $CO_2 - C_{10}$) calculated using the SRK, the CPA and the $CCPA$ EoS. No binary interaction coefficients were used in the calculations ($k_{ij} = 0$). The experimental data are shown in the reference column.

System	ΔT_c (%)			$Ref.$
	SRK	CPA	$CCPA$	
$CO_2 - C_6$	1.7	3.5	1.8	[26, 27]
$CO_2 - C_7$	2.3	4.2	2.5	[26, 28]
$CO_2 - C_8$	4.2	6.1	3.5	[26]
$CO_2 - C_9$	4.2	6.1	3.5	[29]
$CO_2 - C_{10}$	2.8	4.3	2.7	[28, 30]
Avg.	**3.0**	**4.8**	**2.8**	-
System	ΔP_c (%)			$Ref.$
	SRK	CPA	$CCPA$	
$CO_2 - C_6$	6.4	15.9	7.3	[26, 27]
$CO_2 - C_7$	8.1	13.8	6.0	[26, 28]
$CO_2 - C_8$	11.5	22.9	12.0	[26]
$CO_2 - C_9$	5.1	17.9	6.4	[29]
$CO_2 - C_{10}$	7.0	10.4	5.6	[28, 30]
Avg.	**7.6**	**16.2**	**7.5**	-
System	Δv_c (%)			$Ref.$
	SRK	CPA	$CCPA$	
$CO_2 - C_6$	11.7	11.9	11.5	[26, 27]
$CO_2 - C_7$	22.5	11.0	1.6	[26, 28]
$CO_2 - C_8$	12.1	6.51	6.8	[26]
$CO_2 - C_9$	-	-	-	[29]
$CO_2 - C_{10}$	27.3	11.5	4.2	[28, 30]
Avg.	**18.4**	**10.2**	**6.0**	-

Table 5.12: Average AAD of the critical temperature, pressure and volume for binary carbon dioxide/n-alkane systems ($CO_2 - C_6$ to $CO_2 - C_{10}$) calculated using the SRK, the CPA and the $CCPA$ EoS. Binary interaction coefficients regressed from VLE data were used in the calculations (Table 5.2). The experimental data are shown in the reference column.

System	ΔT_c (%)			$Ref.$
	SRK	CPA	$CCPA$	
$CO_2 - C_6$	1.0	1.7	1.9	[26, 27]
$CO_2 - C_7$	1.1	2.6	2.0	[26, 28]
$CO_2 - C_8$	4.8	3.3	3.7	[26]
$CO_2 - C_9$	1.6	3.0	0.9	[29]
$CO_2 - C_{10}$	2.1	2.6	1.7	[28, 30]
Avg.	**2.1**	**2.6**	**2.0**	-
System	ΔP_c (%)			$Ref.$
	SRK	CPA	$CCPA$	
$CO_2 - C_6$	8.1	16.6	11.6	[26, 27]
$CO_2 - C_7$	5.0	15.5	8.8	[26, 28]
$CO_2 - C_8$	9.7	13.5	6.5	[26]
$CO_2 - C_9$	6.7	15.1	4.1	[29]
$CO_2 - C_{10}$	3.9	16.4	13.3	[28, 30]
Avg.	**6.7**	**15.4**	**8.9**	-
System	Δv_c (%)			$Ref.$
	SRK	CPA	$CCPA$	
$CO_2 - C_6$	12.8	12.2	12.0	[26, 27]
$CO_2 - C_7$	17.0	7.5	2.0	[26, 28]
$CO_2 - C_8$	17.4	14.9	15.5	[26]
$CO_2 - C_9$	-	-	-	[29]
$CO_2 - C_{10}$	16.2	5.4	4.9	[28, 30]
Avg.	**15.8**	**10.0**	**8.6**	-

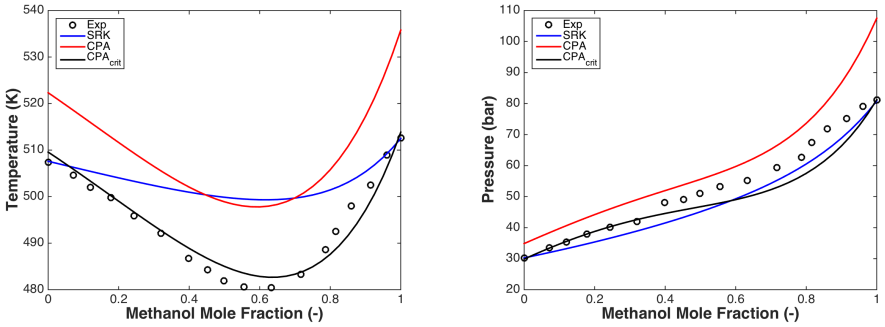

Figure 5.27: Experimental critical pressures (a) and temperatures (b) and the predicted curves ($k_{ij} = 0$) using the SRK and CPA with the literature and rescaled parameters as a function of methanol composition for the methanol/n-hexane system. The experimental data were taken from [27].

for determining the pure component parameters.

Figure 5.28 displays the experimental critical lines for the methanol/n-hexane system and the calculated curves with the binary interaction parameters regressed from LLE data. The comparison of figures 5.27 and 5.28 points out that the representations of the critical points with the association model are not much affected when the k_{ij} is optimized in the LLE region. On the other hand, for the SRK EoS a considerable improvement in the description of the critical temperature is observed, since the minimum critical temperature is lowered from around $500K$ (Figure 5.27a) to a temperature close to $490K$ (Figure 5.28a), while the experimental minimum is around $480K$. Yet, no significant improvements are obtained in the description of the critical pressures, and the model yields a qualitatively erroneous trend for P_c as a function of the mole fraction of methanol.

The performance of the models can be further improved with the optimization of the binary interaction parameters using experimental critical data. The objective function that is minimized for the determination of the k_{ij} is given by the expression:

$$OF = \frac{1}{N}\sum_{i=1}^{N}\left|\frac{T_c^{calc} - T_c^{exp}}{T_c^{exp}}\right| + \frac{1}{N}\sum_{i=1}^{N}\left|\frac{P_c^{calc} - P_c^{exp}}{P_c^{exp}}\right| \tag{5.3}$$

where T_c and P_c are the critical temperatures and pressure, respectively, and

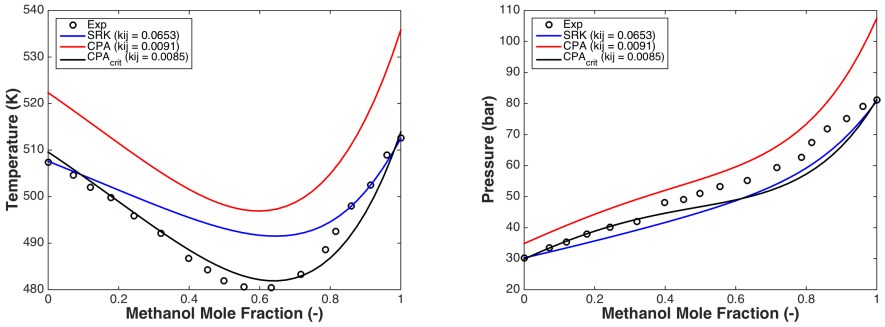

(a) (b)

Figure 5.28: Experimental critical pressures (a) and temperatures (b) and the calculated curves using the SRK and CPA with the literature and rescaled parameters as a function of methanol composition for the methanol/n-hexane system. The k_{ij} were optimized with data from LLE region and critical experimental data were taken from [27].

the superscripts $calc$ and exp are the calculated and experimental properties, respectively.

Figure 5.29 shows the results obtained with the models using a k_{ij} calculated with the fitting of the critical data. The comparison between the curves shows that, for improved representations in the critical region, the cubic and association model with the original parameters require very high binary interaction coefficients, differently from CPA with rescaled parameters. This indicates the importance of the rescaling of the pure component parameters and the hydrogen bonding term in critical point calculations with associating species, since even with large k_{ij}, SRK is qualitatively incorrect for the representation of the critical pressures, while CPA with the literature parameters is not affected in the regions close to the pure species.

In addition to the methanol/n-hexane system, the same calculations were performed for the systems containing methanol and heavier n-alkanes (from n-heptane to n-decane). Figure 5.30 shows the results for all the methanol/n-alkane systems studied, and in the Figure 5.30a no k_{ij} were applied in the calculations, while in the Figure 5.30b the k_{ij} were optimized by fitting the critical experimental data. From the plots, it is possible to conclude that the binary interaction parameters are important for the first two models, in order to improve the representation of the experimental data. On the other hand, it does not affect much the predictions obtained with CPA_{crit}. It can also be

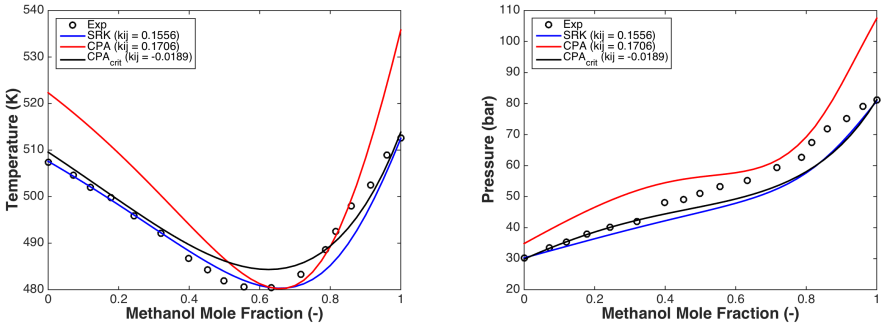

Figure 5.29: Experimental critical pressures (a) and temperatures (b) and the calculated curves using the SRK and CPA with the literature and rescaled parameters as a function of methanol composition for the methanol/n-hexane system. The k_{ij} were optimized with the critical experimental data taken from [27].

seen that the correlations become worse as the molecular weight of the n-alkane increases. In the case of $C_1 - C_{10}$, the model that has the best fitting of the experimental data is CPA, even though it has the biggest deviations near the pure component region. However, it cannot correctly correlate the data of the system $C_1 - C_6$, as discussed before. Therefore, this behavior shows that as the asymmetry between molecules increases, different mixing rules or temperature-dependent binary parameters are needed for improving the descriptions of the experimental data.

After the comparison of the mean-field models, it is important to evaluate the modification obtained with the application of White's recursive procedure to introduce long-range density fluctuations in the model and correctly describe the critical phenomena. As it was shown previously, the $CCPA$ reduces to $CSRK$ when no associating component is present in the system; besides, the association term is also important for the qualitative and quantitative description of the critical behavior in such systems, therefore all the critical point computations were done with the $CCPA$.

Figure 5.31 shows the critical curves of the methanol/n-alkane systems studied in this work. The calculations were pure predictions, as no binary interaction parameters were applied in the estimations. Similar to the CPA EoS with the rescaled pure component parameters, this model is not affected much by the k_{ij} used, hence the comparison with experimental data and the

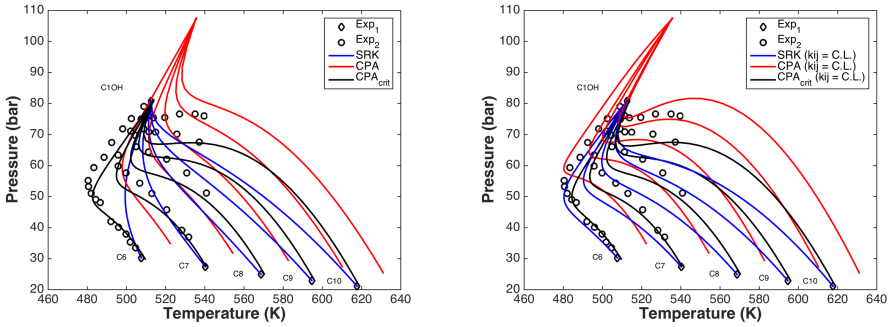

(a) (b)

Figure 5.30: Critical lines of the methanol/n-alkane (from n-hexane to n-decane) systems. Pure component experimental data (Exp_1) were taken from the $DIPPR$ database, while the measurements for the mixtures (Exp_2) were taken from [27, 31]. The curves were calculated with the SRK (blue lines) and $CPA\ EoS$ with literature (red lines) and rescaled parameters (black lines). In the first plot (a), no binary interaction coefficients ($k_{ij} = 0$) were utilized, while in the second (b), the binary interaction parameters were regressed using the experimental critical data.

classical CPA was done using the pure predictions obtained from the models. The comparison of the models with the experimental critical data points out that $CCPA$ is superior to the classical model, as the mean-field model overpredicts the experimental data. Nevertheless, as the molecular weight of the hydrocarbon in increased, the prediction of the pressure in the point of minimum temperature is much lower than the experimental one. Moreover, different temperature-independent k_{ij} were applied in the critical point calculations using the crossover model; nonetheless, no substantial improvements were obtained, hence the results were not plotted in this work.

Table 5.13 presents the performance of each model in the description of the critical properties and the values of the k_{ij} regressed by minimizing the deviations in the experimental critical temperatures and pressures, Equation (5.3). The only exception is the $CCPA\ EoS$, for which the deviations were calculated from the predictive results.

The comparison of the deviations from experimental data calculated with the models are useful for the evaluation of the importance of the incorporation of the density fluctuations in the classical EoS (Table 5.13). It can be seen that the representation of the measured critical points deteriorates with the

Table 5.13: Deviations of the critical properties for the methanol/n-hexane to methanol/n-decane binary systems using the SRK, CPA with the literature and rescaled parameters, and $CCPA$ using k_{ij} optimized with critical experimental data, except for the $CCPA$ EoS.

System	EoS	ΔT_c (%)	ΔP_c (%)	k_{ij}	$Ref.$
$C_1OH - C_6$	SRK	4.4	2.0	0.1556	[27]
	CPA	8.1	8.0	0.1706	
	CPA_{crit}	3.5	2.2	-0.0189	
	$CCPA$	0.7	2.8	0.0000	
$C_1OH - C_7$	SRK	5.9	1.7	0.1581	[31]
	CPA	7.0	9.8	0.1618	
	CPA_{crit}	3.7	1.5	0.0136	
	$CCPA$	0.9	4.0	0.0000	
$C_1OH - C_8$	SRK	7.2	1.7	0.1282	[31]
	CPA	8.5	8.7	0.1759	
	CPA_{crit}	4.7	2.2	0.0003	
	$CCPA$	1.2	4.6	0.0000	
$C_1OH - C_9$	SRK	7.6	1.6	0.0924	[31]
	CPA	7.9	8.0	0.1582	
	CPA_{crit}	5.4	2.0	-0.0055	
	$CCPA$	1.4	5.2	0.0000	
$C_1OH - C_{10}$	SRK	9.5	1.6	0.0983	[31]
	CPA	6.8	6.9	0.1698	
	CPA_{crit}	6.5	2.5	0.0160	
	$CCPA$	1.6	6.4	0.0000	
Avg.	SRK	**6.9**	**1.7**	**-**	**-**
	CPA	**7.7**	**8.3**		
	CPA_{crit}	**4.8**	**2.1**		
	$CCPA$	**1.2**	**4.6**		

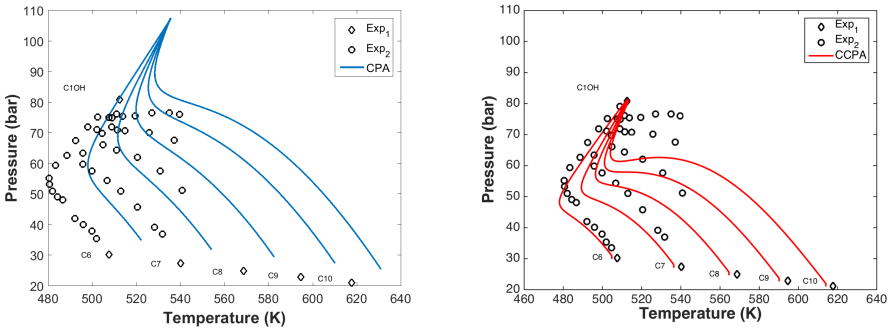

Figure 5.31: Critical lines of the methanol/n-alkanes systems studied in this work. Pure component experimental data (Exp_1) were taken from the $DIPPR$ database, while the measurements for the mixtures (Exp_2) were taken from [27, 31], while calculated curves with $k_{ij} = 0$ were obtained using the CPA (a) and $CCPA$ (b) EoS.

increase of the asymmetry between the components for all the models. However, while SRK and CPA_{crit} are superior to $CCPA$ in the description of the critical pressures, the non-mean-field equation is better in the prediction of the critical temperatures. The calculations have shown that the improved representation of P_c with the classical models are related to the use of k_{ij} optimized with the critical data, which, on the other hand, increased the deviations with respect to T_c. This behavior shows that, although the RG corrections are fundamental for enhancing the results yielded by CPA, a quantitative description of both critical properties needs a different approach to deal with asymmetric systems, as observed before for systems with non-associating molecules.

Xu et al. [114] modeled the methanol/n-hexane to methanol/n-decane series using the crossover $CPA\ EoS$ with a different expression for the initial free energy density (f_0). The overall AAD between the experimental and predicted critical temperatures and pressure were 0.92% and 4.13%, respectively. These values are similar to the ones obtained in this work, i.e. 1.16% for T_c and 4.60% for P_c. The similarity in the results indicates that the models behave equivalently, and possibly more complex mixing rules are necessary for the improvement of the representation of the critical pressures.

The final calculations were done for the methanol/1-propanol and methanol/1-butanol systems. The importance of these calculations is to test the models for representing cross-associating systems. As mentioned in chapter 2, we have

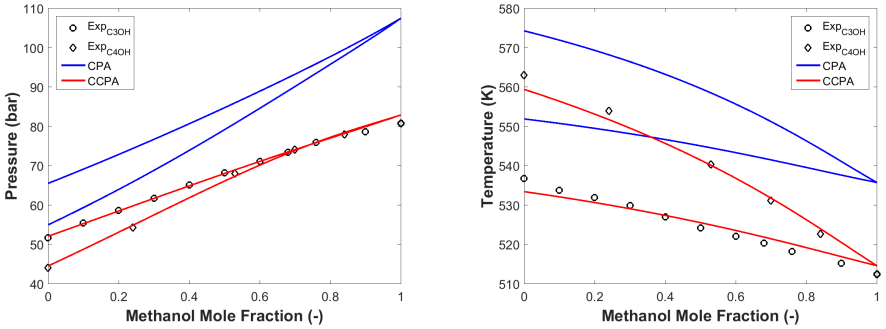

Figure 5.32: Critical temperature (a) and pressure (b) as a function of methanol mole fraction for the methanol/1-propanol and methanol/1-butanol mixtures. Experimental data were taken from [32] and [33], while calculated curves were obtained using the CPA and $CCPA\ EoS$.

used the $CR1$ combining rule to calculate the interaction between the different associating energies and volumes. As seen in Figure 5.32, the trends of the critical pressures and temperatures are similar, although the $CPA\ EoS$ yields larger deviations than the crossover model. The results show that the recursive procedure modifies the predictions of the critical properties, reducing the temperatures and pressures, matching the experimental data. However, the similarity in the trends indicates that the recursive procedure does not change the features of the mean-field equation with the association term, which is essential for the qualitative representation of the critical behavior of mixtures with cross-associating species.

5.3.3 Ternary systems

Experimental data for ternary systems in critical conditions are scarce in the literature. One example of such measurements was done by Soo et al. [165], in which the critical temperatures and pressures of the ternary system composed of ethanol, n-pentane and n-hexane were measured using a dynamic-synthetic apparatus.

In the case of ternary systems, the thermodynamic models yield a critical surface that connects the pure component critical points, as long as the binary systems belong to type I phase behavior according to van Konynenburg and Scott classification [2]. This is the case for the ethanol/n-pentane/n-hexane

mixture. Besides, due to the presence of a hydrogen bonding component (ethanol), the calculations were only done with the CPA and $CCPA\ EoS$.

Before the assessment of the models to represent the critical points of the ternary system, it is important to observe the performance of the models to describe the experimental critical data of the binary systems present in the ternary mixture. Figure 5.33 shows the predicted critical temperatures as a function of the composition of the lighter species in the mixture. The graphs indicate that the RG corrections allow an accurate description of the critical temperatures, reducing the overprediction of the mean-field model, without the need for introducing a binary interaction parameter. The same conclusion can be attained from the plots of the critical pressure as a function of the mole fraction of the lighter component (Figure 5.34). Finally, it can be concluded that the deviations are particularly large when calculated with the mean-field model, for the regions with a high content of ethanol, which is expected due to the reasons discussed previously.

After the modeling of the binary systems, the calculations were performed for the ternary system, and the results were plotted along with experimental data, in order to allow an evaluation of the behavior of the equations to represent the critical surface. Figure 5.35 shows the experimental critical temperature of the $C_2OH - C_5 - C_6$ system as a function of the composition of ethanol and n-hexane, along with the critical surfaces calculated with the CPA and $CCPA\ EoS$, figures 5.35a and 5.35b respectively. The comparison of the results indicates a similarity between the trends predicted by the models, additionally it shows that the difference between the experimental critical temperatures are much higher for CPA close to the limit of the pure alcohol, as seen for the binary mixtures. This behavior is even more pronounced in the case of the critical pressures (Figure 5.36a). The application of the recursive procedure, as observed previously, improves the representation of the pure component critical points and binary critical lines, which allows a correct description of the ternary system in all ranges of composition.

The capability of crossover the model to represent the experimental critical data is easily seen in the plot that gives the deviations regarding the critical temperatures and pressures as a function of the composition of ethanol and n-hexane, figures 5.37 and 5.38. The mole fractions of the experimental points were used as input in the model and the calculated critical properties were compared and plotted using a triangulation procedure to create a surface, where the errors are indicated by the color scale. In the case of the represen-

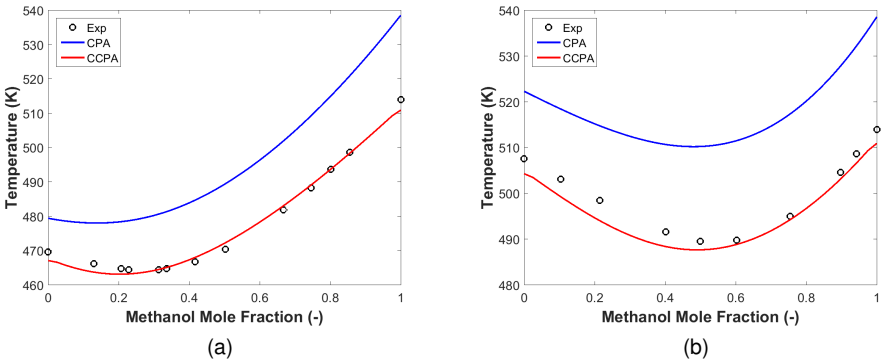

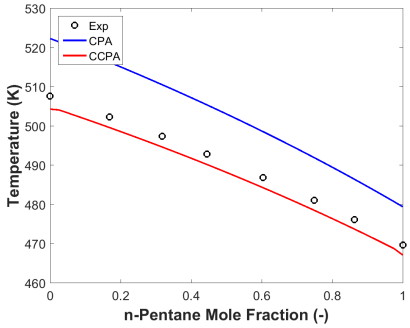

Figure 5.33: Critical temperature as a function of the composition of the lighter component for the systems ethanol/n-pentane (a), ethanol/n-hexane (b) and n-pentane/n-hexane (c). The critical lines were calculated with the CPA (blue lines) and $CCPA$ (red lines) EoS using no interaction parameters ($k_{ij} = 0$), while experimental data were taken from [17].

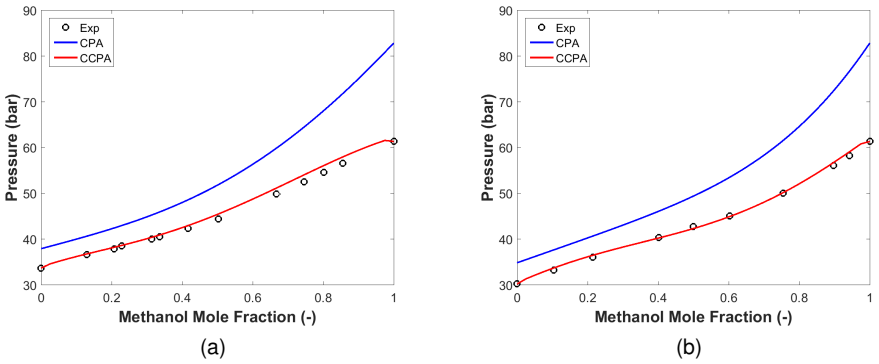

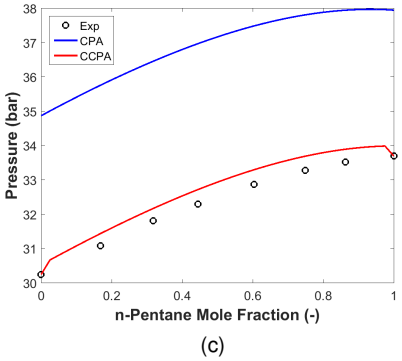

Figure 5.34: Critical pressure as a function of the composition of the lighter component for the systems ethanol/n-pentane (a), ethanol/n-hexane (b) and n-pentane/n-hexane (c). The critical lines were calculated with the CPA (blue lines) and $CCPA$ (red lines) EoS using no interaction parameters ($k_{ij} = 0$), while experimental data were taken from [17].

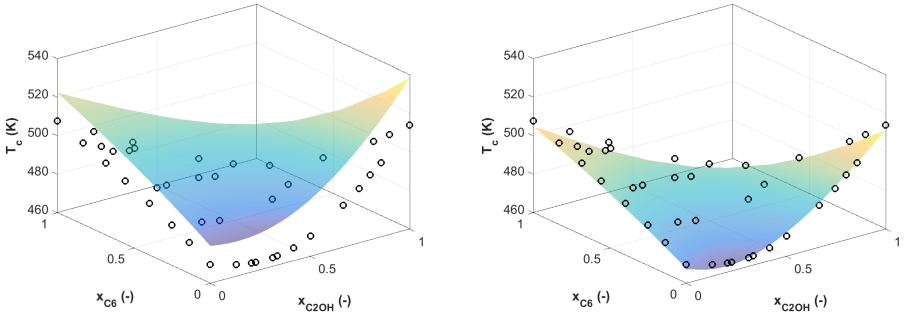

Figure 5.35: Experimental critical temperature of the ternary $C_2OH - C_5 - C_6$ system as a function of the composition of ethanol and n-hexane (open circles), and the calculated critical surfaces using the CPA (a) and the $CCPA$ (b). Experimental data were taken from [17].

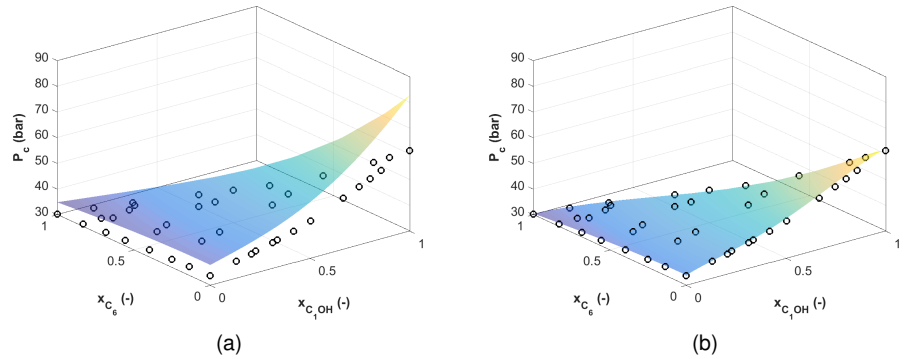

Figure 5.36: Experimental critical pressures of the ternary $C_2OH - C_5 - C_6$ system as a function of the composition of ethanol and n-hexane (open circles), and the calculated critical surfaces using the CPA (a) and the $CCPA$ (b). Experimental data were taken from [17].

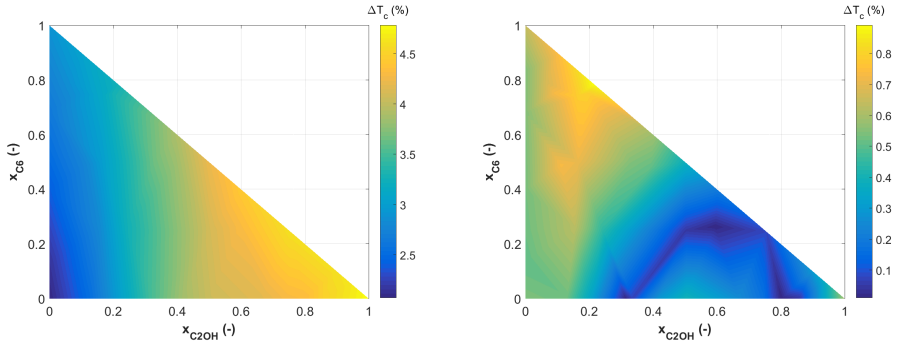

Figure 5.37: Critical temperature AAD of the ternary $C_2OH - C_5 - C_6$ system calculated using the CPA (a) and the $CCPA$ (b). Experimental data were taken from [17].

tation of the critical temperatures, it can be concluded that the $CCPA$ has an excellent agreement with the experimental data, as the maximum deviations are below 1%, while for the mean-field model it is close to 4.5%. On the other hand, for the critical pressures, the deviations were higher, with a maximum AAD of 2.5%; nevertheless, the improvement of the CPA EoS is more significant for this property, as the deviations with the mean-field model can reach 35% close to the limit of pure ethanol.

The results for the $C_2OH - C_5 - C_6$ system indicates that the incorporation of the density fluctuations to the CPA EoS are also important for multicomponent systems, and for this case with an associating molecule (ethanol) and two hydrocarbons of similar size (C_5 and C_6) no binary interaction parameters are necessary for the precise representation of the experimental data. Nevertheless, the generalization of this conclusion to other systems requires the evaluation of other multicomponent mixtures, in particular for mixture possessing a more complex phase behavior in which the pure components critical points are not linked by the critical lines (type III to type V).

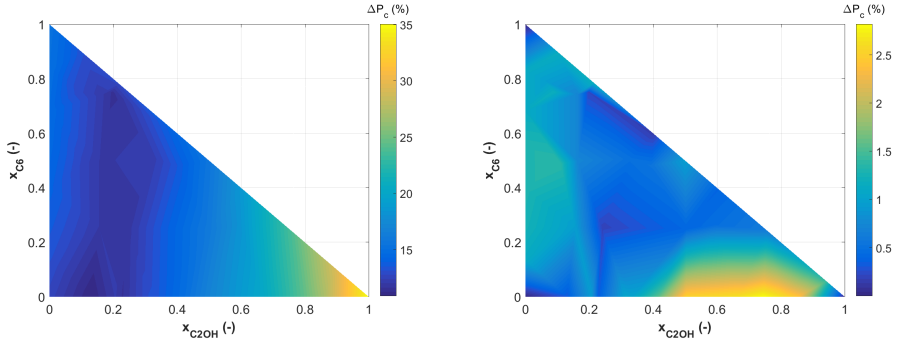

Figure 5.38: Critical pressure AAD of the ternary $C_2OH - C_5 - C_6$ system calculated using the CPA (a) and the $CCPA$ (b). Experimental data were taken from [17].

Chapter 6

Conclusions

This thesis is devoted to the improvement of the thermodynamic models that are widely used to represent the phase equilibria of fluids relevant to the oil and gas industry. The SRK and $CPA\ EoS$ were corrected with a recursive procedure based on the renormalization group theory, which introduces density fluctuations in the mean-field equations, thus allowing the correct representation of the non-analytical and asymptotic behavior of fluids in the critical region. Far away from the critical point, the fluctuations become negligible and the model reduces to the classical one, yielding the analytical behavior of fluids of traditional EoS. Such models are referred to as crossover EoS and are useful for applications in the oil & gas sector, as well as other industries, because they are able of precisely representing the phase behavior of systems in a wide range of conditions, i.e. in conditions close to and far away from critical. If applied to process simulators, they might increase the reliability of the calculations and help in the design of equipment and process optimization containing complex fluids in broad ranges of temperatures, pressures and compositions, e.g. the compositional reservoir simulation of deep high-temperature/high-pressure reservoirs.

In this work, different classical thermodynamic models were applied in the calculation of the phase equilibria of non-associating and hydrogen bonding species, then the results were compared with experimental data, with the aim to assess the advantages and shortcommings of the distinct approaches. Moreover, a new procedure for rescaling the pure compound parameters of CPA was developed, using the PSO method to minimize an objective function containing critical point information, in an attempt to overcome one of the

limitations of this equation, i.e. the overprediction of the critical properties. In addition to these computations, White's recursive procedure was used with SRK and CPA and the non-mean-field equations were systematically compared to experimental data and the underlying models, in order to obtain a complete overview of the improvements achieved with the incorporation of the density fluctuations, along with the limitations of the crossover models. The mixtures studied in the thesis were comprised of hydrocarbon (from methane to decane), carbon dioxide, methanol and others. Besides, various homologous series were investigated in order to evaluate effects like asymmetry, hydrogen bonding and others.

In the initial calculations, mean-field models (SRK, PT and CPA with the literature and rescaled pure component parameters) were utilized to represent the saturated properties of pure species, including non-associating and associating compounds. The comparison of the results showed that the the additional constant of the PT EoS improves the description of liquid phase saturated volume of non-associating properties, yet the two cubic models are unable to correctly describe pure hydrogen bonding fluids. On the other hand, CPA with the parameters optimized through the matching of experimental data away from the critical point overestimates the critical pressures and temperatures, while precisely represents the saturated properties. The use of the rescaled parameters improved the representation of the critical properties of pure fluids with the CPA EoS at the cost of an increase in the deviation of the saturated liquid phase volume and the critical volume. These deviations can be reduced with the application of a volume translation method; however, the model still gives an analytical representation of the near-critical region, which is not in accordance with the real behavior of fluids.

These deficiencies were corrected with the application of White's recursive procedure to two mean-field EoS studied in this work, i.e. SRK and CPA. The behavior of the classical thermodynamic models were modified in the critical region via inclusion of density fluctuations. This procedure allowed a precise description of the thermodynamic properties, both phase equilibrium and critical, of the pure species. For hydrogen bonding components, the association term plays an important role in the calculation of the saturated properties, thus only $CCPA$ were used to describe such systems. Additionally, the crossover models are capable of producing non-mean-field critical exponents that are close to experimental values.

The VLE calculations of non-associating fluid mixtures (methane/n-alkane

and CO_2/n-alkane) showed that all models are capable of representing such properties. However, the deviations increase with the asymmetry between the components, that is when one of the components molecular weight is much higher than the other. As the critical point is approached, CPA predicts a bigger phase envelope, which is corrected with the crossover model. Furthermore, the incorporation of density fluctuations is fundamental for the correct representation of the volume of the liquid phase, especially close to the critical point. In the case of hydrogen bonding species, it was observed that the association term is needed for the quantitative description of the phase diagrams, and that both $CCPA$ and CPA with the rescaled parameters can describe the measured data, although higher k_{ij} are required in comparison to the classical $CPA\ EoS$. The $CCPA\ EoS$ behaves equivalently to the underlying mean-field model, but it improves the representation of the phase equilibrium properties as the critical point is reached.

For the LLE computations, it was seen that only CPA with parameters obtained from the fitting of the saturated properties far from the critical point and the $CCPA\ EoS$ can correctly describe both the hydrocarbon rich and the oil rich phase compositions. Thus, it indicates that the rescaling procedure is useful if applied to specific regions of the phase diagram. On the other hand, a superior global representation of the equilibrium data is attained with the application of the crossover approach.

Finally, the critical point calculations pointed out that the $SRK\ EoS$ is able to accuratly represent the critical pressures and temperatures of the fluid mixtures containing non-associating compounds, as long as the difference in size between the components is not too large. Nonetheless, this model yields the worst description of the critical volumes. The $CCPA\ EoS$ corrects the overestimation of the critical lines with the mean-field model, and it yields the best representations of the critical volumes of the systems studied. It is important to note that the capability of the models to reproduce the phase behavior of mixtures deteriorates with the increase of asymmetry between the components in the system, meaning that different approaches, i.e. more complex mixing rules or temperature-dependent interaction parameters, might be necessary for the quantitative description of the experimental data for these mixtures. For systems with associating and cross-associating components, it was seen that the recursive procedure improves the predictions of CPA, and excellent results for the critical temperature and pressure are obtained, except for the more asymmetric cases. One ternary system with a hydrogen bonding molecule

was investigated, and the critical surface are in good agreement with the measured experimental critical points.

In summary, this work has shown that a simple procedure can be used to correct the limitations regarding the near-critical behavior of mean-field models widely used in the Oil & Gas industry. Still, further improvements should be analyzed, and this is the topic of the next section.

6.1 Suggestions to Future Work

This study covered the application of mean-field and crossover models to describe thermodynamic properties of pure fluids and mixtures containing non-associating and hydrogen bonding species over a wide range of conditions. The results showed some of the advantages and shortcomings of the different EoS; however, further investigations will be useful for clarifying certain points that were not evaluated in this work. Some suggestions are given below:

- Evaluate the performance of the $CCPA\ EoS$ in the representation of the phase equilibrium properties of different fluids that are useful for the oil & gas industry, e.g. glycols and asphaltenes, and compare to the mean-field approaches.
- Parametrize and compare the results of the crossover models with different mean-field equations for other species, like the ones cited above.
- Apply a sensitivity and uncertainty analysis of the crossover EoS pure component parameters, with the aim to evaluate the ones that are more important the phase behavior calculations.
- Test the models with respect to the representation of derivative properties, e.g. heat capacity, compressibility, etc.
- Introduce new mixing rules and mean-field models in order to account for the asymmetry of the molecules present in the system.
- Investigate the effect of solvation with CO_2 and a self-associating system.
- Extend the crossover approach to take into account the fluctuations in the LLE critical phenomena, for which the order parameter becomes

the difference between the composition of one of the components in the different phases in equilibrium.

- Evaluate and optimize the computational speed of the recursive model by using volume-based thermodynamics, and compare the phase equilibrium calculations with cubic and non-cubic EoS.

Bibliography

[1] Horstmann, S. *Theoretische und Experimentelle Untersuchungen zum Hochdruckphasengleichgewichtsverhalten Fluider Stoffgemische für die Erweiterung der PSRK-Gruppenbeitragszustandsgleichung*. Ph.d. thesis (2000). xix, 27

[2] van Konynenburg, P. & Scott., R. Critical lines and phase equilibria in binary van der Waals mixtures. *Philosophical Transactions of the Royal Society A* 495–540 (1980). xix, 23, 28, 31, 87, 114, 128, 145

[3] Vinhal, A. P., Yan, W. & Kontogeorgios, G. M. Evaluation of equations of state for simultaneous representation of phase equilibrium and critical phenomena. *Fluid Phase Equilib.* **437**, 140–154 (2017). xx, 56, 57, 104, 107, 111

[4] Palma, A., Oliveira, M., Queimada, A. & Coutinho, J. Re-evaluating the CPA EOS for improving critical points and derivative properties description. *Fluid Phase Equilib.* **436**, 85–97 (2017). xx, xxxi, xxxii, 57, 58, 59, 60, 107, 113

[5] Vinhal, A. P. C. M., Yan, W. & Kontogeorgis, G. M. Application of a crossover equation of state to describe phase equilibrium and critical properties of n-alkanes and methane/n-alkane mixtures. *J. Chem. Eng. Data* **63**, 981–993 (2018). xx, 61, 62, 87

[6] Zielkiewicz, J. (Vapor + liquid) equilibria in (propan-1-ol + heptane + octane) at the temperature 313.15 K. *J. Chem. Thermodyn.* 455–62 (1992). xxii, 87

[7] Wichterle, O. & Kobayashi, R. Vapor-liquid equilibrium of methane-ethane system at low temperatures and high pressures. *J. Chem. Eng. Data* **17**, 9–12 (1972). xxii, 89, 93

[8] Davalos, J., Anderson, W., Phelps, R. & Kidnay, A. Liquid-vapor equilibria at 150.00 K for systems containing methane, ethane and carbon dioxide. *Chem. Eng. Data* **21**, 81–84 (1976). xxii, 89, 93

[9] Sage, B., Hicks, B. & Lacey, W. Phase equilibria in hydrocarbon systems: The methane-n-butane system in the two-phase region. *Ind. Eng. Chem.* **32**, 1085–1092 (1940). xxii, 90, 93

[10] Roberts, L., Wang, R., Azarnoosh, A. & McKetta, J. Methane-n-butane system in the two-phase region. *Chem. Eng. Data* **7**, 484–485 (1962). xxii, 90, 93

[11] Reamer, H., Sage, B. & Lacey, W. Phase equilibria in hydrocarbon systems. Volumetric and phase behavior of the methane-n-heptane system. *Chem. Eng. Data Ser.* **1**, 29–42 (1956). xxiii, 92, 93

[12] Wei, M.-W., Brown, T., Kidnay, A. & Sloan, E. Vapor + liquid equilibria for the ternary system methane + ethane + carbon dioxide at 230 K and its constituent binaries at temperatures from 207 to 270 K. *J. Chem. Eng. Data* **40**, 726–731 (1995). xxiii, 95, 97, 101

[13] Olds, R., Reamer, H., Sage, B. & Lacey, W. The n-butane-carbon dioxide system. *J. Ind. Eng. Chem.* **41**, 475–482 (1949). xxiii, xxv, xxvi, 98, 100, 101, 102, 125, 126, 127, 129, 130, 131

[14] Reamer, H. & Sage, B. Phase equilibria in hydrocarbon systems. volumetric and phase behavior of the n-decane-CO2 system. *J. Chem. Eng. Data* **8**, 508–513 (1963). xxiii, 101, 102

[15] Koennecke, H. G. Ergebnisse von Dampfflüssigkeits-Phasengleichgewichtsuntersuchungen am System n-Hexan-Methylcyclohexan-Methanol bei 60°C. *J. Prakt. Chem.* **311**, 974–982 (1969). xxiii, xxiv, 105, 106, 107

[16] Hongo, M., Tsuji, T., Fukuchi, K. & Arai, Y. Vapor-liquid equilibria of methanol + hexane, methanol + heptane, ethanol + hexane, ethanol + heptane, and ethanol + octane at 298.15 K. *J. Chem. Eng. Data* **39**, 688–691 (1994). xxiii, 105, 106

[17] Seo, J., Lee, J. & Kim, H. Isothermal vapor-liquid equilibria for the system ethanol and n-hexane in the near critical region. *Fluid Phase Equi-*

lib. **182**, 199–207 (2001). xxiv, xxviii, xxix, 109, 147, 148, 149, 150, 151

[18] Skrzecz, A. Critical evaluation of solubility data in binary systems formed by methanol with n-hydrocarbons. *Thermochim. Acta* **182**, 123–131 (1991). xxiv, 108, 111, 112, 113

[19] Higashiuchi, H. & Sakuragi, Y. Measurement and correlation of liquid-liquid equilibria of binary and ternary systems containing methanol and hydrocarbons. *Fluid Phase Equilib.* **36**, 35–47 (1987). xxiv, 108, 111, 112, 113

[20] Hicks, C. P. & Young, C. L. The gas-liquid critical properties of binary mixtures. *Chem. Rev.* **75**, 119–175 (1975). xxiv, xxv, xxxiii, 116, 117, 118, 119, 120, 121, 123

[21] Mraw, S., Hwangand, S.-C. & Kobayashi, R. Vapor-liquid equilibrium of the methane-carbon dioxide system at low temperatures. *J. Chem. Eng. Data* **23**, 135–139 (1978). xxv, xxvi, 125, 126, 127, 129, 130, 131

[22] Horstmann, S., Fischer, K., Gmehling, J. & Kolar, P. Experimental determination of the critical line for (carbon dioxide + ethane) and calculation of various thermodynamic properties for (carbon dioxide + n-alkane) using the PSRK model. *J. Chem. Thermodyn.* **32**, 451–464 (2000). 130, 131

[23] Roof, J. & Baron, J. Critical loci of binary mixtures of propane with methane, carbon dioxide, and nitrogen. *J. Chem. Eng. Data* **12**, 292–293 (1967). 130, 131

[24] Poettmann, F. & Katz, D. Phase behavior of binary carbon dioxide-paraffin systems. *J. Ind. Eng. Chem.* **37**, 847–853 (1945). 130, 131

[25] Reamer, H., Sage, B. & Lacey, W. Phase equilibria in hydrocarbon systems. Volumetric and phase behavior of the propane-carbon dioxide system. *J. Ind. Eng. Chem.* **43**, 2515–2520 (1951). xxv, xxvi, 125, 126, 127, 129, 130, 131

[26] Sun, Y., Li, Y., Zhou, J., Zhua, R. & Tiana, Y. Experimental determination and calculation of the critical curves for the binary systems of CO2 containing ketone, alkane, ester and alcohol, respectively. *Fluid Phase Equilib.* **307**, 72–77 (2011). xxvi, xxvii, 132, 133, 134, 135, 137, 138

[27] Liu, J., Qin, Z., Wang, G., Hou, X. & Wang, J. Critical properties of binary and ternary mixtures of hexane + methanol, hexane + carbon dioxide, methanol + carbon dioxide, and hexane + carbon dioxide + methanol. *J. Chem. Eng. Data* **48**, 1610–1613 (2003). xxvii, xxviii, 3, 136, 137, 138, 139, 140, 141, 142, 143, 144

[28] Juntarachat, N., Bello, S. & R. Privat, J.-N. J. Validation of a new apparatus using the dynamic method for determining the critical properties of binary mixtures containing CO2 and a n-alkane. *Fluid Phase Equilib.* **325**, 66–70 (2012). 137, 138

[29] Choi, E.-J. & Yeo, S.-D. Critical properties for carbon dioxide + n-alkane mixtures using a variable-volume view cell. *J. Chem. Eng. Data* **43**, 714–716 (1998). 137, 138

[30] Remy, B. & Degiovanni, A. Measurements of the thermal conductivity and thermal diffusivity of liquids. Part II: Convective and radiative effects. *Int. J. Thermophys.* **27**, 949–969 (2006). xxvi, xxvii, 132, 133, 134, 135, 137, 138

[31] de Loos, T. W., Poot, W. & de Swaan Arons, J. Vapour-liquid equilibria and critical phenomena in methanol + n-alkane systems. *Fluid Phase Equilib.* **42**, 209–227 (1998). xxviii, 106, 142, 143, 144

[32] Nazmutdinov, A., Alekina, E. & Nesterova, T. Concentration dependences of the critical temperatures of binary mixtures of nonaqueous components. *Russ. J. Phys. Chem. A.* **82**, 1857–1862 (2008). xxviii, 145

[33] Wang, L., Han, K., Xia, S., Ma, P. & Yan, F. Measurement and correlation of critical properties for binary mixtures and ternary mixtures containing gasoline additives. *J. Chem. Thermodyn.* **74**, 161–168 (2014). xxviii, 145

[34] Tsivintzelis, I. *et al.* The Cubic-Plus-Association EOS. Parameters for pure compounds and interaction parameters. Tech. Rep., Technical University of Denmark, CERE, Center for Energy Resources Engineering Department of Chemical and Biochemical Engineering (2012). xxxi, 46, 47

[35] Hendriks, E. *et al.* Industrial requirements for thermodynamics and transport properties. *Ind. Eng. Chem. Res.* **49**, 11131–11141 (2010). 1, 10

[36] Moser, B. & Kistenmacher, H. An analysis of the industrial use of a phase equilibria prediction model based on thermodynamic perturbation theory. *Fluid Phase Equilib.* **34**, 189–201 (1987). 1

[37] Wei, Y., Chen, Z., Satyro, M., Dong, C. & H., D. Compositional simulation using the advanced Peng-Robinson equation of state. In *SPE Reservoir Simulation Symposium* (Society of Petroleum Engineers, The Woodlands, Texas, USA, 2011). SPE141898. 2

[38] Kontogeorgis, G. M. & Folas, G. K. *Thermodynamic Models for Industrial Applications: From Classical and Advanced Mixing Rules to Association Theories* (Wiley, Chichester, West Sussex, United Kingdom, 2010), 1st edn. 2, 17, 18, 19, 20, 21, 46, 51, 55, 104

[39] Anisimov, M. A. & Sengers, J. V. *Supercritical Fluids*, vol. 366, chap. Critical and Crossover Phenomena in Fluids and Fluid Mixtures, 89–121 (Springer Netherlands, Dordrecht, 2000). 2, 3, 10, 25, 48, 57

[40] Kontogeorgis, G. M. *et al.* Ten years with the CPA (Cubic-Plus-Association) equation of state. Part 1. Pure compounds and self-associating systems. *Ind. Eng. Chem. Res.* **45**, 4855–4868 (2006). 2, 3, 17, 45, 107

[41] Shinta, A. & Firoozabadi, A. Equation of state representation of aqueous mixtures using an association model. *Can. J. Chem. Eng.* **73**, 367–379 (1995). 2

[42] Economou, I. G. & Donohue, M. D. Chemical, quasi-chemical and perturbation theories for associating fluids. *AIChE J.* **37**, 1875–1894 (1991). 2

[43] Economou, I. G. & Donohue, M. D. Equations of state for hydrogen bonding systems. *Fluid Phase Equilib.* **116**, 518–529 (1996). 2, 15, 103

[44] Chapman, W., Gubbins, K., Jackson, G. & Radosz, M. SAFT: Equation-of-state solution model for associating fluids. *Fluid Phase Equilib.* **52**, 31–38 (1989). 2, 16

[45] Kontogeorgis, G. M., Voutsas, E. C., Yakoumis, I. V. & Tassios, D. P. An equation of state for associating fluids. *Ind. Eng. Chem. Res.* **35**, 4310–4318 (1996). 2, 16, 53

[46] Kontogeorgis, G. M. *et al.* Ten years with the CPA (Cubic-Plus-Association) equation of state. Part 2. Cross-associating and multicomponent systems. *Ind. Eng. Chem. Res.* **45**, 4869–4878 (2006). 3, 17, 45

[47] Wyczalkowska, A. K., Sengers, J. V. & Anisimov, M. A. Critical fluctuations and the equation of state of van der Waals. *Physica A* **334**, 482–512 (2004). 3, 10, 26, 32

[48] Kiselev, S. B. Cubic crossover equation of state. *Fluid Phase Equilib.* **147**, 7–23 (1998). 3, 26, 32, 34, 36, 53

[49] Pizarro, J. O. d. S. & Branco, C. C. M. Challenges in implementing an EOR project in the pre-salt province in deep offshore brasil. In *Society of Petroleum Engineers* (Society of Petroleum Engineers, Oman, 2012). SPE-155665. 3

[50] Ma, T. *et al.* Selective synthesis of gasoline from syngas in near-critical phase. *Catalysis Today* **228**, 167–174 (2014). 3

[51] Zhang, Q., Liu, P., Fujiyama, Y., Chen, C. & Li, X. Synthesis of light hydrocarbons from syngas in near-critical phase. *Applied Catalysis A: General* **401**, 147–152 (2011). 3

[52] Demirbas, M. F. & Balat, M. Recent advances on the production and utilization trends of bio-fuels: A global perspective. *Energy Convers. Manage.* **47**, 2371–2381 (2006). 3

[53] Oliveira, M. B., Coutinho, J. A. P. & Queimada, A. J. Mutual solubilities of hydrocarbons and water with the CPA EOS. *Fluid Phase Equilib.* **258**, 58–66 (2007). 3

[54] Llovell, F., Pamies, J. C. & Vega, L. F. Thermodynamic properties of Lennard-Jones chain molecules: Renormalization-Group corrections to a modified Statistical Associating Fluid Theory. *J. Chem. Phys.* **121**, 10715–10724 (2004). 3, 39, 63, 82, 86

[55] Llovell, F. & Vega, L. F. Global fluid phase equilib. and critical phenomena of selected mixtures using the crossover Soft-SAFT equation. *J. Phys. Chem. B* **110**, 1350–1362 (2006). 3, 32, 39, 63

[56] Kiselev, S. & Friend, D. Cubic crossover equation of state for mixtures. *Fluid Phase Equilib.* **162**, 51–82 (1999). 3, 4, 26, 34, 36, 42, 53

[57] Wilson, K. G. Renormalization Group and critical phenomena. I. Renormalization Group and the Kadanoff scaling picture. *Phys. Rev. B* **4**, 3174–3183 (1971). 3, 26, 37

[58] Salvino, L. W. & White, J. A. Calculation of density fluctuation contributions to thermodynamic properties of simple fluids. *J. Chem. Phys.* **96**, 4559–4568 (1992). 4, 26, 37, 39, 41, 42, 53, 62, 67, 73, 82

[59] White, J. A. Contribution of fluctuations to thermal properties of fluids with attractive forces of limited range: Theory compared with PvT and Cv data for argon. *Fluid Phase Equilib.* **75**, 53–64 (1992). 32, 37, 64

[60] White, J. A. & Zhang, S. Renormalization Group theory for fluids. *J. Chem. Phys.* **99**, 2012–2019 (1993). 41

[61] White, J. A. & Zhang, S. Renormalization theory of nonuniversal thermal properties of fluids. *J. Chem. Phys.* **103**, 1922–1928 (1995). 4, 26, 53

[62] Fisher, M. E. Renormalization of critical exponents by hidden variables. *Phys. Rev.* **176**, 257–272 (1968). 4, 42

[63] Anisimov, M. A. & Sengers, J. V. *Equations of State for Fluids and Fluid Mixtures* (Elsevier, Amsterdam, The Netherlands, 2000), 1st edn. Critical Region. 7, 10, 25

[64] Binney, J. J., Dowrick, N. J., Fisher, A. J. & Newman, M. E. J. *The Theory of Critical Phenomena. An Introducion to the Renormalization Group* (Clarendon Press, Oxford, 1992). 7, 8, 26, 82

[65] van der Waals, J. D. *Over de Continuiteit van den Gas- en Vloeistoftoestand*. Ph.D. thesis, Leiden, Holanda (1873). 9, 10

[66] Sandler, S. I. *Chemical, Biochemical, and Engineering Thermodynamics* (Wiley, Hoboken, 2006), 4 edn. 9, 11

[67] Sengers, J. & Sengers, J. L. Thermodynamic behavior of fluids near the critical point. *Annu. Rev. Phys. Chem.* **37**, 189–222 (1986). 10

[68] Danesh, A. *PVT and Phase Behaviour of Petroleum Reservoir Fluids* (Elsevier Science, Amsterdam, 1998). 10, 13, 18

[69] Valderrama, J. O. The state of the cubic equations of state. *Ind. Eng. Chem. Res.* **42**, 1603–1618 (2003). 10, 11, 18

[70] Redlich, O. & Kwong, J. N. S. On the thermodynamics of solutions. V: An equation of state. Fugacities of gaseous solutions. *Chem. Rev.* **44**, 233–244 (1949). 11

[71] Soave, G. Equilibrium constants from a modified Redlich-Kwong equation of state. *Chem. Eng. Sci.* **27**, 1197–1203 (1972). 12

[72] Peng, D. Y. & Robinson, D. B. A new two-constant equation of state. *Ind. Eng. Chem. Fundam.* **15**, 59–64 (1976). 12

[73] Peng, D. Y. & Robinson, D. B. Two and three phase equilibrium calculations for systems containing water. *Can. J. Chem. Eng.* **54**, 595–599 (1976). 12

[74] Schmidt, G. & Wenzel, H. A modified van der Waals type equation of state. *Chem. Eng. Sci.* **35**, 1503–1512 (1980). 13, 14, 15, 19

[75] Patel, N. C. & Teja, A. S. A new cubic equation of state for fluids and fluid mixtures. *Chem. Eng. Sci.* **37**, 463–473 (1982). 14, 46

[76] Cismondi, M. & Mollerup, J. Development and application of a three-parameter RK-PR equation of state. *Fluid Phase Equilib.* **232**, 74–89 (2005). 15, 103

[77] Anderko, A. A simple equation of state incorporating association. *Fluid Phase Equilib.* **45**, 39–67 (1989). 15

[78] Anderko, A. Phase equilibria in aqueous systems from an equation of state based on the chemical approach. *Fluid Phase Equilib.* **65**, 89–110 (1991). 15

[79] Wertheim, M. S. Fluids with highly directional attractive forces. I. Statistical thermodynamics. *J. Stat. Phys.* **35**, 19–34 (1984). 16

[80] Huang, S. H. & Radosz, M. Equation of state for small, large, polydisperse, and associating molecules. *Ind. Eng. Chem. Res.* **29**, 2284–2294 (1990). 17

[81] Kontogeorgis, G. *et al.* Modelling of associating mixtures for applications in the oil and gas and chemical industries. *Fluid Phase Equilib.* **261**, 205–211 (2007). 17

[82] Alay, A., Liang, X., von Solms, N. & Kontogeorgis, G. Modeling of asphaltene precipitation from crude oil with the Cubic-Plus-Association equation of state. *Energy Fuels* **31**, 2063–2075 (2017). 17

[83] Alay, A., Liang, X., von Solms, N. & Kontogeorgis, G. Prediction of gas injection effect on asphaltene precipitation onset using the cubic and Cubic-Plus-Association equations of state. *Energy Fuels* **31**, 3313–3328 (2017). 17

[84] Linder, B. *Thermodynamics and Introductory Statistical Mechanics* (John Wiley & Sons, Inc., 2004). 24

[85] Uzunov, D. *Theory of Critical Phenomena* (World Scientific Publishing Co. Pte. Ltd., River Edge, NJ, USA, 1993). 25

[86] Llovell, F. *Accurate Description of the Critical Region by a Molecular-Based Equation of State with a Crossover Treatment*. Ph.d. thesis, Universitat Autonoma de Barcelona, Barcelona (2006). 26

[87] Chen, Z., Albright, P. & Sengers, J. Crossover from singular critical to regular classical thermodynamic behavior of fluids. *Phys. Rev. A* **41**, 3161–3177 (1990). 26, 32, 33, 34

[88] Wilson, G. M. A modified Redlich-Kwong equation of state, application to general physical data calculations. *Fluid Phase Equilib.* **53**, 113 (1969). 26, 185

[89] Wilson, K. G. & Fisher, M. E. Critical exponents in 3.99 dimensions. *Physical Review Letters* **4**, 240–243 (1972). 26, 37

[90] White, J. A. & Zhang, S. Renormalization Group theory for fluids to greater density distances from the critical point. *Int. J. Thermophys.* **19**, 1019–1027 (1998). 26

[91] Polishuk, I., Wisniak, J. & Segura, H. Prediction of the critical locus in binary mixtures using equation of state. *Fluid Phase Equilib.* **164**, 13–47 (1999). 28, 30, 87, 114, 115, 118, 122

[92] Prausnitz, J. M., Lichtenthaler, R. N. & Azevedo, E. G. *Molecular Thermodynamics of Fluid-Phase Equilibria* (Prentice-Hall Inc., Englewood Cliffs, 1986), 2nd edn. 28

[93] Polishuk, I., Wisniak, J. & Segura, H. Simultaneous prediction of the critical and sub-critical phase behavior in mixtures using equations of state III. Methane-n-alkanes. *Chem. Eng. Sci.* **58**, 4363–4376 (2003). 30, 87, 114, 115, 122

[94] Polishuk, I., Wisniak, J. & Segura, H. Simultaneous prediction of the critical and sub-critical phase behavior in mixtures using equations of state II. Carbon dioxide-heavy n-alkanes. *Chem. Eng. Sci.* **58**, 2529–2550 (2003). 30, 103, 124

[95] Kiselev, S., Kostyukova, I. & Povodyrev, A. Universal crossover behavior of fluids and fluid mixtures in the critical region. *Int. J. Thermophys.* **12**, 877–895 (1991). 32

[96] McCabe, C. & Kiselev, S. Application of crossover theory to the SAFT-VR equation of state: SAFT-VRX for pure fluids. *Ind. Eng. Chem. Res.* **43**, 2839–2851 (2004). 32, 34, 36

[97] Lue, L. & Prausnitz, J. M. Renormalization-Group corrections to an approximate free-energy model for simple fluids near to and far from the critical region. *J. Chem. Phys.* **108**, 5529–5536 (1998). 32, 39

[98] Xu, X. H. & Duan, Y. Y. Crossover CPA equation of state for associating fluids. *Fluid Phase Equilib.* **290**, 148–152 (2010). 32, 39, 63, 68, 82

[99] Ma, S.-k. *Modern Theory of Critical Phenomena* (Westview Press, New York, NY, USA, 2000). 32

[100] Chen, Z., Abbaci, A., Tang, S. & Sengers, J. Global thermodynamic behavior of fluids in the critical region. *Phys. Rev. A* **42**, 4470–4484 (1990). 33, 34

[101] Kiselev, S. & Ely, J. Simplified crossover SAFT equation of state for pure fluids and fluid mixtures. *Fluid Phase Equilib.* **174**, 93–113 (2000). 34, 36

[102] Janecek, J., Paricaud, P., Dicko, M. & Coquelet, C. A generalized Kiselev crossover approach applied to Soave-Redlich-Kwong equation of state. *Fluid Phase Equilib.* **401**, 16–26 (2015). 36

[103] Sun, L., Zhao, H., Kiselev, S. & McCabe, C. Predicting mixture phase equilibria and critical behavior using the SAFT-VRX approach. *J. Phys. Chem. B* **109**, 9047–9058 (2005). 36, 124, 135

[104] Percus, J. & Yevick, G. Analysis of classical statistical mechanics by means of collective coordinates. *Phys. Rev.* **110**, 1–13 (1958). 37

[105] Jiang, J. & Prausnitz, J. M. Critical temperatures and pressures for hydrocarbon mixtures from an equation of state with Renormalization-Group theory corrections. *Fluid Phase Equilib.* **169**, 127–147 (2000). 39

[106] Llovell, F. & Vega, L. F. Phase equilibria, critical behavior and derivative properties of selected n-alkane/n-alkane and n-alkane/1-alkanol mixtures by the crossover Soft-SAFT equation of state. *J. Supercrit. Fluids* **41**, 204–216 (2007). 39, 63, 87, 94, 122

[107] Forte, E., Llovell, F., Vega, L., Trusler, M. & Galindo, A. Application of a Renormalization-Group treatment to the Statistical Associating Fluid Theory for potentials of variable range (SAFT-VR). *J. Chem. Phys.* **134**, 154102 (2011). 39

[108] Forte, E., Llovell, F., Trusler, M. & Galindo, A. Application of the Statistical Associating Fluid Theory for potentials of variable range (SAFT-VR) coupled with renormalisation-group (RG) theory to model the phase equilibria and second-derivative properties of pure fluids. *Fluid Phase Equilib.* **337**, 274–287 (2013). 39

[109] Bymaster, A., Emborsky, C., Dominik, A. & Chapman, W. Renormalization-Group corrections to a Perturbed-Chain Statistical Associating Fluid Theory for pure fluids near to and far from the critical region. *Ind. Eng. Chem. Res.* **47**, 6264–6274 (2008). 39

[110] Tang, X. & Gross, J. Density functional theory for calculating surface tensions with a simple renormalization formalism for the critical point. *J. Supercrit. Fluids* **55**, 735–742 (2010).

[111] Tang, X. & Gross, J. Renormalization-Group corrections to the Perturbed-Chain Statistical Associating Fluid Theory for binary mixtures. *Ind. Eng. Chem. Res.* **49**, 9436–9444 (2010). 39, 70

[112] Cai, J. & Prausnitz, J. M. Thermodynamics for fluid mixtures near to and far from the vapor-liquid critical point. *Fluid Phase Equilib.* **219**, 205–217 (2004). 39, 42, 61, 62, 63

[113] Cai, J., Qiu, D., Zhang, L. & Hu, Y. Vapor-liquid critical properties of multi-component fluid mixtures. *Fluid Phase Equilib.* **241**, 229–235 (2006). 39

[114] Xu, X.-H., Duan, Y.-Y. & Yang, Z. Prediction of the critical properties of binary alkanol + alkane mixtures using a crossover CPA equation of state. *Fluid Phase Equilib.* **309**, 168–173 (2011). 39, 63, 105, 144

[115] Griffiths, R. & Wheeler, J. Critical points in multicomponent systems. *Phys Rev A* **2**, 1047–1064 (1970). 42

[116] Llovell, F., Vega, L., Seiltgens, D., Mejía, A. & Segura, H. An accurate direct technique for parametrizing cubic equations of state. Part III. application of a crossover treatment. *Fluid Phase Equilib.* **264**, 201–210 (2008). 42, 63

[117] Yakoumis, I. V., Kontogeorgis, G. M., Voutsas, E. C. & Tassios, D. P. Vapor-liquid equilibria for alcohol/hydrocarbon systems using the CPA equation of state. *Fluid Phase Equilib.* **130**, 31–47 (1997). 45

[118] Yakoumis, I. V., Kontogeorgis, G. M., Voutsas, E. C., Hendriks, E. M. & Tassios, D. P. Prediction of phase equilibria in binary aqueous systems containing alkanes, cycloalkanes, and alkenes with the Cubic-Plus-Association equation of state. *Ind. Eng. Chem. Res.* **37**, 4175–4182 (1998). 55

[119] Voutsas, E. C., Kontogeorgis, G. M., Yakoumis, I. V. & Tassios, D. P. Correlation of liquid-liquid equilibria for alcohol/hydrocarbon mixtures using the CPA equation of state. *Fluid Phase Equilib.* **132**, 61–75 (1997). 45

[120] Cismondi, M., Brignole, E. A. & Mollerup, J. Rescaling of three-parameter equations of state: PC-SAFT and SPHCT. *Fluid Phase Equilib.* **234**, 108–121 (2005). 48

[121] Tsonopoulos, C. & Tan, Z. The critical constants of normal alkanes from methane to polyethylene II. Application of the flory theory. *Fluid Phase Equilib.* **83**, 127–138 (1993). 52

[122] Anselme, M. J., Gude, M. & Teja, A. S. The critical temperatures and densities of the n-alkanes from pentane to octadecane. *Fluid Phase Equilib.* **57**, 317–326 (1990). 52

[123] Siepmann, J. I., Karaborni, S. & Smit, B. Simulating the critical behaviour of complex fluids. *Nature* **365**, 330–332 (1993). 52

[124] Blas, F. J. & Galindo, A. Study of the high pressure phase behaviour of CO2+n-alkane mixtures using the SAFT-VR approach with transferable parameters. *Fluid Phase Equilib.* **194-197**, 501–509 (2002). 53

[125] Galindo, A. & Blas, F. J. Theoretical examination of the global fluid phase behavior and critical phenomena in carbon dioxide + n-alkane binary mixtures. *J. Phys. Chem. B* **106**, 4503–4515 (2002).

[126] Pamies, J. C. & Vega, L. F. Critical properties of homopolymer fluids studied by a Lennard-Jones Statistical Associating Fluid Theory. *Mol. Phys.* **100**, 2519–2529 (2002). 53

[127] Kennedy, J. & Eberhart, R. Particle Swarm Optimization. In *Proceedings of the 1995 IEEE international conference on neural networks*, 1942–1948 (IEEE Service Center, Piscataway, NJ, 1995). 54

[128] Clerc, M. Stagnation analysis in Particle Swarm Optimization or what happens when nothing happens. Technical Report CSM-460, Department of Computer Science, University of Essex, Essex, UK (2006). 54

[129] Santos, L. C., Abunahman, S. S., Tavares, F. W., Ahon, V. R. R. & Kontogeorgis, G. M. Modeling water saturation points in natural gas streams containing CO2 and H2S - Comparisons with different equations of state. *Ind. Eng. Chem. Res.* **54**, 743–757 (2015). 55, 113

[130] Santos, L. C., Tavares, F. W., Ahón, V. R. R. & Kontogeorgis, G. M. Modeling MEA with the CPA equation of state: A parameter estimation study adding local search to PSO algorithm. *Fluid Phase Equilib.* **400**, 76–86 (2015). 55, 113

[131] Peneloux, A., Rauzy, E. & Freze, R. A consistent correction for Redlich-Kwong-Soave volumes. *Fluid Phase Equilib.* **8**, 7–23 (1982). 57, 58, 113

[132] Mathias, P. M. & Copeman, T. W. Extension of the Peng-Robinson equation of state to complex mixtures: Evaluation of the various forms of the local composition concept. *Fluid Phase Equilib.* **13**, 91–108 (1984). 58, 113

[133] Carnahan, N. & Starling, K. Equation of state for nonattracting rigid spheres. *J. Chem. Phys.* **51**, 635– (1959). 61

[134] Pedersen, K. S. & Christensen, P. L. *Phase Behavior of Petroleum Reservoir Fluids* (Taylor & Francis, Boca Raton, 2006). 86

[135] Cismondi, M., Galdo, M., Gomez, M., Tassin, N. & Yanes, M. High pressure phase behavior modeling of asymmetric alkane + alkane binary systems with the RKPR EOS. *Fluid Phase Equilib.* **362**, 125–135 (2014). 86, 87, 122

[136] Cismondi, M., Cruz, J., Gomez, M. & Montoya, G. Modelling the phase behavior of alkane mixtures in wide ranges of conditions: New parameterization and predictive correlations of binary interactions for the RKPR EOS. *Fluid Phase Equilib.* **403**, 49–59 (2015). 86, 87, 91, 94, 115, 122

[137] Sage, B., Lacey, W. & Schaafsma, J. Phase equilibria in hydrocarbon systems: II - Methane-propane system. *Ind. Eng. Chem.* **26**, 214–217 (1934). 93

[138] Berry, V. & Sage, B. Phase behavior in binary and multicomponent systems at elevated pressures: n-Pentane and methane-n -pentane. Tech. Rep., National Bureau of Standards (1970). 93

[139] Poston, R. & McKetta, J. Vapor-liquid equilibrium in the methane-n-hexane system. *Chem. Eng. Data* **11**, 362–363 (1966). 93

[140] Shipman, L. & Kohn, J. Heterogeneous phase and volumetric equilibrium in the methane-n-nonane system. *Chem. Eng. Data* **11**, 176–180 (1966). 93

[141] Reamer, H., Olds, R., Sage, B. & Lacey, W. Phase equilibria in hydrocarbon systems: Methane-decane system. *Ind. Eng. Chem.* **34**, 1526–1531 (1942). 93

[142] Tsivintzelis, I., Kontogeorgis, G. M., Michelsen, M. L. & Stenby, E. H. Modeling phase equilibria for acid gas mixtures using the CPA equation of state. Part II: Binary mixtures with CO2. *Fluid Phase Equilib.* **306**, 38–56 (2011). 94, 95

[143] Cismondi, M., Rodriguez-Reartes, S., Milanesio, J. & Zabaloy, M. Phase equilibria of CO2 + n-alkane binary systems in wide ranges of conditions: Development of predictive correlations based on cubic mixing rules. *Ind. Eng. Chem. Res.* **51**, 6232–6250 (2012). 94, 99, 103, 124, 136

[144] Naderi, K. & Babadagli, T. Use of CO2 as solvent during steam over solvent injection in fractured reservoirs (SOS-FR) method for heavy oil recovery. In *International Petroleum Technology Conference* (International Petroleum Technology Conference, Bangkok, 2012). IPTC14918. 94

[145] Ikawa, N., Nagase, Y., Tada, T., Furuta, S. & Fukuzato, R. Separation process of ethanol from aqueous solutions using supercritical carbon dioxide. *Fluid Phase Equilib.* **83**, 167–174 (1993). 94

[146] Reilly, J., Bokis, C. & Donohue, M. An experimental investigation of lewis acid-base interactions of liquid carbon dioxide using fourier transform infrared (ft-ir) spectroscopy. *Int. J. Thermophys.* **16**, 599–610 (1995). 94

[147] Polishuk, I., Wisniak, J. & Segura, H. Estimation of liquid-liquid-vapor equilibria using predictive EOS models. 1. Carbon dioxide-n-alkanes. *J. Phys. Chem. B* **107**, 1864–1874 (2003). 94

[148] Bjørner, M. & M.Kontogeorgis, G. Modeling derivative properties and binary mixtures with CO2 using the CPA and the quadrupolar CPA equations of state. *Fluid Phase Equilib.* **408**, 151–169 (2016). 95, 96

[149] Kukarni, A., Zarah, B., Luks, K. & Kohn, J. Phase-equilbriums behavior of system carbon dioxide-n-decane at low temperatures. *J. Chem. Eng. Data* **19**, 92–94 (1974). 96

[150] Cismondi, M., Mollerup, J. & Zabaloy, M. Equation of state modeling of the phase equilibria of asymmetric CO2 + n-alkane binary systems using mixing rules cubic with respect to mole fraction. *J. Supercrit. Fluids* **55**, 671–681 (2010). 99, 124

[151] Zabaloy, M. Cubic mixing rules. *Ind. Eng. Chem. Res.* **47**, 5063–5079 (2008). 99, 122

[152] Webster, L. & Kidnay, A. Vapor-liquid equilibria for the methane-propane-carbon dioxide systems at 230 K and 270 K. *J. Chem. Eng. Data* **46**, 759–764 (2001). 101

[153] Cheng, H., de Fernandez, M. P., Zollweg, J. & Streett, W. Vapor-liquid equilibrium in the system carbon dioxide + n-pentane from 252 to 458 K at pressures to 10 MPa. *J. Chem. Eng. Data* **34**, 319–323 (1989). 101

[154] Li, Y.-H., Dillard, K. & Jr., R. R. Vapor-liquid phase equilibrium for carbon dioxide-n-hexane at 40, 80, and 120 .degree.C. *J. Chem. Eng. Data* **26**, 53–55 (1981). 101

[155] Kalra, H., Kubota, H., Robinson, D. & Ng, H.-J. Equilibrium phase properties of the carbon dioxide-n-heptane system. *J. Chem. Eng. Data* **23**, 317–321 (1978). 101

[156] Jimenez-Gallegos, R., Galicia-Luna, L. & Elizalde-Solis, O. Experimental vapor-liquid equilibria for the carbon dioxide + octane and carbon dioxide + decane systems. *J. Chem. Eng. Data* **51**, 1624–1628 (2006). 101

[157] Camacho-Camacho, L., Galicia-Luna, L., Elizalde-Solis, O. & Martínez-Ramírez, Z. New isothermal vapor-liquid equilibria for the CO2 + n-nonane, and co2 + n-undecane systems. *Fluid Phase Equilib.* **259**, 45–50 (2007). 101

[158] Vitu, S., Privat, R. & Mutelet, J.-N. J. F. Predicting the phase equilibria of CO2 + hydrocarbon systems with the PPR78 model (PR EOS and kij calculated through a group contribution method). *J. Supercrit. Fluids* **45**, 1–26 (2008). 103

[159] Fu, D., Liang, L., Li, X.-S., Yan, S. & Liao, T. Investigation of vapor-liquid equilibria for supercritical carbon dioxide and hydrocarbon mixtures by Perturbed-Chain Statistical Associating Fluid Theory. *Ind. Eng. Chem. Res.* **45**, 4364–4370 (2006). 103

[160] Ferguson, J. The system methyl alcohol-n-hexane at 45 degrees. *J. Phys. Chem.* **36**, 1123–1128 (1932). 106

[161] Palma, A. *Predictive Methods for the Association Parameters of Multifunctional Molecules with the CPA EoS*. Ph.D. thesis (2017). 113

[162] Creek, J., Knobler, C. & Scott, R. Tricritical phenomena in quasibinary mixtures of hydrocarbons. I. Methane systems. *J. Chem. Phys.* **74**, 3489–3499 (1981). 114

[163] Deiters, U. & Pegg, I. Systematic investigation of the phase behavior in binary fluid mixtures. I. Calculations based on the Redlich-Kwong equation of state. *J. Chem. Phys.* **90**, 6632–6641 (1989). 114

[164] Sengers, H. C. M. A. J. Prediction of thermodynamic and transport properties in the one-phase region of methane + n-hexane mixtures near their critical end points. *Fluid Phase Equilib.* **128**, 67–97 (1997). 118

[165] Soo, C.-B., Theveneau, P., Coquelet, C., Ramjugernath, D. & Richon, D. Determination of critical properties of pure and multi-component mixtures using a dynamic-synthetic apparatus. *J. Supercrit. Fluids* **55**, 545–553 (2010). 145

[166] Michelsen, M. & Mollerup, J. *Thermodynamic Models: Fundamentals and Computational Aspects* (Tie-Line Publications, Denmark, 2007). 178

[167] Michelsen, M. L. Calculation of phase envelopes and critical points for multicomponent mixtures. *Fluid Phase Equilib.* **4**, 1–10 (1980). 189

[168] Heidemann, R. A. & Khalil, A. M. The calculation of critical points. *AIChE J.* **26**, 769–779 (1980). 189

Appendix A

Thermodynamic Calculations with a Crossover EoS

This appendix contains the mathematical expression for calculating the crossover contributions of the thermodynamic variables needed for the with the application of the crossover CPA. The solution of the pressure EoS will be presented in the fist section, and in the second section the expression for the calculation of the fugacity coefficients is derived.

A.1 Pressure expression for a crossover EoS

Using White's approach, the pressure expression for a crossover EoS is described by the equations:

$$P = \rho^2 \left(\frac{\partial A}{\partial \rho} \right) ; A = \frac{f_n}{\rho} \tag{A.1}$$

$$P = P_{EoS} + \rho \left(\frac{\partial \delta f_n}{\partial \rho} \right) - \delta f_n \tag{A.2}$$

where P_0 is the initial mean field equation and δf_m are the density fluctuation contributions.

A.2 Volume calculation with a crossover EoS

The calculation of the volume of a system in a certain specified pressure (P) is given by the expressions:

$$H(V) = P - P_{EoS} + \rho\left(\frac{\partial \delta f_n}{\partial \rho}\right) - \delta f_n \tag{A.3}$$

$$V^{new} = V - {}^{H(V)}/_{H'(V)} \tag{A.4}$$

The final volume is attained numerically when $H(V)$ is smaller than a tolerance pre-determined.

A.3 Fugacity coefficient calculation with a crossover EoS

The fugacity coefficient of a component in a mixture is given by [166]:

$$RT\ln(\phi_i) = \frac{\partial}{\partial x_i}(A^r) - RT\ln Z \tag{A.5}$$

The residual Helmholtz energy can be obtained from the Helmholtz density function by:

$$A^r = A - A_{i.g.} = {}^{f_n}/_{\rho} - {}^{f_{i.g.}}/_{\rho} \tag{A.6}$$

where $A_{i.g.}$ and $f_{i.g.}$ are the Helmholtz energy and the free energy density of the ideal gas.

Substituting the residual Helmholtz function in the equation of the fugacity coefficient:

$$RT\ln(\phi_i) = \frac{\partial}{\partial x_i}(A^r_{EoS}) - RT\ln Z + \frac{1}{\rho}\frac{\partial \delta f_n}{\partial x_i} \tag{A.7}$$

The term $\frac{\partial}{\partial x_i}(A^r_{EoS}) - \ln Z$ is the molar fugacity coefficient given by the EoS, while $\frac{1}{\rho}\frac{\partial \delta f_n}{\partial x_i}$ are the correction of the long-scale fluctuations.

A.4 Derivative of δf_n with respect to density

The calculation of pressure with the crossover EoS requires the expression for the derivative of δf_n with respect to ρ, which is obtained as follows:

$$\frac{\partial \delta f_n}{\partial \rho} = \frac{\partial - K_n \ln\left(\frac{\Omega_n^s}{\Omega_n^l}\right)}{\partial \rho} = -K_n \left[\frac{\left(\frac{\partial \Omega_n^s}{\partial \rho}\right)}{\Omega_n^s} - \frac{\left(\frac{\partial \Omega_n^l}{\partial \rho}\right)}{\Omega_n^l} \right] \tag{A.8}$$

The terms $\frac{\partial \Omega_n^s}{\partial \rho}$ and $\frac{\partial \Omega_n^l}{\partial \rho}$ are defined by the expressions:

$$\frac{\partial \Omega_n^s}{\partial \rho} = \frac{\partial \int_0^{\min(\rho, \rho_{max}-\rho)} \left\{ \exp\left[\frac{-G_n^s(\rho,y)}{K_n}\right] \right\} dy}{\partial \rho} = \int_0^{\min(\rho, \rho_{max}-\rho)} \left\{ \exp\left[\frac{-G_n^s(\rho,y)}{K_n}\right] \left(\frac{-1}{K_n}\right) \left[\frac{\partial G_n(\rho,y)}{\partial \rho}\right] \right\} dy + \exp\left[\frac{-G_n^s(\rho,\rho)}{K_n}\right] \tag{A.9}$$

$$\frac{\partial \Omega_n^l}{\partial \rho} = \frac{\partial \int_0^{\min(\rho, \rho_{max}-\rho)} \left\{ \exp\left[\frac{-G_n^l(\rho,y)}{K_n}\right] \right\} dy}{\partial \rho} = \int_0^{\min(\rho, \rho_{max}-\rho)} \left\{ \exp\left[\frac{-G_n^l(\rho,y)}{K_n}\right] \left(\frac{-1}{K_n}\right) \left[\frac{\partial G_n(\rho,y)}{\partial \rho}\right] \right\} dy + \exp\left[\frac{-G_n^l(\rho,\rho)}{K_n}\right] \tag{A.10}$$

The equation to calculate $\frac{\partial G_n(\rho,y)}{\partial \rho}$ is:

$$\begin{aligned} \frac{\partial G_n(\rho,y)}{\partial \rho} &= \frac{\partial}{\partial \rho}\left(\frac{\bar{f}_{n-1}(\rho+y) + \bar{f}_{n-1}(\rho-y) - 2\bar{f}_{n-1}(\rho)}{2} \right) \\ &= \frac{1}{2}\left(\frac{\partial \bar{f}_{n-1}(\rho+y)}{\partial \rho} - 2\frac{\partial \bar{f}_{n-1}(\rho)}{\partial \rho} + \frac{\partial \bar{f}_{n-1}(\rho-y)}{\partial \rho} \right) \end{aligned} \tag{A.11}$$

Finally, $\frac{\partial \bar{f}_{n-1}}{\partial \rho}$ is given by:

$$\frac{\partial \bar{f}_{n-1}}{\partial \rho} = \frac{\partial \bar{A}_{n-1}\rho}{\partial \rho} = \rho \frac{\partial \bar{A}_{n-1}}{\partial \rho} + \bar{A}_{n-1} = \frac{P_{n-1}}{\rho} + \bar{A}_{n-1} \tag{A.12}$$

A.5 Derivative of δf_n with respect to mole fraction

The calculation of the fugacity coefficient with the crossover EoS requires the expression for the derivatives of δf_n with respect to x_i, which is obtained as follows:

$$\frac{\partial \delta f_n}{\partial x_i} = \frac{\partial - K_n \ln\left(\frac{\Omega_n^s}{\Omega_n^l}\right)}{\partial x_i} = -\left(\frac{\partial K_n}{\partial x_i}\right)\ln\left(\frac{\Omega_n^s}{\Omega_n^l}\right) - K_n\left[\frac{\left(\frac{\partial \Omega_n^s}{\partial x_i}\right)}{\Omega_n^s} - \frac{\left(\frac{\partial \Omega_n^l}{\partial x_i}\right)}{\Omega_n^l}\right] \tag{A.13}$$

The term $\frac{\partial K_n}{\partial x_i}$ is given by the expression:

$$\frac{\partial K_n}{\partial x_i} = \frac{\partial\left[\frac{k_B T}{(2^n L)^3}\right]}{\partial x_i} = -K_n\left(\frac{L_i}{L}\right)^3 \tag{A.14}$$

The term $\frac{\partial \Omega_n^s}{\partial x_i}$ is defined by the expression:

$$\frac{\partial \Omega_n^s}{\partial x_i} = \frac{\partial \int_0^{\min(\rho,\rho_{max}-\rho)}\left\{\exp\left[\frac{-G_n^s(\rho,y)}{K_n}\right]\right\}dy}{\partial x_i} = \int_0^{\min(\rho,\rho_{max}-\rho)}\left\{\exp\left[\frac{-G_n^s(\rho,y)}{K_n}\right]\left[-\frac{\frac{\partial G_n^s(\rho,y)}{\partial x_i}}{K_n} + \frac{\left(\frac{\partial K_n}{\partial x_i}\right)G_n^s(\rho,y)}{K_n^2}\right]\right\}dy \tag{A.15}$$

To calculate $\frac{\partial G_n^s(\rho,y)}{\partial x_i}$ we use the expression:

$$\frac{\partial G_n^s(\rho,y)}{\partial x_i} = \frac{\partial}{\partial x_i}\left(\frac{\bar{f^s}_n(\rho+y) + \bar{f^s}_n(\rho-y) - 2\bar{f^s}_n(\rho)}{2}\right) = \frac{1}{2}\left(\frac{\partial \bar{f^s}_n(\rho+y)}{\partial x_i} - 2\frac{\partial \bar{f^s}_n(\rho)}{\partial x_i} + \frac{\partial \bar{f^s}_n(\rho-y)}{\partial x_i}\right) \tag{A.16}$$

where $\frac{\partial \bar{f^s}_n(\rho)}{\partial x_i}$ is:

$$\frac{\partial \bar{f^s}_n(\rho)}{\partial x_i} = \frac{\partial\left[\bar{f^s}_{n-1}(\rho) + \frac{a\phi\rho^2}{2^{2n}}\right]}{\partial x_i} = \frac{\partial\left[\bar{f^s}_{n-1}(\rho)\right]}{\partial x_i} + \frac{\rho^2}{2^{2n}}\left[a\left(\frac{\partial \phi}{\partial x_i}\right) + \phi\left(\frac{\partial a}{\partial x_i}\right)\right] \tag{A.17}$$

The similar term $\frac{\partial \Omega_n^l}{\partial x_i}$ is given by:

$$\frac{\partial \Omega_n^l}{\partial x_i} = \frac{\partial \int_0^{\min(\rho,\rho_{max}-\rho)} \left\{ \exp\left[\frac{-G_n^l(\rho,y)}{K_n} \right] \right\} dy}{\partial x_i} = \int_0^{\min(\rho,\rho_{max}-\rho)} \left\{ \exp\left[\frac{-G_n^l(\rho,y)}{K_n} \right] \left[-\frac{\frac{\partial G_n^l(\rho,y)}{\partial x_i}}{K_n} + \frac{\left(\frac{\partial K_n}{\partial x_i} \right) G_n^l(\rho,y)}{K_n^2} \right] \right\} dy \tag{A.18}$$

while $\frac{\partial G_n^l(\rho,y)}{\partial x_i}$ is given by:

$$\frac{\partial G_n^l(\rho,y)}{\partial x_i} = \frac{\partial}{\partial x_i} \left(\frac{\bar{f}^l{}_n(\rho+y) + \bar{f}^l{}_n(\rho-y) - 2\bar{f}^l{}_n(\rho)}{2} \right) = \frac{1}{2} \left(\frac{\partial \bar{f}^l{}_n(\rho+y)}{\partial x_i} - 2\frac{\partial \bar{f}^l{}_n(\rho)}{\partial x_i} + \frac{\partial \bar{f}^l{}_n(\rho-y)}{\partial x_i} \right) \tag{A.19}$$

where $\frac{\partial \bar{f}^l{}_n(\rho)}{\partial x_i}$ is:

$$\frac{\partial \bar{f}^l{}_n(\rho)}{\partial x_i} = \frac{\partial \left[\bar{f}^l{}_{n-1}(\rho) + a\rho^2 \right]}{\partial x_i} = \frac{\partial \left[\bar{f}^l{}_{n-1}(\rho) \right]}{\partial x_i} + \rho^2 \left(\frac{\partial a}{\partial x_i} \right)$$

Using the mixing and combining rules presented in the previous chapters, the terms $\frac{\partial a}{\partial x_i}$ and $\frac{\partial \phi}{\partial x_i}$ are determined by:

$$\frac{\partial a}{\partial x_i} = \frac{\partial \sum_i \sum_i x_i x_j \sqrt{a_i a_j}\,(1-k_{ij})}{\partial x_i} = 2\sum_j x_j \sqrt{a_i a_j}\,(1-k_{ij})$$

$$\frac{\partial \phi}{\partial x_i} = \frac{\partial \sum_i x_i \phi_i}{\partial x_i} = \phi_i$$

Appendix B

Description of Algorithms with a Crossover EoS

This appendix describes the procedures for calculating the equilibrium and critical properties of pure fluids and mixtures using a crossover EoS. In the first part, a procedure to compute the volume of the liquid and vapor phases will be presented. Then, a description of the algorithm to calculate the vapor and bubble point pressures, as well as the PT-flash and critical point is given. These procedures are the basis for the results obtained in this thesis.

B.1 Calculation of volume using a Crossover EoS

The expression for calculating the volume of a system using a crossover EoS is given by equations (A.3) and (A.4). Figure (B.1) describe the algorithm implemented to calculate the molar volume of a system at fixed P and T using the Crossover EoS. For the liquid phase calculations, the initial molar volume value is $1.001b$ while for the vapor phase, the ideal gas volume ($\frac{RT}{P}$) is used.

B.2 Calculation of vapor and bubble pressure using a Crossover EoS

For the calculations of vapor and bubble pressure of thermodynamic systems it is necessary to determine first an expression for the fugacity coefficient

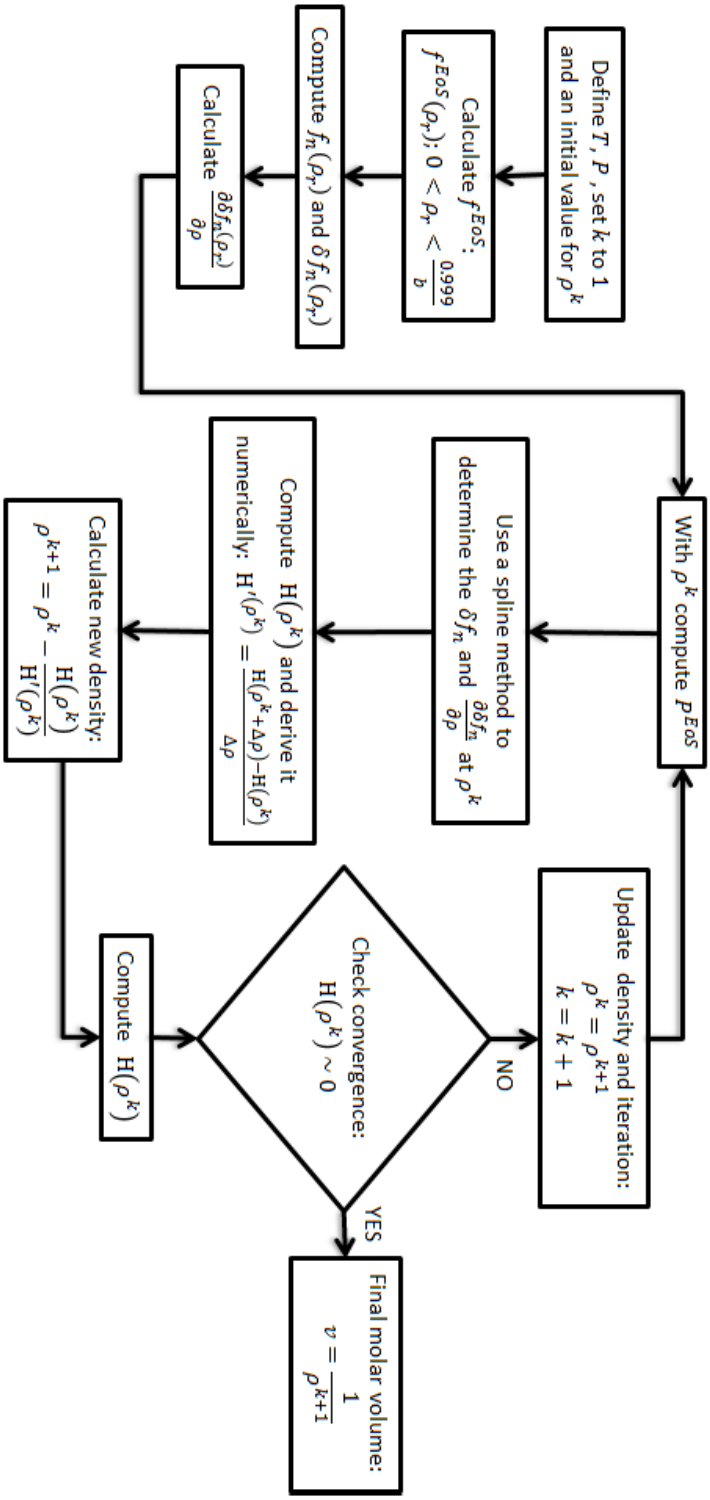

Figure B.1: Procedure for calculating the molar volume of a system using a crossover EoS

ϕ_i, which is obtained from Equation (A.7).

The procedure for the calculation of the vapor pressure of a component is described in Figure B.2. From the figure it is possible to see that once the free energy curves with the corrections for the density fluctuations are determined, it is only a matter of finding the density and pressure corresponding to the equilibrium of the system at a desired temperature.

The bubble point pressure is determined in a procedure similar to the vapor pressure. Unlike the previous algorithm, the system is composed of more than one component, and by defining the composition of the liquid phase, the composition of the vapor phase can be obtained initially from a correlation for the equilibrium ratios ($K_i = \frac{y_i}{x_i}$), e.g. Wilson's correlation [88]. Then, the vapor phase mole fractions are changed until the equilibrium conditions are attained, i.e. $x_i\phi_{i,liq} = y_i\phi_{i,vap}$. Additionally, due to the different compositions that the vapor phase assume in the algorithm, the free energy curve of the vapor phase must be changed at each iteration, as described in Figure B.3.

B.3 Calculation of the PT Flash

The PT flash algorithm is used to calculate the compositions of the phases in equilibrium of a system in a predefined temperature, pressure and feed composition (z). This procedure is schematically represented in Figure B.4. For the determination of equilibrium condition, it is necessary to compute the volume fraction (β) using the Rachford-Rice equation:

$$g(\beta) = \sum_{i=1}^{N} \frac{K_i - 1}{1 - \beta + \beta K_i} = 0 \tag{B.1}$$

where K_i are the equilibrium ratios. The composition of each phase is given by the expressions:

$$x_i = \frac{z_i}{1 - \beta + \beta K_i} \tag{B.2}$$

$$y_i = K_i x_i \tag{B.3}$$

It is important to note that the recursive procedure must be repeated with change in the composition of the phases (Figure B.4).

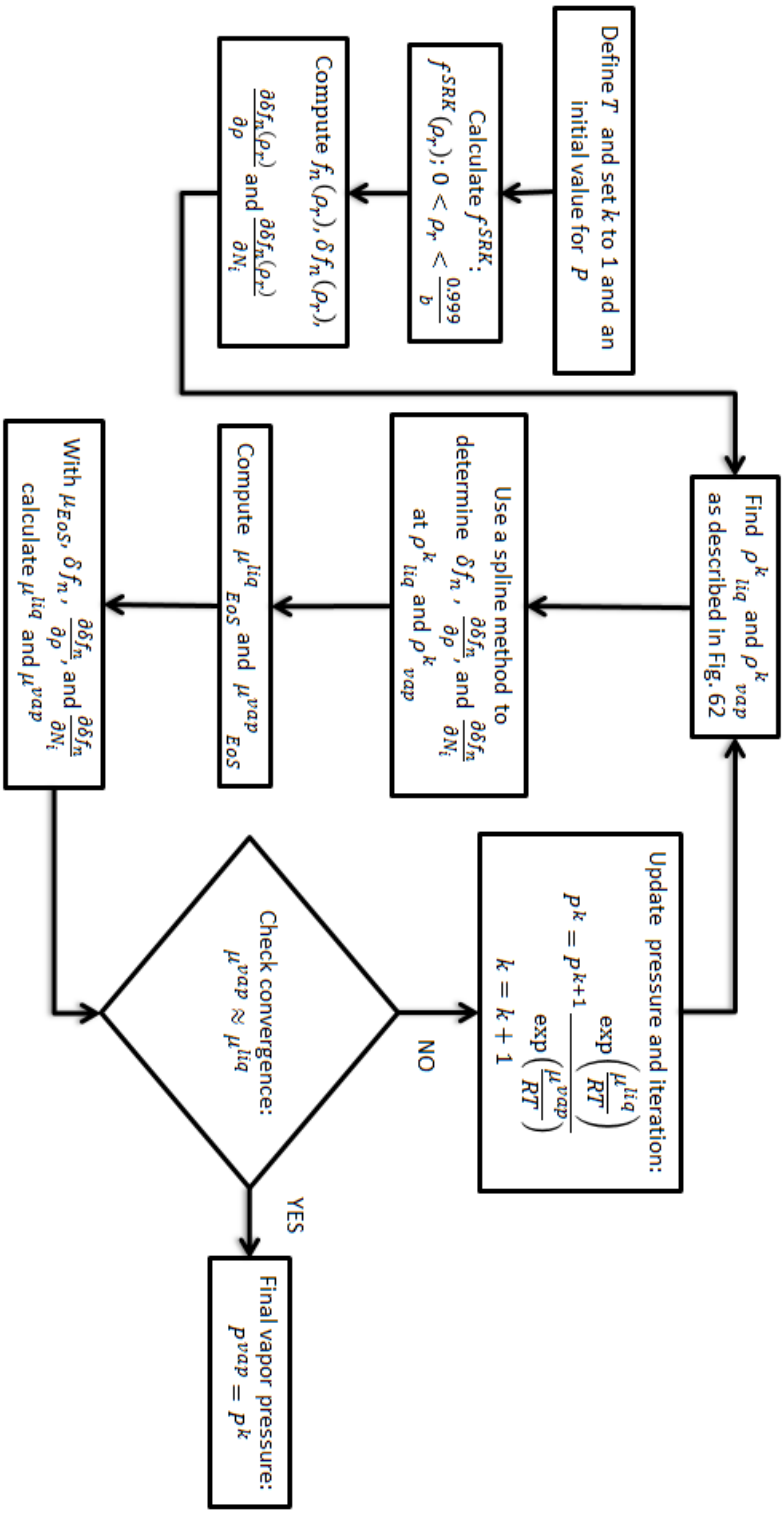

Figure B.2: Procedure for calculating the vapor pressure of a system using a crossover EoS

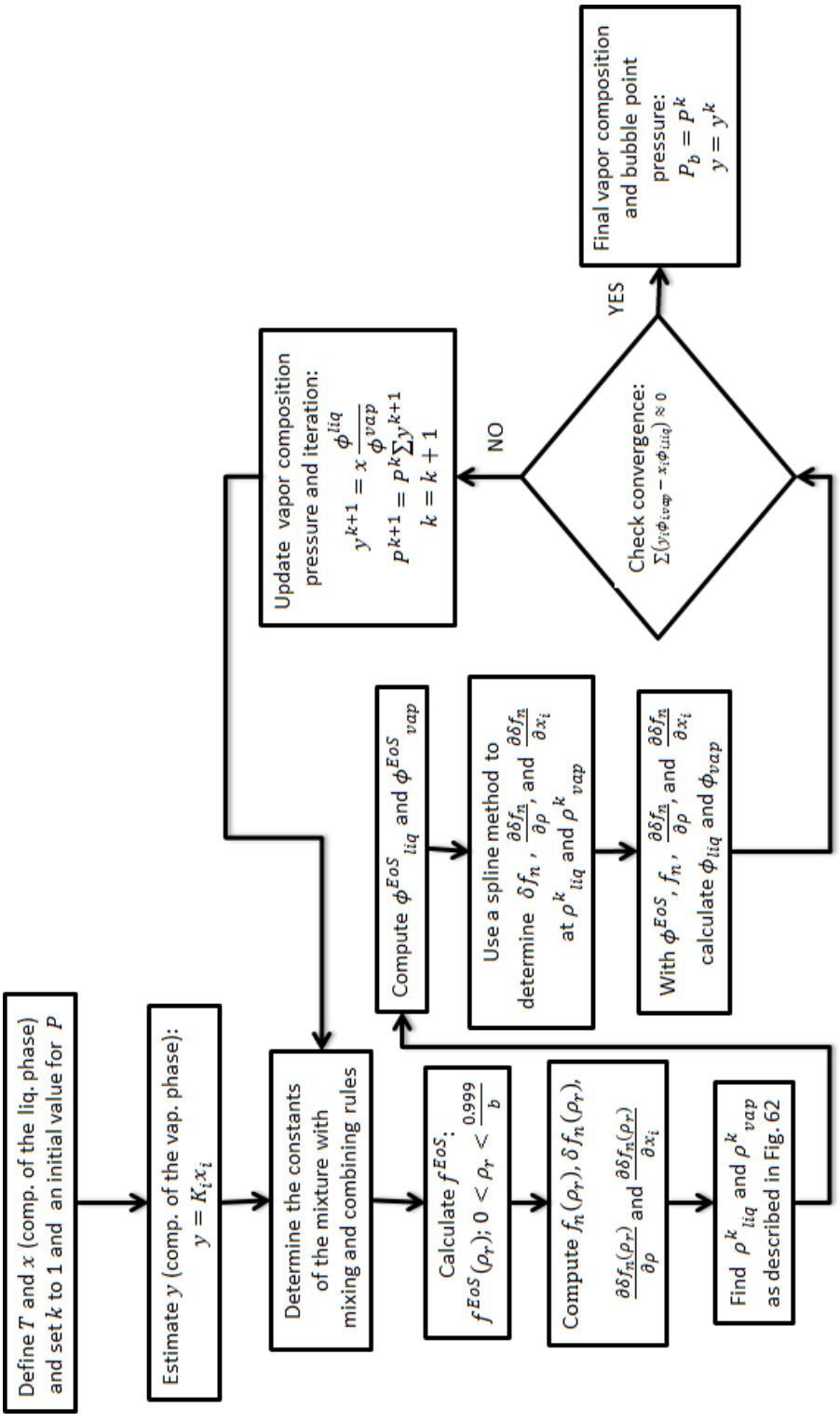

Figure B.3: Procedure for calculating the bubble point pressure of a system using a crossover EoS

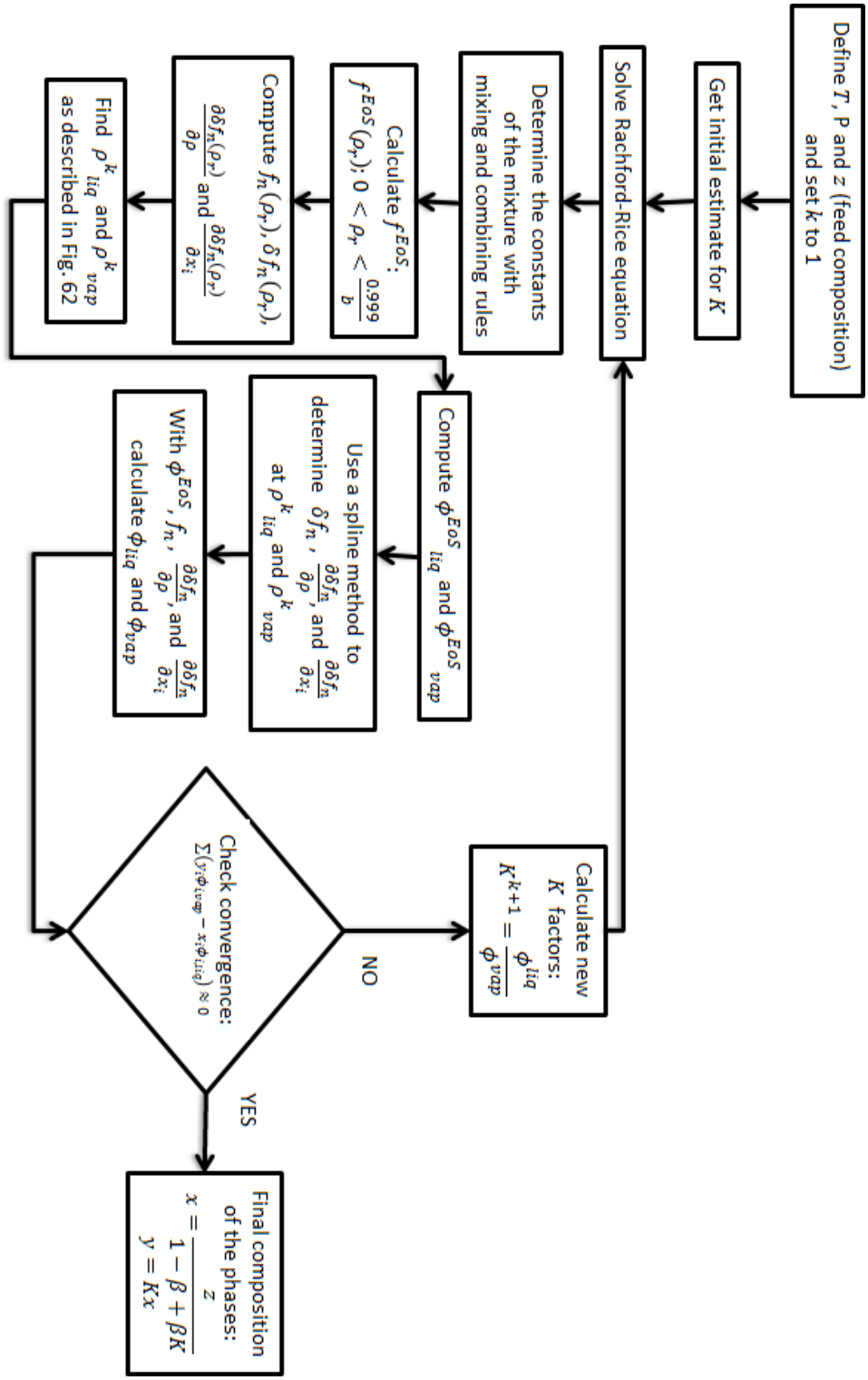

Figure B.4: Procedure for calculating the compositions of the phases in equilibrium using the PT flash algorithm with a crossover EoS

B.4 Calculation of critical lines

For the critical point calculations, Michelsen's [167] modification of Heideman and Khalil's [168] algorithm was applied. The method is used to solve the stability and criticality conditions given by:

$$\left(\frac{\partial^2 A}{\partial n_i \partial n_j}\right)_{T,V,n_{l\neq i,j}} = 0 \tag{B.4}$$

$$\left(\frac{\partial^3 A}{\partial n_i \partial n_j \partial n_k}\right)_{T,V,n_{l\neq i,j,k}} = 0 \tag{B.5}$$

and the algorithm is described in Figure B.5. The efficient computation of the stability condition is based on the approach that, for a point to lie on the limit of stability, the matrix $\mathbf{Q}$ with elements $q_{ij} = \left(\frac{\partial^2 A}{\partial n_i \partial n_j}\right)$ should have a zero determinant:

$$\det(\mathbf{Q}) = 0 \tag{B.6}$$

Thus if this condition is not respected, the temperature is changed until convergence is reached. Besides, with the change of T it is required to re-evaluate f_n, the free energy density. If the previous condition holds, there should be a vector Δn that satisfy the equation:

$$\mathsf{Q} \cdot \Delta n = 0 \tag{B.7}$$

and if a non-zero vector Δn is found, the criticality condition has to be considered. Michelsen [167] proposed the following condition to replace Equation (B.5):

$$C = \Delta n \cdot \left[\frac{\partial q_{ij}\,(n + s\Delta n)}{\partial s}\right] \cdot \Delta n = 0 \tag{B.8}$$

where $\frac{\partial q_{ij}(n+s\Delta n)}{\partial s}$ is the derivative of q_{ij} with respect to the directional increment s. Consequently, if Equation (B.8) is greater than a predetermined tolerance, the volume of the system is changed and the the free energy density, f_n, needs to be re-evaluated. The critical point is reached at a certain T and v when both $\det(\mathbf{Q})$ and C are close to zero. The critical pressure is calculated using Equation (A.2).

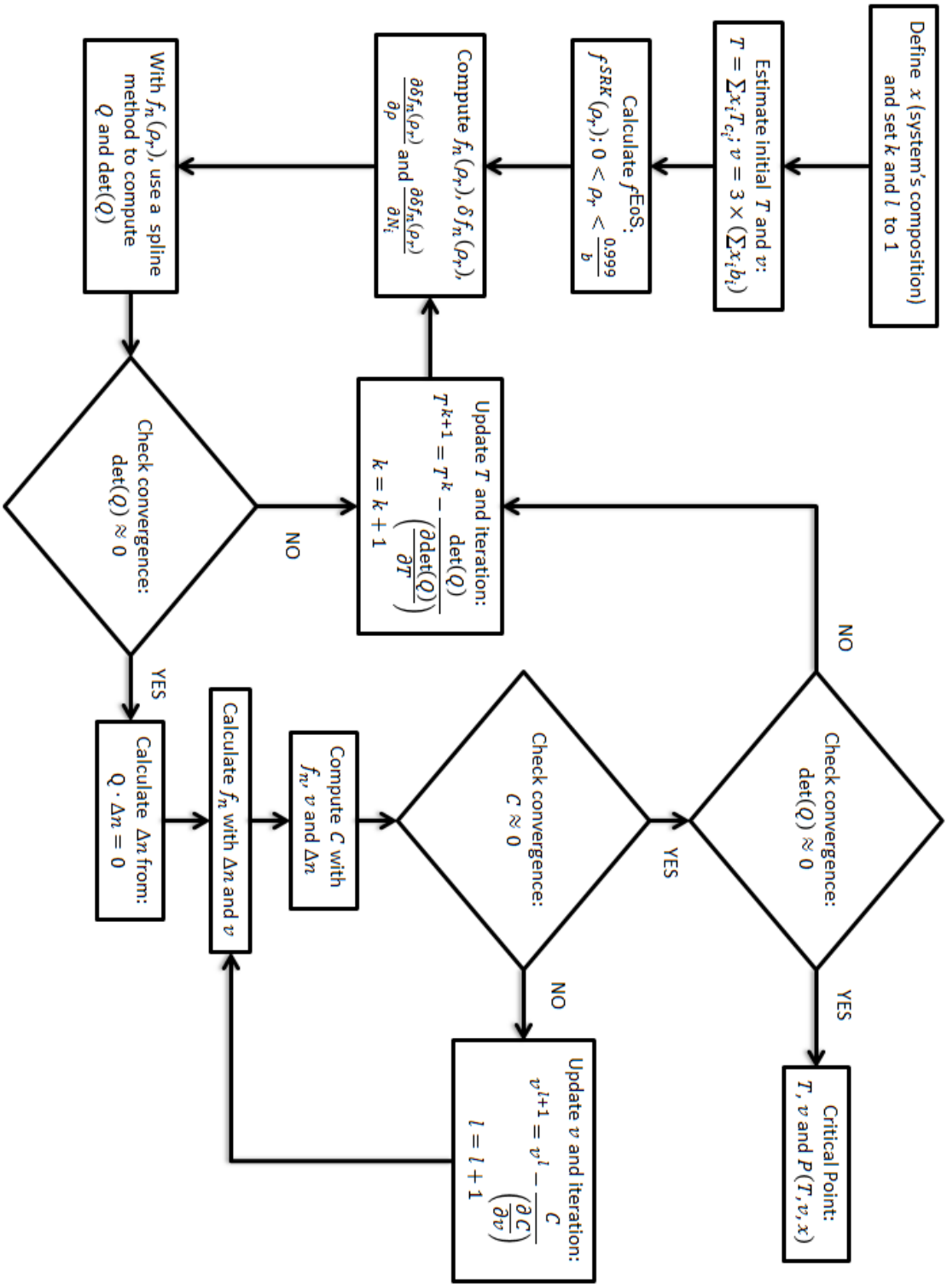

Figure B.5: Procedure for calculating the critical point of a mixture using a crossover EoS

Appendix C

List of Publications

The results obtained in this work allowed the completion of the scientific articles that were published in international journals relevant to the field of chemical engineering. Below are the list of publications:

1. Evaluation of equations of state for simultaneous representation of phase equilibrium and critical phenomena
   Andre P.C.M. Vinhal, Wei Yan, Georgios M. Kontogeorgis
   Fluid Phase Equilibria 437, 140-154, 2017
   http://dx.doi.org/10.1016/j.fluid.2017.01.011

2. Application of a Crossover Equation of State to Describe Phase Equilibrium and Critical Properties of n-Alkanes and Methane/n-Alkane Mixtures
   Andre P. C. M. Vinhal , Wei Yan, Georgios M. Kontogeorgis
   Journal of Chemical Engineering Data 63, 4, 981-993
   http://pubs.acs.org/doi/abs/10.1021/acs.jced.7b00779

Søltofts Plads, Building 229
2800 Kongens Lyngby, Denmark
Tlf. +45 4525 2800

www.kt.dtu.dk